



MONASH University

**OCEAN-ATMOSPHERE COUPLED MODES
OF DECADAL VARIABILITY
IN THE SOUTHERN HEMISPHERE**

GANG WANG

A thesis submitted for the degree of Doctor of Philosophy at
Monash University in 2015
School of Earth, Atmosphere and Environment

Copyright notice

© Gang Wang (2015). Except as provided in the Copyright Act 1968, this thesis may not be reproduced in any form without the written permission of the author.

I certify that I have made all reasonable efforts to secure copyright permissions for third-party content included in this thesis and have not knowingly added copyright content to my work without the owner's permission.

TABLE OF CONTENTS

Abstract	I
Publications during Enrolment	III
General Declaration	III
Acknowledgements	V

Chapter 1. Introduction 1

1.1 Background	3
1.1.1 Climate Modes	3
1.1.2 Southern Ocean	6
1.1.3 Long-term Variability in the Southern Ocean	8
1.1.4 CMIP Models	13
1.2 Aims	14
1.3 Outline of Thesis	15

Chapter 2. Model Evaluation 17

Declaration for Chapter 2	19
2.1 Introduction	21
2.2 Data and Method	23
2.2.1 Data	23
2.2.2 Comparison of EOF Modes	27
2.3 Formulation of null hypotheses	31
2.3.1 Sampling Uncertainties of Eigenvalues	32
2.3.2 Slab Ocean Model	34
2.3.3 Isotropic diffusion	34
2.4 Comparison of the Eigenvalue (EV)-Spectrum	36
2.4.1 North Pacific	38
2.4.2 Uncertainties in the SST Modes in the Global Oceans	43
2.4.3 Comparison between Models	54
2.5 Summary and Discussion	56

Chapter 3. Basic Long-term Modes in the Southern Ocean 63

Declaration for Chapter 3	65
3.1 Introduction	67
3.2 Data, Model Simulations and Methods	69
3.3 Model Evaluation	71
3.4 Leading Modes in the Southern Ocean	75
3.4.1 Mode 1: The Annular Mode	83
3.4.2 Mode 2: Basin Wide Monopole Mode	87
3.4.3 Mode 3: Dipole Mode in the South Pacific	90
3.5 Summary and Discussion	93

Chapter 4. Factors Influencing SST Variability in the Southern Ocean	99
4.1 Introduction	101
4.2 The HYCOM Ocean Model	103
4.3 Atmospheric Forcing	109
4.4 Ocean Dynamics	114
4.5 Sea Ice	117
4.6 Summary and Discussion	121
Chapter 5. Mechanism of Long-term Variability	125
5.1 Mixed Layer Depth	128
5.2 Advection Mode HYCOM Experiment	132
5.3 Simple Band Model Experiment	137
5.4 Summary and Discussion	143
Chapter 6. Conclusions	147
6.1 Summary of Findings	149
6.2 Synthesis of Results	150
6.3 Future Work	151
Reference	154
Abbreviations	170

ABSTRACT

The Southern Ocean has a critical influence on the global climate, and any long-term variability in the Southern Ocean can have both regional and global impacts significantly. However, sparse observations limit the study of the long-term variation. To test the quality of models simulating the natural sea surface temperature (SST) variability, the SST variability in the global oceans is evaluated in simulations of the Climate Model Intercomparison Project Phase 3 (CMIP3) and CMIP5 models. The result shows that some models demonstrate good skill in simulating the observed spatial structure of the SST variability in the tropical domains and less so in the extra-tropical domains. The CMIP5 ensemble exhibits some improvement over the CMIP3 ensemble, mostly in the tropical domains on SST variability simulation. Further, the spatial structure of the SST modes of the CMIP3 and CMIP5 super ensemble is more realistic than any single model, which is mostly used for the following study.

Several SST leading modes in the Southern Ocean are discussed on decadal and even larger time scales using CMIP5 data set based on EOF analysis. We compare the modes against several simple null hypotheses, such as isotropic diffusion (red noise) and a Slab Ocean model, to investigate the sources of decadal variability and the factors affecting the propagation and decay of long-term anomalies. The result reveals that the annular mode with largest amplitudes in the Pacific, the basin-wide monopole mode and South Pacific dipole are the principle patterns with low-frequency variability, which contain the dual effects of internal intrinsic processes as well as external forcing and teleconnections. The annular mode is mostly affected by El Niño Southern Oscillation (ENSO) via teleconnection especially in the South Pacific domain and by local Southern Annular Mode (SAM) over the whole Southern Ocean.

The monopole mode and South Pacific dipole mode, while they both demonstrate pronounced multi-decadal and longer time scales variability, are firstly inducted by the Wave-3 patterns in the atmosphere and further developed via ocean dynamics.

The causes and characteristics of interannual-decadal SST variability in the Southern Ocean are further investigated with an ocean general circulation model and a simplified band ocean model. Possible factors are examined affecting the generation, propagation and decay of long-term anomalies with a series of sensitivity experiments. We found that the atmospheric forcing not only affects the SST modes on shorter time-scales directly, but also shows its influence on longer time scales via air-sea interaction, amplification and oceanic feedback. The deep mixed layer in the Southern Ocean is an essential element to maintain the long-term SST variability. The ocean dynamics connect the entire ocean and create the homogeneous-like spatial patterns. The ocean advection is the key factor to create SST spectral structure, which concentrates the spectrum on interannual scale synchronizing with the transport of Antarctic Circumpolar Current (ACC).

Publications During Enrolment

Wang G, Dommenges D, Frauen C (2015) An evaluation of the CMIP3 and CMIP5 simulations in their skill of simulating the spatial structure of SST variability. *Climate Dynamics* 44: 95-114.

Wang G, Dommenges D (2015) The leading modes of decadal SST variability in the Southern Ocean in CMIP5 simulations. *Climate Dynamics*. Submitted

General Declaration

I hereby declare that this thesis contains no material which has been accepted for the award of any other degree or diploma at any university or equivalent institution and that, to the best of my knowledge and belief, this thesis contains no material previously published or written by another person, except where due reference is made in the text of the thesis.

This thesis includes 1 original papers published in peer reviewed journals and 1 unpublished publications. The core theme of the thesis is “decadal SST variability in the Southern Ocean”. The ideas, development and writing up of all the papers in the thesis were the principal responsibility of myself, the candidate, working within the School of Earth, Atmosphere and Environment under the supervision of Dr. Dietmar Dommenges.

The inclusion of co-authors reflects the fact that the work came from active collaboration between researchers and acknowledges input into team-based research.

In the case of chapter 2 and 3, my contribution to the work involved the following:

Thesis chapter	Publication title	Publication status	Nature and extent of candidate's contribution
2	An evaluation of the CMIP3 and CMIP5 simulations in their skill of simulating the spatial structure of SST variability	Published	Data analysis. Writing and preparation of the manuscript. Main author of the manuscript. 75% contribution
3	The leading modes of decadal SST variability in the Southern Ocean in CMIP5 simulations	Submitted	Data analysis. Writing and preparation of the manuscript. Main author of the manuscript. 80% contribution

I have not renumbered sections of submitted or published papers in order to generate a consistent presentation within the thesis.

Student signature: 

Date: 27/10/2015

The undersigned hereby certify that the above declaration correctly reflects the nature and extent of the student and co-authors' contributions to this work.

Main Supervisor signature: 

Date: 27/10/2015

Acknowledgements

First and foremost I would like to express my sincerest appreciation to my supervisor Dr. Dietmar Dommenges for his excellent guidance and patience. It has been such an honour to be his first Ph.D. student at Monash University. Dietmar, by his example as a successful scientist, motivates and inspires me throughout my Ph.D. study.

My deep gratitude also goes to my associate supervisor, Prof. Christian Jakob. He would always take time out from his busy schedule and give me many valuable suggestions from different angles.

I want to thank all Dommenges group members, including Claudia, Tobias, Yanshan, Nick, Byju and Asha for their friendship and help. Special thanks to Dr Claudia Frauen who helps me a lot for the ACCESS model study.

It has been such a big pleasure to work at Monash University and Australian Research Council Centre of Excellence for Climate System Science. The various excellent researchers and kind staff have contributed in many ways towards my research. I would like to thank all of them.

And finally, I would like to thank my parents, sister, brother-in-law and my lovely nephew for their consistent support and encouragement.

My candidature is supported by the Monash Graduate Scholarship and Faculty of Science Dean's International Scholarship. This project is funded under the Australian Research Council Centre of Excellence for Climate System Science (CE110001028). The model simulations were computed on the National Computational Infrastructure in Canberra.

Chapter 1

Introduction

In recent decades, there has been growing interests in decadal and longer time scale climate modes of variability, which is motivated by a desire to better understand the climate system especially the recent observed variations and warming trends. However, neither the decadal and longer modes of variability nor the processes that cause this low-frequency variability are well understood due to the lack of qualified observation data, especially in the Southern Hemisphere (SH).

The analysis of long climate simulations provides a promising alternative for study of decadal variability. This thesis examines the long-term atmospheric-ocean coupled modes of variability in the Southern Hemisphere based on the combination of observed data and model output, with a focus on the low-frequency variability of sea surface temperature (SST) in the Southern Ocean (SO) and its mechanisms.

In this chapter, we briefly introduce the background of the study including the definition of climate modes, the climate variability in the Southern Ocean, and development of CMIP models, followed by the goals and structures of the thesis.

1.1 Background

1.1.1 Climate Modes

Climate variability refers to variations in the mean state and other statistics of the climate on all temporal and spatial scales beyond that of individual weather events (IPCC, 2001). An important process in understanding the climate variability is to simplify the complex climate system to a minimum number of climate modes that can explain a maximal part of the variation (Dima and Lohmann, 2004). Thus, climate variability tends to take place mainly with a series of spatial modes fluctuating about a mean climate state, and the combination of several leading modes can simply

represent most variation of the high-dimensional climate system. In climatology, “mode” is usually used to describe a spatial structure with at least two strongly coupled centres of action (Wang and Schimel, 2003). Most dynamical modes are represented from the variability of the primary climate variability like temperature, pressure and precipitation.

There are two types of methods to measure the climate modes. The simpler definition is to get the mode time evolution first, and then obtain the associated spatial structure by regressing the temporal series on to the spatial field. An example is the Southern Oscillation Index (SOI, e.g. Chen, 1982), which is used to represent the strength of El Niño-Southern Oscillation (ENSO). Warm ENSO events lead to warm sea surface anomalies in east-central equatorial Pacific, and vice versa. The SOI is defined as the sea surface pressure gradient between Tahiti and Darwin that essentially infers the zonal wind variability over tropical west Pacific. The correlation between SOI and the sea surface temperature field demonstrates the spatial features of ENSO. During warm ENSO events (El Niño), the pressure decreases to below average in Tahiti and becomes above average in Darwin, then the SOI is negative. For cold ENSO events (La Niña), the SOI tends to be positive as the pressures behave oppositely (Fig. 1.1).

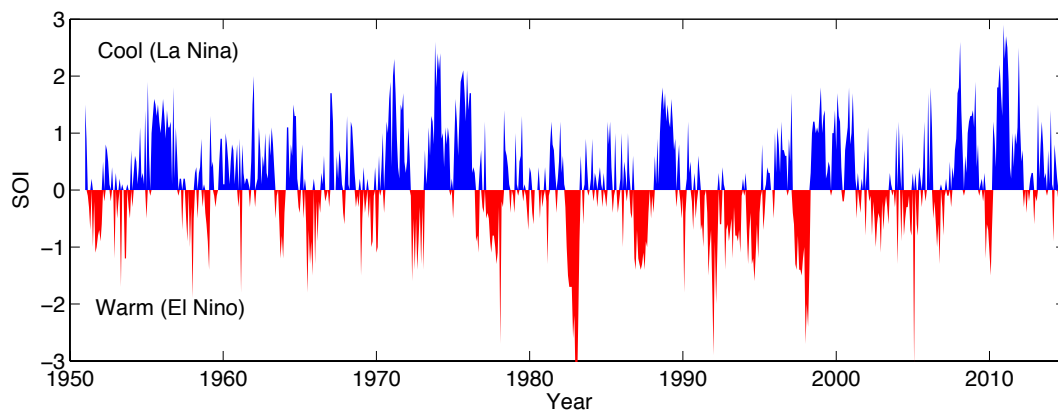


Fig. 1.1 Monthly standardized Southern Oscillation Index (SOI) from 1951 to 2014. (Data source: <http://www.cpc.ncep.noaa.gov/data/indices/soi>)

Another more complicated method is empirical orthogonal function (EOF) analysis. This analysis is used to decompose a climate dataset into pairs of eigenvectors (EOFs, namely the spatial patterns) and corresponding principal components (PCs, namely the functions of time, time series or time indices). As a result, it can find the time series and spatial patterns at the same time. The EOFs describe the spatial structures of the modes and associated time indices present the temporal variation of specific modes. However, as EOF is a purely statistical technique, further analysis is required to guarantee the EOF pattern (mode) have physical meaning beyond noise.

For instance, the Pacific Decadal Oscillation (PDO) is described as the leading EOF mode of the SST anomaly in the North Pacific on decadal time scale (north of 20°N, Fig. 1.2a, e.g. Mantua et al, 1997). The PDO index, therefore, is the standardized PC time series, which illustrates a decadal to multi-decadal variation (Fig. 1.2b). When the index is positive, the PDO is in a warm phase, the northwest Pacific surface becomes cooler and the eastern coastal part becomes warmer, and vice versa.

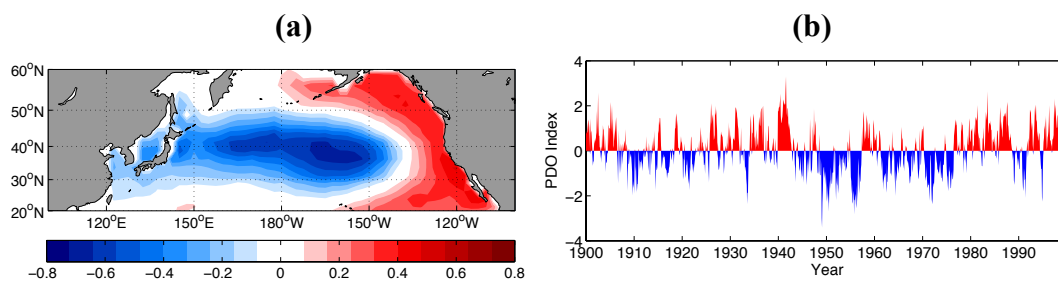


Fig. 1.2 (a): Leading EOF pattern of detrended monthly SST anomaly in the North Pacific for HadISST (Hadley Centre Sea Ice and Sea Surface Temperature data set, see Rayner et al., 2002); (b): Time series of the EOF pattern in (a).

The combination of several leading modes can simply represent most variation of the high-dimensional global climate system. These include, among many others, the

North Atlantic Oscillation (Walker and Bliss, 1932; Wallace and Gutzler, 1981; Hurrell, 1995), the Arctic Oscillation and its SH counterpart, the Antarctic Oscillation (also known as the northern and southern annular modes, respectively) (Limpasuvan and Hartmann, 1999; Thompson and Wallace, 1998, 2001;), ENSO (Walker and Bliss, 1932; Wallace and Gutzler, 1981; Philander 1985), and the PDO (Mantua et al, 1997).

While climate modes in the Northern Hemisphere (NH) oceans on decadal to multi-decadal scales has been the subject of numerous studies (Deser and Blackmon, 1993; Graham, 1994; Kushnir, 1994; Trenberth and Hurrell, 1994; Latif and Barnett, 1996 and references therein), far less work has been done on the similar low frequency variability in the SH oceans regions since the oceans in SH especially the Southern Ocean represent perhaps the largest spatial data voids on the globe.

1.1.2 Southern Ocean

The Southern Ocean (south of 30°S) plays an important role in the global climate system for its significant heat and carbon capacity as it absorbs about 40% of the total global ocean uptake of anthropogenic CO₂ (e.g. Patra et al., 2005; Gruber et al., 2009). It has the largest current in the world ocean, the Antarctic Circumpolar Current (ACC, Fig. 1.3), which flows eastward driven by the strong westerly wind above, connects Pacific, Atlantic and Indian Ocean and has a profound influence on the global ocean circulation and climate (Bindoff et al., 2007).

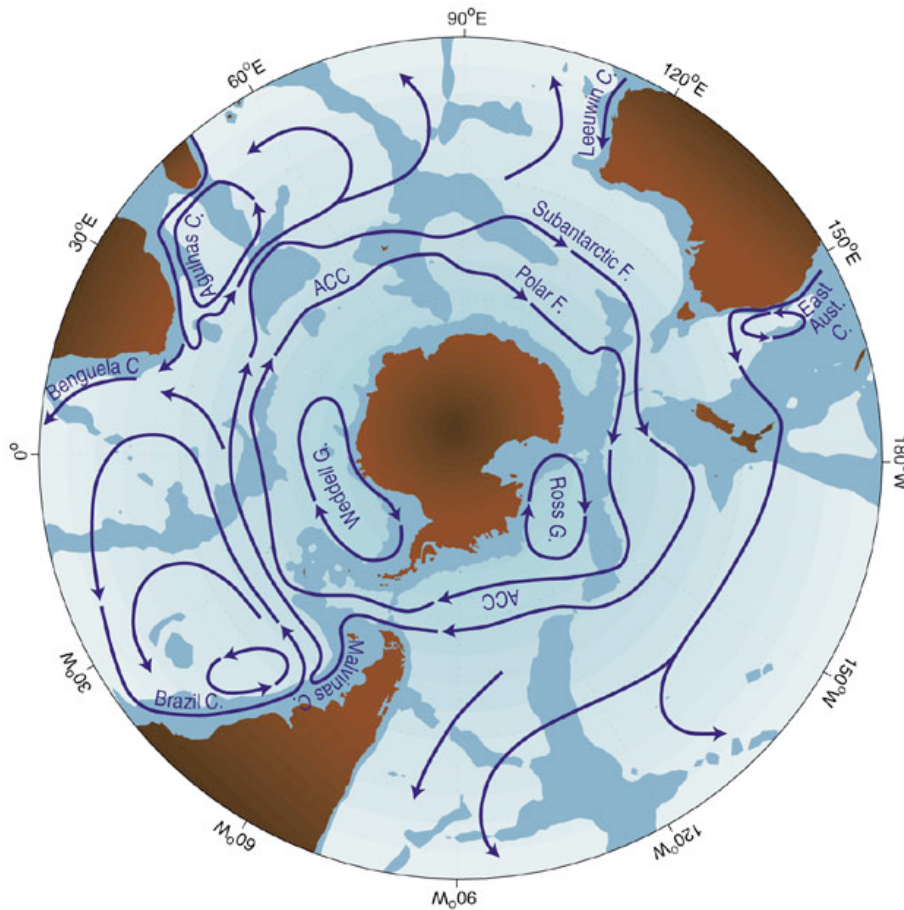


Fig. 1.3 The diagram of Southern Ocean surface circulation. C = Current (e.g. ACC = Antarctic Circumpolar Current); F = Front; G = Gyre. (Rintoul et al., 2001)

The Southern Ocean also is the essential part of the overturning circulation and responsible for the deep and bottom water masses generation and transportation (Marsh et al., 2000). In addition, the active air-sea interaction transports the heat and moisture and further determines the regional climate. Given the importance of the Southern Ocean in the global climate system, it is pertinent to understand the variability in this region.

However, the research of Southern Ocean is mostly restricted by the lack of data. In-situ observations were rare in the Southern Ocean before the 1950s (Gordon and Molinelli, 1982). After the 1960s, the increased instrumental observations were mostly focused on specific regions like the Drake Passage. From the 1980s, vast

amount of satellite data has been acquired and applied into oceanography study, which has significantly increased the spatial coverage of observation. However, for the long-term variability research, only 30 years of satellite observation is still not long enough.

Another difficulty for Southern Ocean study is mainly caused by the dynamical complexity of the Southern Ocean. As Southern Ocean is one of the extremely energetic regions, eddies play an important role in the dynamics (e.g. Johnson and Bryden, 1989; Sallée and Rintoul, 2011; Hogg et al., 2015). According to the Rossby deformation radius, eddies occur on the order of 10~30 km in the Southern Ocean (Chelton et al., 1998). This fact makes it difficult for Southern Ocean modelling. Thus, models must have eddy-resolving (0.1°) horizontal resolution, otherwise models are largely depends on eddy parameterizations.

However, the computational cost is too high for long-term eddy-resolving model simulations. For coupled climate experiments, simulations with eddy-resolving resolution have only been attempted recently with short integrations (McClean et al., 2011; Kirtman et al., 2012; Bryan et al., 2014), which is still not enough for low-frequency analysis. Thus, some climate centres take the compromise that they use eddy-permitting resolution ($0.25^\circ\sim 0.5^\circ$) combined with eddy parameterizations and make long integrations of the climate model simulation (e.g. Menemenlis et al., 2008; Mazloff et al., 2010).

1.1.3. Long-term Variability in the Southern Ocean

In the recent decades, the Southern Ocean demonstrates an unusual negative trend of the surface temperature under the global warming background (e.g. SST trend in Fig.

1.4). Similarly, opposite to the Arctic, the Antarctica has also cooled and even increased its ice extent since 1980s (e.g., Cavalieri and Parkinson 2008; Comiso and Nishio 2008) These imply that there might be internal variability existing within the Southern Ocean, which shows a negative phase currently and offsets the climate change effect.

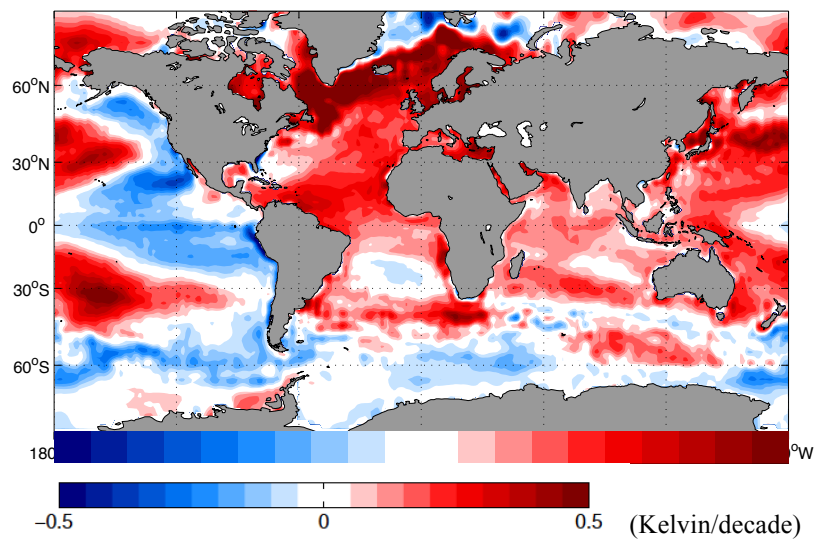


Fig. 1.3 Satellite observed SST Trend in 1982-2010 for OISST (Optimum Interpolation Sea Surface Temperature, Reynolds et al., 2002)

Other evidences are from the proxy data. Take the tree ring for example; Fig. 1.5 shows the time series of tree-ring reconstructed surface temperature of several locations within Southern Hemisphere (Jansen et al, 2007). Clearly all these paleo records demonstrate strong low-frequency variation. In particular, the reconstructed temperature in Tasmania and New Zealand both illustrate decadal to multi-decadal oscillations among last 1000 years, which further supports the existence of the long-term variability in the Southern Ocean.

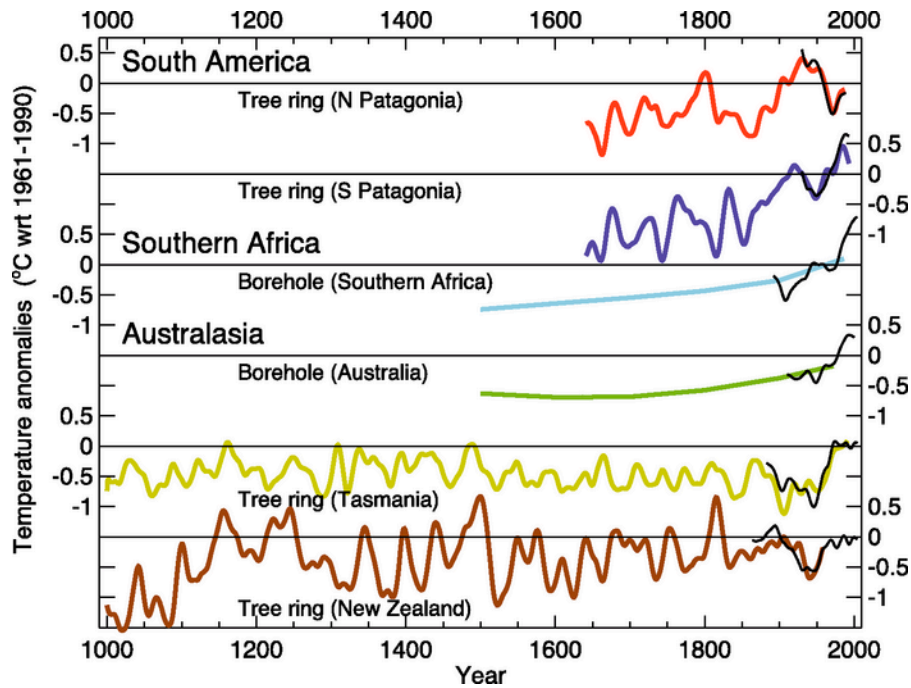


Fig. 1.5 Temperature reconstructions for regions in the SH: two annual temperature series from South American tree ring data (Villalba et al., 2003); annual temperature estimates from borehole inversions for southern Africa and Australasia (Huang et al, 2000); summer temperature series from Tasmania and New Zealand tree ring data (Cook et al., 2000, 2002). The black curves show summer or annual instrumental temperatures for each region. All tree ring and instrumental series were smoothed with a 25-year filter and represent anomalies ($^{\circ}\text{C}$) from the 1961 to 1990 mean (indicated by the horizontal lines). (Jason et al., 2007)

Most research focuses on the long-term variation caused by ENSO and the Southern Annular Mode (SAM). ENSO is the most prominent coupled ocean-atmosphere phenomenon that causes global climate variability on interannual time scale. It is an oscillation of the surface temperature in the tropical Pacific. Warm events of ENSO (El Niño) accompany SST warming in the tropical eastern Pacific and weakening of the trade winds and Walker Circulation, and enhance the convection in central tropical Pacific (McPhaden et al., 2006). The convection creates anomalous potential vorticity and poleward advection in the atmosphere, and further excites Rossby wave teleconnection patterns in the Southern Hemisphere, known as the Pacific South America (PSA) patterns (Fig. 1.6, Hoskins and Karoly, 1981; Mo and Higgins 1998).

The PSA transports the ENSO anomalous signals to high southern latitudes (e.g. Mo and Higgins, 1998; Renwick, 2002; Turner, 2004), and has a significant influence on the atmospheric circulation in the South Pacific and the surface air variability in the Antarctic Peninsula (Kwok and Comiso, 2002). In addition, ENSO also demonstrates its impact on SST and sea ice variability in the Southern Ocean via its related anomalous sensible and latent heat flux exchange (Garreaud and Battisi, 1999; Lefebvre et al., 2004; Yuan and Martinson, 2000; Yeo and Kim, 2015).

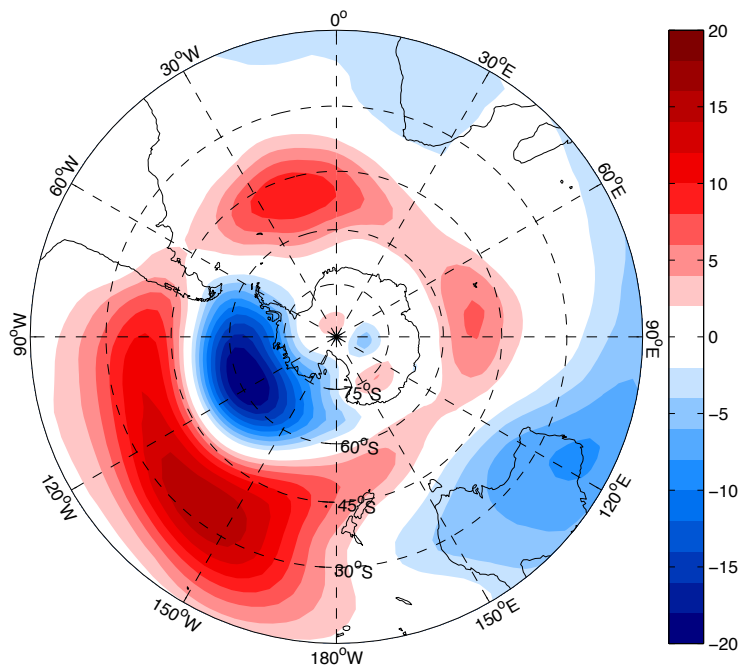


Fig. 1.6 Regression of 700mb atmospheric geopotential height anomalies onto the SOI on monthly time scale (1979-2014, unit: metre). The geopotential height data is from NCEP-DOE Reanalysis 2 (Kanamitsu et al., 2002). The regression demonstrates the PSA pattern in extra-tropical Southern Hemisphere.

Another important factor is Southern Annular Mode, also named Antarctic Oscillation. SAM is the dominant mode of Southern Hemisphere climate variability from intraseasonal to interannual time scale, which is defined as the leading EOF pattern of sea level pressure (SLP) to the south of 20°S and is approximately zonally symmetric (Fig. 1.7, Thompson and Wallace 2000, Jones et al. 2009). It is

characterized by pressure anomalies of different signs over the mid-latitudes and high-latitudes. Positive SAM is associated with a positive pressure anomaly in the mid-latitudes and a negative anomaly in the high-latitudes, and vice versa. The variation of the pressure gradient drives the meridional shift of the westerly winds over the Southern Ocean (e.g. Hartmann and Lo, 1998). Thus, SAM can affect the westerly circumpolar flow, then further influence the circulation, mixed layer depth and heat capacity in the ocean substantially (e.g. Boer et al. 2001; Cai and Watterson, 2002; Fyfe, 2003).

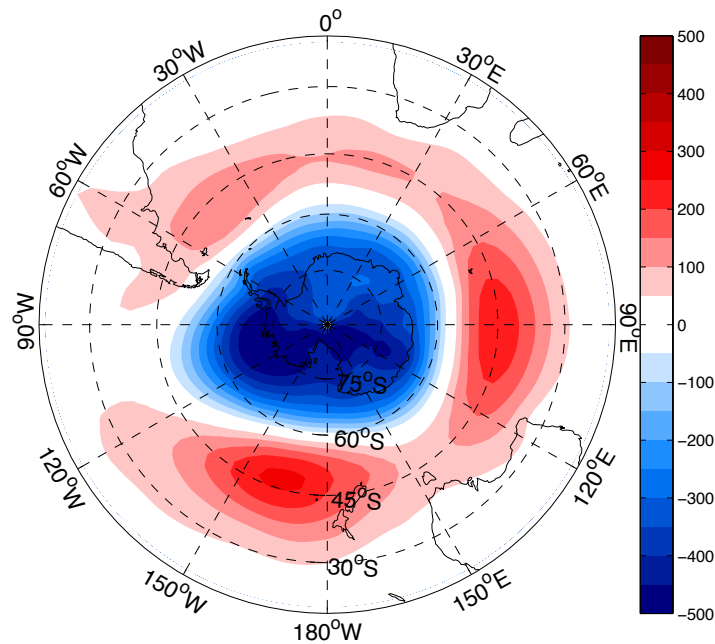


Fig. 1.7 Leading EOF pattern (25%) of monthly sea level pressure anomaly in extra-tropical Southern Hemisphere for NCEP-DOE Reanalysis 2 in 1979-2014.

Further, a number of coupled modes in the atmosphere-ocean system have been identified in the Southern Hemisphere, such as the Trans-Polar Index (TPI, Jones et al, 1999), Antarctic Circumpolar Wave (ACW, e.g. White and Peterson, 1996) and South Pacific subtropical Dipole (Morioka et al., 2013). They might also exhibit

decadal variations. The length of observation records and limitations of models restrict our understanding of the long-term variability in the Southern Ocean.

1.1.4 CMIP Models

Since the begin of the 21st century, coupled climate models have been well developed and further applied to the climate study especially for the long-term variation research. Long-term coupled climate simulation provides another beneficial resource for low-frequency climate study in addition to the observations. Therefore, the statistical analysis in combination with coupled model simulations can build a very good tool to study the decadal climate modes.

The Coupled Model Intercomparison Project (CMIP) presents a highly valued resource to the climate science research for the understanding of natural variability and future climate change (Meehl et al., 2007; Taylor et al., 2012). Now the CMIP datasets mainly include the Phase 3 (CMIP3) and Phase 5 (CMIP5), both of which contains the output from a great number of models with long-term simulation to advance our study of climate processes and their effects.

CMIP3 was released in 2010 for the Intergovernmental Panel on Climate Change (IPCC) Fourth Assessment Report (AR4). It has 25 coupled models and includes scenarios for past and present climate forcing. On the basis of CMIP3, CMIP5 was released in 2013 for IPCC AR5. It contains 56 models with higher spatial resolution (e.g. 0.2~2.0° for ocean components compared to 0.2~5.0° in CMIP3), more complete representation of the climate system (e.g. coupled biogeochemical components, aerosol and dynamical vegetation) and improved parameterizations compared to CMIP3.

However, given the complexity of the global climate system especially in the Southern Ocean, it is important to know whether the CMIP models are capable of simulating the long-term variability and related modes, which requires proper model evaluation prior.

1.2 Aims

The motivation of this thesis is to better understand of the leading modes in the Southern Ocean on long time scales. Sea surface temperature is taken as the primary research variable as it represents the interaction between the atmosphere and the ocean. We will analyse the long-term modes of SST variability in the Southern Ocean based on CMIP simulation output and limited observations.

There are two aims in this project:

1. To find out the leading coupled modes and their basic characteristics.
2. To examine the possible factors and mechanisms affecting the generation, propagation and decay of long-term anomalies.

The first aim is achieved by the analyses based on model output and observations. The second aim is mainly realized by null hypotheses comparison and sensitivity numerical experiments.

Throughout the thesis, we will attempt to address four questions below:

1. How good are CMIP models at simulating the coupled modes in the global ocean especially in the Southern Ocean?
2. What are the basic modes with in the Southern Ocean around the decadal scale?

3. What are the elements affecting the strength, propagation and spatial structure of the modes?
4. What are the key factors affecting the long-term variability and its specific spectral structure in the Southern Ocean?

These questions and related answers will consist of the main body of the thesis and lead us to the following chapters.

1.3 Outline of Thesis

First of all we will start from the model evaluation. Chapter 2 will show the details of the evaluation of the CMIP3 and CMIP5 simulations in their skill of simulating the spatial structure of SST variability. We will examine the models on different time scales on the basis of their EOF-modes, and compare the models and observations against simple null hypotheses to illustrate the models skill in simulating realistic patterns of variability and get the suitable models for following study.

In chapter 3, we will use the CMIP5 dataset and discuss the leading SST modes and their basic features. We will also compare modes against several simple null hypotheses to investigate the sources of mode generation and development.

Based on the results of chapter 3, we will address the spatial mechanism of the Southern Ocean variability in chapter 4. We will design a series of different sensitivity experiments with an ocean general circulation model and test the roles of different possible factors influences the modes, such as atmospheric forcing, ocean dynamics and sea ice. This part constructs the basic idea that how the complex climate system affects the long-term modes generally.

Chapter 5 focuses on the temporal structure of the Southern Ocean SST variability. It will answer the question why the Southern Ocean maintains the long-term variability and why the SST spectrum concentrates over some certain frequency and decreases over other period bands using simplified model experiments.

Finally, we will summarise the conclusions of each chapter in Chapter 6 and briefly discuss the possible prospect of future work.

Chapter 2

Model Evaluation

The content presented in Chapter 2 was published as the following paper:

Wang G, Dommenges D, Frauen C (2015) An evaluation of the CMIP3 and CMIP5 simulations in their skill of simulating the spatial structure of SST variability. *Climate Dynamics* 44: 95-114.

Declaration for Thesis Chapter 2

Declaration by candidate

In the case of Chapter 2, the nature and extent of my contribution to the work was the following:

Nature of contribution	Extent of contribution (%)
Data analysis. Writing and preparation of the manuscript. Main author of the manuscript. 75% contribution	75%

The following co-authors contributed to the work. If co-authors are students at Monash University, the extent of their contribution in percentage terms must be stated:

Name	Nature of contribution	Extent of contribution (%) for student co-authors only
Dietmar Dommenges	Methodology development	
Claudia Frauen	Slab Ocean model simulation	

The undersigned hereby certify that the above declaration correctly reflects the nature and extent of the candidate's and co-authors' contributions to this work*.

Candidate's Signature		Date 27/10/2015
------------------------------	---	---------------------------

Main Supervisor's Signature		Date 27/10/2015
------------------------------------	---	---------------------------

The CMIP models provide an unprecedented collection of data output for climate study. However, given that the CMIP models are from different institutions with different model components and parameterizations, they demonstrate significant disagreements with each other and even with the observation. Thus, before we use the CMIP output for long-term climate study, it is important to understand how capable are these CMIP models of simulating the coupled variability, and it must begin with understanding the simulated SST variability in other ocean basins before we compare the SST simulation in the sparsely observed Southern Ocean.

In this chapter, the natural sea surface temperature (SST) variability in the global oceans is evaluated in simulations of the Climate Model Intercomparison Project Phase 3 (CMIP3) and CMIP5 models. In this evaluation, we examine how well the spatial structure of the SST variability matches between the observations and simulations on the basis of their Empirical Orthogonal Functions (EOF)-modes. We will compare the models and observations against simple null hypotheses, such as isotropic diffusion (red noise) or a Slab Ocean model, to illustrate the models skill in simulating realistic patterns of variability. The results will guide us what models should be taken for the further long-term climate variation analysis in the following chapters.

2.1. Introduction

The Coupled Model Intercomparison Project (CMIP) presents a highly valued resource to the climate science research for the understanding of natural variability and future climate change (Meehl et al., 2007; Taylor et al., 2012). However, the models of CMIP are different in their structures and physical parameterizations and have shown significant disagreement and uncertainties on their performance (e.g.

Gleckler et al., 2008, Jamison and Kravtsov, 2010). The aim of the chapter presented here is to evaluate the CMIP models skill in simulating the natural internal spatial structure of SST variability in all major ocean basins (tropical Indo-Pacific, North Pacific, tropical and North Atlantic and the Southern Ocean, see Fig. 2.1 for domain boundaries). This should guide the climate community in the understanding of natural modes of SST variability and support the development of seasonal to decadal forecasting systems.

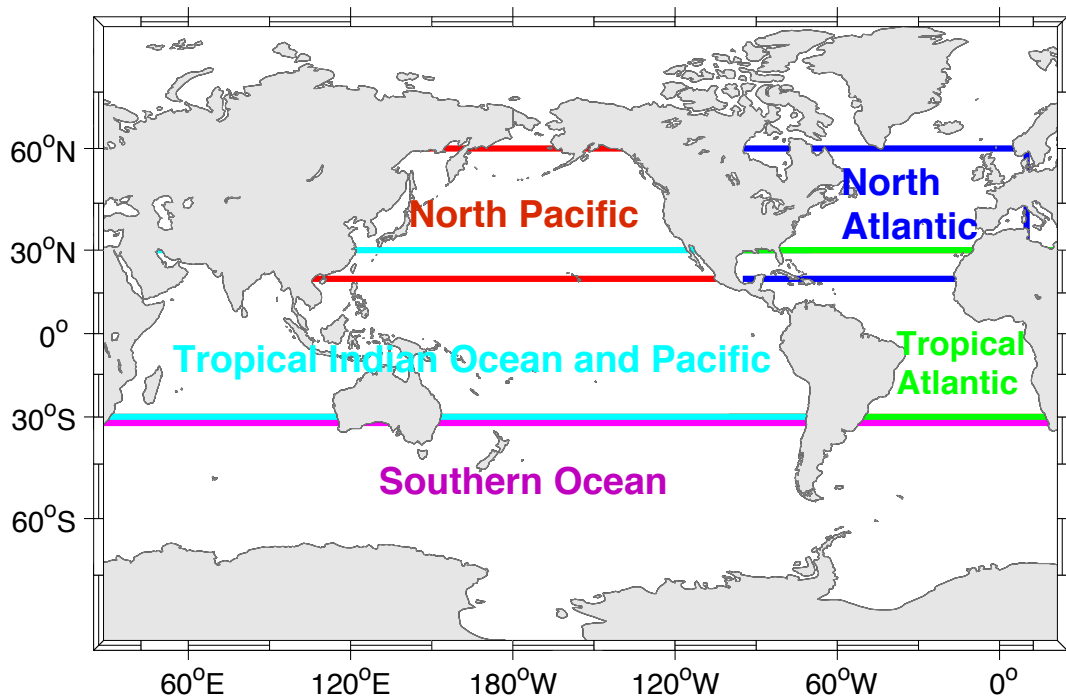


Fig. 2.1 Illustration of the domain boundaries for the EOF-analyses.

Previous model evaluations focused on the mean state climate (Taylor, 2001, Boer and Lambert 2001, Murphy et al. 2004, Gleckler et al., 2008), the general strength of climate variability (Boer and Lambert 2001, Gleckler et al., 2008) or on some regional aspects of climate variability (Guilyardi, 2006, Zhou et al. 2009, Jamison and Kravtsov, 2010, Xavier et al., 2010). Missing is a model evaluation of the SST variability on the global scale.

In the study presented here we will base our model evaluation on the comparison of the empirical orthogonal function (EOF) modes of SST variability for the different major ocean basins in the model simulations and observations. We will consider the EOF modes of shorter time scales of monthly mean high-pass filtered variability and on longer time scales of 5yrs low-pass filtered SST to get some understanding of how the evaluation may change with different time scales. The method of comparing EOF-modes is based on the studies of Dommenges (2007) and Bayr and Dommenges (2014). Similar methods are also discussed in Jolliffe (2002, chapter 13.5) and Krzanowski (1979). This method allows quantifying the agreement in the spatial structure of SST variability in a systematic and objective way. An important aspect in such an evaluation is to put the results of this relatively abstract and complicated analysis into the perspective of some simple null hypotheses, which should help to guide the researchers in evaluating the significance of the results. The simple null hypotheses used in this study describe the spatial structure of SST variability, as they would result from simplified physical processes such as isotropic diffusion (red noise) or atmospheric forcings only (Slab Ocean).

The chapter is organized as follows: firstly, section 2 presents the data and methodology used. Section 3 introduces the null hypotheses chosen for the evaluation and section 4 shows results of the EOF-mode comparison, which are the main results of this study. Finally a summary and discussion are provided in section 5.

2.2. Data and Method

2.2.1 Data

The observed global monthly mean SSTs are taken from the Hadley Centre Sea Ice and SST data set (HadISST, referred as “observations” below; Rayner et al., 2003) from 1900 to 1999, and the NOAA Extended Reconstructed sea surface temperature data set (ERSST, Smith et al., 2008) was chosen as an auxiliary.

Model simulations are taken from all CMIP3 and CMIP5 databases available (Meehl et al., 2007; Taylor et al., 2012). Our analysis focuses on the 20th century SST simulations corresponding to the scenarios of “20c3m” in CMIP3 and “historical run” in CMIP5, respectively. Table 2.1 and 2.2 list all available simulations for this study.

Table. 2.1 List of CMIP3 models

Number	Originating Group(s)	Country	Model
1	Bjerknes Centre for Climate Research	Norway	BCCR-BCM2.0
2	Canadian Centre for Climate Modelling & Analysis	Canada	CGCM3.1 (T47)
3	Canadian Centre for Climate Modelling & Analysis	Canada	CGCM3.1 (T63)
4	Météo-France / Centre National de Recherches Météorologiques	France	CNRM-CM3
5	CSIRO Atmospheric Research	Australia	CSIRO-Mk3.0
6	CSIRO Atmospheric Research	Australia	CSIRO-Mk3.5
7	US Dept. of Commerce / NOAA / Geophysical Fluid Dynamics Laboratory	USA	GFDL-CM2.0
8	US Dept. of Commerce / NOAA / Geophysical Fluid Dynamics Laboratory	USA	GFDL-CM2.1
9	NASA / Goddard Institute for Space Studies	USA	GISS-AOM
10	NASA / Goddard Institute for Space Studies	USA	GISS-EH
11	NASA / Goddard Institute for Space Studies	USA	GISS-ER
12	LASG / Institute of Atmospheric Physics	China	FGOALS-g1.0
13	Instituto Nazionale di Geofisica e Vulcanologia	Italy	INGV-SXG
14	Institute for Numerical Mathematics	Russia	INM-CM3.0
15	Institut Pierre Simon Laplace	France	IPSL-CM4
16	Center for Climate System Research (The University of Tokyo), National Institute for Environmental Studies, and Frontier Research Center for Global Change (JAMSTEC)	Japan	MIROC3.2 (hires)
17	Center for Climate System Research (The University of Tokyo), National Institute for Environmental Studies, and Frontier Research Center for Global Change (JAMSTEC)	Japan	MIROC3.2 (medres)
18	Max Planck Institute for Meteorology	Germany	ECHAM5/MPI-OM
19	Meteorological Research Institute	Japan	MRI-CGCM2.3.2
20	National Center for Atmospheric Research	USA	CCSM3
21	National Center for Atmospheric Research	USA	PCM
22	Hadley Centre for Climate Prediction and Research / Met Office	UK	UKMO-HadCM3
23	Hadley Centre for Climate Prediction and Research / Met Office	UK	UKMO-HadGEM1

Table. 2.2 List of CMIP5 models

Number	Originating Group(s)	Country	Model
1	CSIRO and BOM	Australia	ACCESS1.0
2	Beijing Climate Center, China Meteorological Administration	China	BCC-CSM1.1
3	National Center for Atmospheric Research	USA	CCSM4
4	Météo-France / Centre National de Recherches Météorologiques	France	CNRM-CM5
5	Canadian Centre for Climate Modelling and Analysis	Canada	CanESM2
6	Geophysical Fluid Dynamics Laboratory	USA	GFDL-CM3
7	Geophysical Fluid Dynamics Laboratory	USA	GFDL-ESM2G
8	Geophysical Fluid Dynamics Laboratory	USA	GFDL-ESM2M
9	NASA / Goddard Institute for Space Studies	USA	GISS-E2-H
10	NASA / Goddard Institute for Space Studies	USA	GISS-E2-R
11	Hadley Centre for Climate Prediction and Research / Met Office	UK	HadCM3
12	Hadley Centre for Climate Prediction and Research / Met Office	UK	HadGEM2-CC
13	Hadley Centre for Climate Prediction and Research / Met Office	UK	HadGEM2-ES
14	Institute for Numerical Mathematics	Russia	INM-CM4
15	Institut Pierre Simon Laplace	France	IPSL-CM5A-LR
16	Institut Pierre Simon Laplace	France	IPSL-CM5A-MR
17	Institut Pierre Simon Laplace	France	IPSL-CM5B-LR
18	Atmosphere and Ocean Research Institute (The University of Tokyo), National Institute for Environmental Studies, and Japan Agency for Marine-Earth Science and Technology	Japan	MIROC5
19	Max Planck Institute for Meteorology	Germany	MPI-ESM-LR
20	Max Planck Institute for Meteorology	Germany	MPI-ESM-P
21	Meteorological Research Institute	Japan	MRI-CGCM3
22	Norwegian Climate Centre	Norway	NorESM1-M
23	Norwegian Climate Centre	Norway	NorESM1-ME

An output of a simple Slab Ocean coupled experiment is also used to compare versus the CMIP models in this study. The atmospheric component of the model is based on the UK Meteorological Office Unified Model general circulation model with HadGEM2 atmospheric physics (Davies et al., 2005; Martin et al., 2010; Martin et al., 2011). For our study the atmospheric resolution is reduced to N48 ($3.75^\circ \times 2.5^\circ$). For regions with all-year open ocean conditions the model is coupled to a simple Slab Ocean model with constant 50m depth (e.g. Washington and Meehl, 1984; Dommenges and Latif, 2002; Murphy et al., 2004; Dommenges, 2010) and otherwise

a SST and sea ice monthly climatology of 1950-2010 based on the HadISST data set is prescribed.

The slab ocean cannot reproduce realistic mean SST without calibration, as it does not include ocean circulation to maintain the observed surface energy balance. Therefore, a flux correction scheme is used to force the model SST to closely follow the Hadley Centre Sea Ice and SST data set (HadISST) SST climatology (for more details see Wang et al., 2015). The flux corrections are a function of location and calendar month, but are identical in every year and are thus not state dependent. They are constant fluxes that lead to the correct seasonal mean SST, but do not directly force any SST anomalies. The application of a flux correction to the ocean surface energy balance is an alternative way of introducing a parameterization of the ocean circulation, however, the circulation in the slab ocean model is effectively fixed and does not change in response to atmospheric forcings. We take 500 years output from this simulation and divide the data into five 100-year chunks for the analysis. Unless otherwise noted we show the mean result of the 5 subsamples for the Slab Ocean data analysis.

All data sets (models and observations) were analysed for the period 1900 to 1999, interpolated to a common 2.5° latitude \times longitude grid and linearly detrended to remove the global warming signal prior to the analysis. We used a high-pass filter (cut off at 5 yr) to obtain the high frequency monthly mean SST anomalies (SSTA) for each model and the observations individually, referred as high pass below. A 5yr-running mean was also used to get the low frequency annual mean SSTA on decadal or longer time scales, referred as low pass below.

In addition to analysing the models individually we also combined all the CMIP3 and CMIP5 ensembles to super model data sets to provide a synthesis. The CMIP3 SST anomalies (computed for each model individually) were concatenated to generate a CMIP3 super model with 2300 years of data. Similarly, a CMIP5 super model with 2300 years of data and a CMIP3+5 with 4600 years of data were also constructed. It has to be noted here that combining the anomalies of simulations, which have different modes of variability, will lead to some changes in the characteristics in the EOF-modes. We will point out some of these limitations through out the analysis part.

2.2.2 Comparison of EOF modes

We base our comparison of the spatial structure of SST variability in different data sets on the comparison of the EOF-modes, assuming that the leading EOF-modes give a good representation of the large-scale SST variability. This is done by defining the EOF-modes of one data set as the reference modes and projecting the EOF-modes of the other data set onto these modes to estimate the amount of variance that the reference EOF-modes explain in this projected data set. This concept is based on Dommenges (2007) and Bayr and Dommenges (2014) and briefly summarized here:

An EOF eigenvector (mode) of the reference data set \mathbf{A} , \vec{E}_i^A and its corresponding eigenvalue (EV) e_i^A are compared with the eigenvector \vec{E}_j^B and eigenvalue e_j^B of another data set \mathbf{B} by projecting the eigenvectors \vec{E}_i^A onto the \vec{E}_j^B ,

$$c_{ij} = \frac{\vec{E}_i^A \vec{E}_j^B}{|\vec{E}_i^A| |\vec{E}_j^B|} \quad (2.1)$$

where c_{ij} is the uncentered pattern correlation coefficient describing the spatial similarity between the two EOF-patterns. The projected explained variance (PEV) of

mode \vec{E}_i^A in data set \mathbf{B} , $pe_i^{A \rightarrow B}$, is estimated by the accumulation of all eigenvalues of \mathbf{B} (Dommenget, 2007):

$$pe_i^{A \rightarrow B} = \sum_{j=1}^N c_{ij}^2 e_j^B \quad (2.2)$$

The value $pe_i^{A \rightarrow B}$ represents the total variance of data set B that is explained by the reference mode \vec{E}_i^A , with N the number of EOF-modes considered. In this paper N is set to be 60, which is sufficient to give us stable results. Increasing N does not change the outcomes in any of the domains. The $pe_i^{A \rightarrow B}$ values do not need to be monotonically decreasing, as the e_i^A do, since an EOF-mode of A may explain more variance in the data set B than it does in A and vice versa.

We illustrate this method in a simple example of comparing two data sets: In Fig. 2.2a-f we show the leading EOF modes of the North Pacific for the observations and the GFDL-cm2.1 model simulation. We note here that the two data sets have slightly different leading modes of variability and that the explained variances of each of these modes are also slightly different. To compare the overall spatial structure of variability in the two data sets we choose the observed EOF-modes as the reference modes (\vec{E}_i^A) and project the EOF-modes of the GFDL-cm2.1 model simulation (\vec{E}_i^B) onto these modes. Fig. 2.3a shows the eigenvalues of the observed EOF-modes (e_i^A) against the projected explained variance from the GFDL-cm2.1 model simulation ($pe_i^{A \rightarrow B}$). The leading observed mode (EOF-1 in Fig. 2.2a), for instance, explains only half as much variance in the GFDL-cm2.1 model simulation (red line in Fig. 2.3a) than it does in the observations (black line in Fig. 2.3a). In turn, the observed EOF-10, for instance, mode has more relative explained variance in the GFDL-cm2.1 simulation. Therefore, comparing the overall spatial structure of variability essentially

means to estimate how much variance each of the reference modes explains in both data sets, and essentially quantify the discrepancy based on the mismatch of the variances explained.

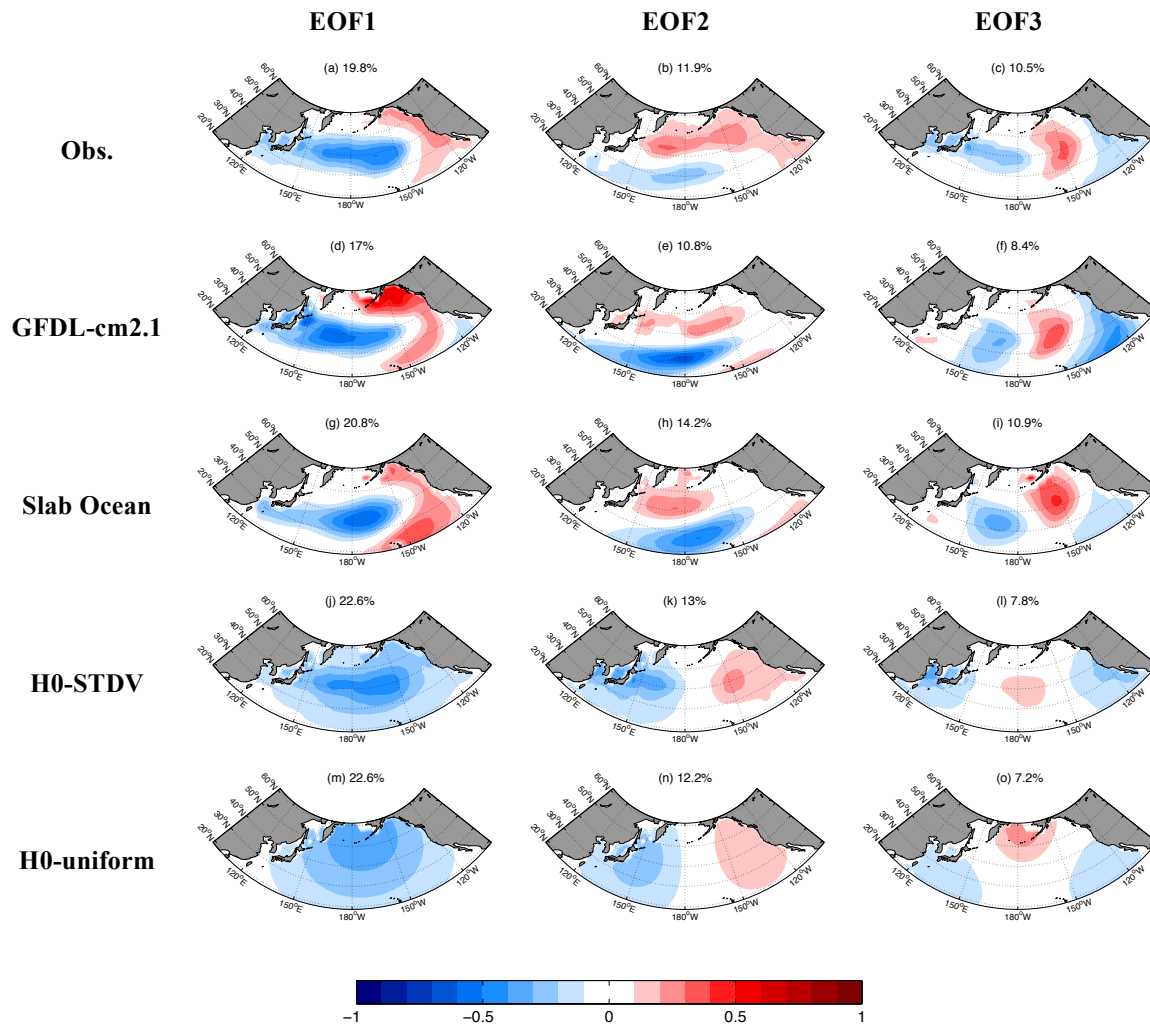


Fig. 2.2 First three leading EOF patterns of detrended monthly SSTA in the North Pacific after 5-year high-pass filter for (a-c): observations (HadISST); (d-f): GFDL-cm2.1; (g-i): slab ocean experiment; (j-l): fitted isotropic diffusion process with inhomogeneous standard deviation forcing; (m-o): as in (j-l): but with homogeneous forcing. The values in the headings of each panel are the explained variances of each EOF-mode.

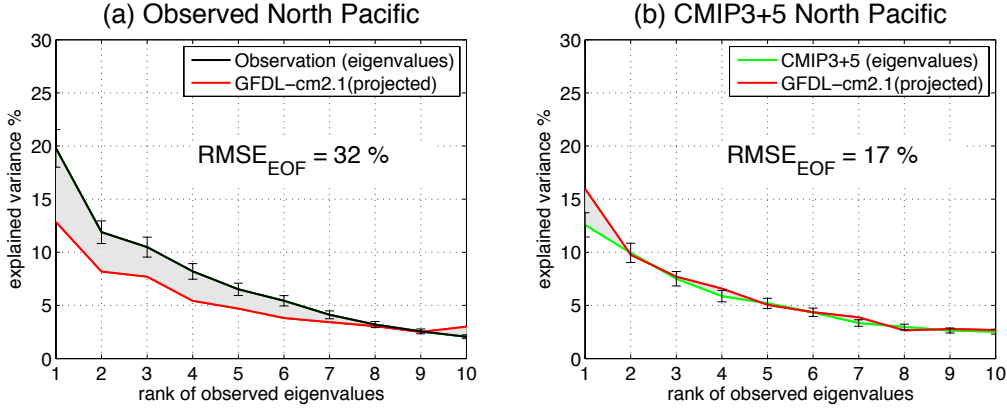


Fig. 2.3 (a) Eigenvalue spectrum of the observed leading EOF-modes in the North Pacific and the PEV values of the GFDL-CM2.1. The bars mark the sampling uncertainty interval of the eigenvalues after North et al. (1982) (b): as (a) but for the leading EOF-modes of the CMIP3+5 super model in the North Pacific. Here the bars mark the sampling uncertainty interval of the eigenvalues after North et al. (1982) based on length of the time series in the GFDL-CM2.1 simulation.

We further see in this comparison that the explained variances of the observed leading modes are significantly less in the GFDL-cm2.1 model simulation. This overall mismatch (grey band in Fig. 2.3a) in the explained variances is quantified by a normalized root-mean-square error ($RMSE_{EOF}$) between the e_i^A and $pe_i^{A \rightarrow B}$ values:

$$RMSE_{EOF}(A, B) = \sqrt{\frac{\sum_{i=1}^{N_A} (pe_i^{A \rightarrow B} - e_i^A)^2}{\sum_{i=1}^{N_A} (e_i^A)^2}} \quad (2.3)$$

The normalization allows a better comparison of the $RMSE_{EOF}$ values among different domains with different sampling uncertainties. Here N_A corresponds to the number of EOF modes considered. In our analysis we choose N_A equal to the effective number degrees of freedom, $N_{spatial}$, also known as the number of independent modes after Bretherton et al. (1999):

$$N_{spatial} = \frac{1}{\sum (e_i)^2} \quad (2.4)$$

The sum $\text{RMSE}_{\text{EOF}}(A, B)$ is dominated by the mismatches in the leading modes between e^A and $pe^{A \rightarrow B}$, as they have larger uncertainties. Uncertainties in the higher order modes are less important in this estimate. Fig. 2.3 shows the RMSE_{EOF} values for two examples. A RMSE_{EOF} value of 100% corresponds to errors that are as big as the eigenvalues. Thus, the RMSE_{EOF} value (32%, see Fig. 2.3a) of the GFDL-cm2.1 model relative to the observations reflects an uncertainty of the leading EOF-modes of about 32% of the eigenvalues, which is a substantial uncertainty. Similarly, the relative smaller RMSE_{EOF} value (17%) in Fig. 2.3b, which represents an uncertainty of about 17% within the leading modes, suggests less fluctuation and better matches between the PEV of GFDL-cm2.1 and the eigenvalues of the CMIP3+5 super model.

2.3 Formulation of null hypotheses

The comparison of the spatial patterns of SST variability in different data sets in this study is based on projecting EOF-modes and estimating the RMSE_{EOF} values. These RMSE_{EOF} values are quite abstract and it is important to put these values into perspective with some simple null hypotheses to understand the significance of these values. We therefore formulate a number of theoretical reference null hypotheses: first we estimate the RMSE_{EOF} for sampling uncertainties after North et al. (1982). We then formulate three simple physical models for the spatial patterns of SST variability: the first is the Slab Ocean models modes of variability. The second and third physical models are based on the assumption that the spatial patterns of SST variability are just a reflection of isotropic diffusion with two different assumptions for the spatial distribution of variances.

2.3.1 Sampling Uncertainties of Eigenvalues

North et al. (1982) give the statistical uncertainties of the eigenvalues e_i due to sampling errors:

$$\delta e_i = e_i(2/N_{sample})^{1/2} \quad (2.5)$$

where N_{sample} is the number of independent samples. In this study $N_{spatial}$ is estimated as N_{len}/t_d , while N_{len} is the length of the time series and t_d is the average e-folding decorrelation time based on the first five leading Principal Components (PCs). To maintain consistency, we estimate N_{len} from the shorter time series of the CMIP models rather than the much longer references. The $RMSE_{EOF}$ for sampling uncertainties is then

$$RMSE_{EOF}(\delta e_i^A) = \sqrt{\frac{\sum_{i=1}^{N_A} (\delta e_i^A)^2}{N_A}} / \sqrt{\frac{\sum_{i=1}^{N_A} (e_i^A)^2}{N_A}} = \sqrt{\frac{2}{N_{sample}^A}} \quad (2.6)$$

Thus, the $RMSE_{EOF}(\delta e_i)$ could be deemed as the confidence level of a data set. If two data sets are just different stochastic realizations of the same process (have the same spatial patterns of SST variability), we expect the $RMSE_{EOF}$ to be in average $RMSE_{EOF}(\delta e_i)$.

Fig. 2.4 illustrates an example based on subsampling the CMIP5 super model. Here we computed the EOF-modes for the North Pacific for high-pass (5 yrs) and low-pass (5yrs) SST. For subsampling the CMIP5 super ensemble we split the data from each model into average chunks with 5yrs/60mon data and concatenated the chunks into the CMIP5 super subsamples. Here, the total number of samples N_{len} is set to be 1380 (60*23) for the high pass and 115 (5*23) for the low pass. For high-pass data analysis

the average decorrelation time of the leading five principal components $t_d = 8.8$. Therefore, we get $N_{sample} = 1380/8.8 = 156.8$. Similarly $N_{sample} = 115/5.8 = 19.8$ for the low-pass analysis.

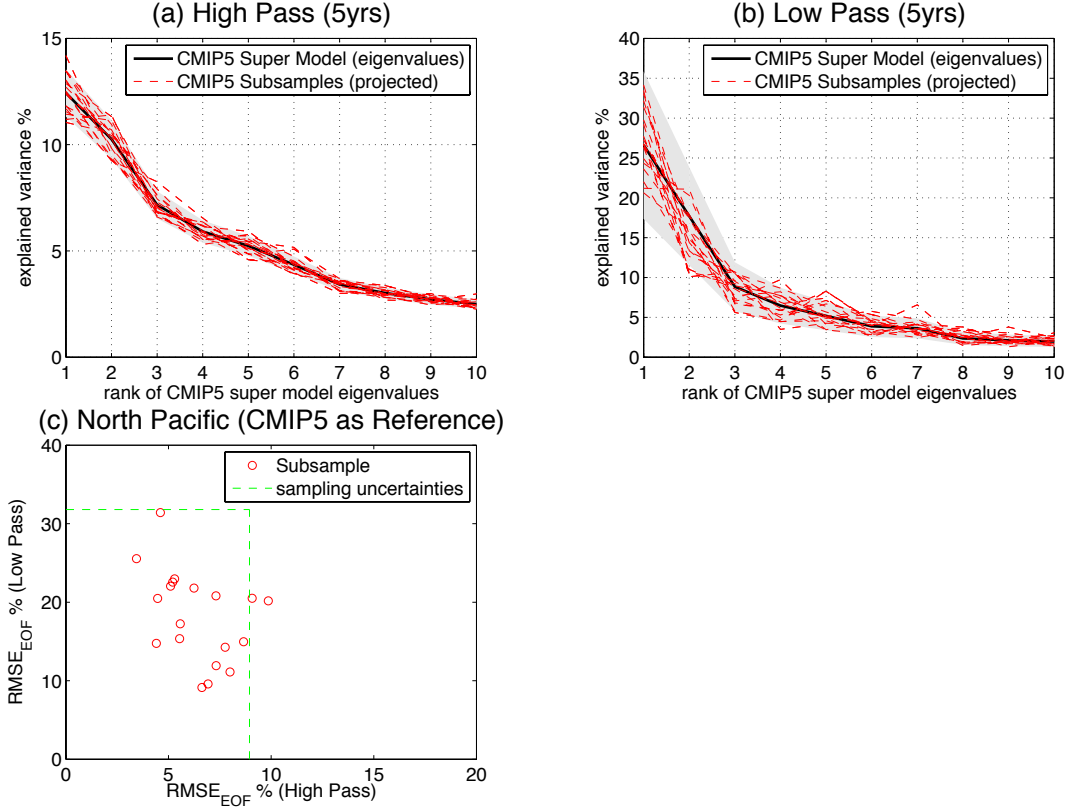


Fig. 2.4 Eigenvalue spectrum of CMIP5 super model and the PEV of its subsamples in the North Pacific. The shaded area marks the uncertainty interval of the eigenvalues after North et al. (1982) (a): high-pass result; (b): low-pass result; (c): $RMSE_{EOF}$ values of the subsamples in (a) on the x-axis and (b) on the y-axis.

We note from Fig. 2.4a-b that the subsamples $pe_i^{A \rightarrow B}$ values fluctuate around the e_i^A values of the CMIP5 super model, caused here by sampling uncertainties and not by differences in the physical system. Subsequently, the $RMSE_{EOF}$ values of the subsamples fluctuate around the $RMSE_{EOF}(\delta e_i)$ (see Fig. 2.4c). For the 5yrs-running mean SST it seems that the subsamples fluctuate less than expected by the $RMSE_{EOF}(\delta e_i)$, which could indicate that our subsampling of the models is not quite representative of the sampling uncertainties in the CMIP5 super model as they are

from the same data sets.

2.3.2 Slab Ocean Model

The spatial structure of the SST variability is a result of the coupled dynamics between atmosphere and oceans. A Slab Ocean model coupled to an AGCM (see data section for model details) estimates the spatial structure of the SST variability that is caused by the atmosphere only. Compared to a fully CGCM, the slab ocean model only introduces the error of atmospheric simulation without significant error addition or amplification by the coupling process or ocean dynamics. It is therefore a good null hypothesis to evaluate the models: if the spatial structure of the SST variability agrees better with the slab ocean model (smaller $RMSE_{EOF}$) than with a CGCM, this is indicating that the coupling procedures and ocean dynamics are causing unrealistic SST patterns.

Fig. 2.2 shows the observed EOF-modes of the high-pass monthly mean SST variability in the North Pacific in comparison with the EOF-modes of the slab ocean simulation, for an example. The EOF-modes of the slab simulation are already quite realistic, suggesting that much of the large-scale structure of the SST variability is to first order simulated in the slab simulation, which is consistent with what has been found in other studies as well (e.g. Pierce et. al, 2001).

2.3.3 Isotropic diffusion

Cahalan et al. (1996) and Dommenges (2007) used the null hypothesis of isotropic diffusion to explain the leading EOF-modes of climate variability. The isotropic diffusion process leads to EOF-modes that are a hierarchy of multi-poles, starting with a monopole (largest scale), followed by a dipole, and followed by multi-poles

with increasing complexity (smaller scales). It essentially represents a spatial red noise process (Dommenget 2007). Fig. 2.2m-o illustrates the EOF-modes of isotropic diffusion for the North Pacific domain. The EOF-modes are pure geometric deconstructions of the domain not considering any structure in the SST standard deviation (STDV, Fig. 2.5), but assuming the same $N_{spatial}$ as observed. Thus, the spectrum of the explained variance of the eigenvalues has a structure similar to what is observed. We refer to this null hypothesis as $H0_{uniform}$.

This null hypothesis is further extended by also using the observed inhomogeneous SST STDV field (see Fig. 2.5a and b) and therefore focusing the leading EOF-modes onto regions where the observed SST STDV is large (see Dommenget 2007 for details). This concept has also been applied to study the structure of the Indian Ocean SST variability, for instance, by Dommenget (2011).

Much of the spatial structure in SST variability is already highlighted by the spatial structure in the SST STDV field (see Fig. 2.5a and b). The regions with large SST STDV will be the regions where most of the leading EOF-modes have large variance. Here we can already see that the SST STDV deviation is different on different time scales, which will be reflected in slightly or significantly different SST modes. The CMIP3 and CMIP5 ensembles capture most of the main observed structures and even the Slab Ocean simulation captures some of it (see Fig. 2.5c-h).

Fig. 2.2j-l illustrates the EOF-modes of isotropic diffusion with observed SST STDV for the North Pacific domain. The EOF-modes are still a hierarchy of multi-poles, but now the modes are centred on regions of large SST STDV (for comparison with STDV of observations see Fig. 2.5a). These EOF-modes now have some more realistic features. We refer to this null hypothesis as $H0_{STDV}$.

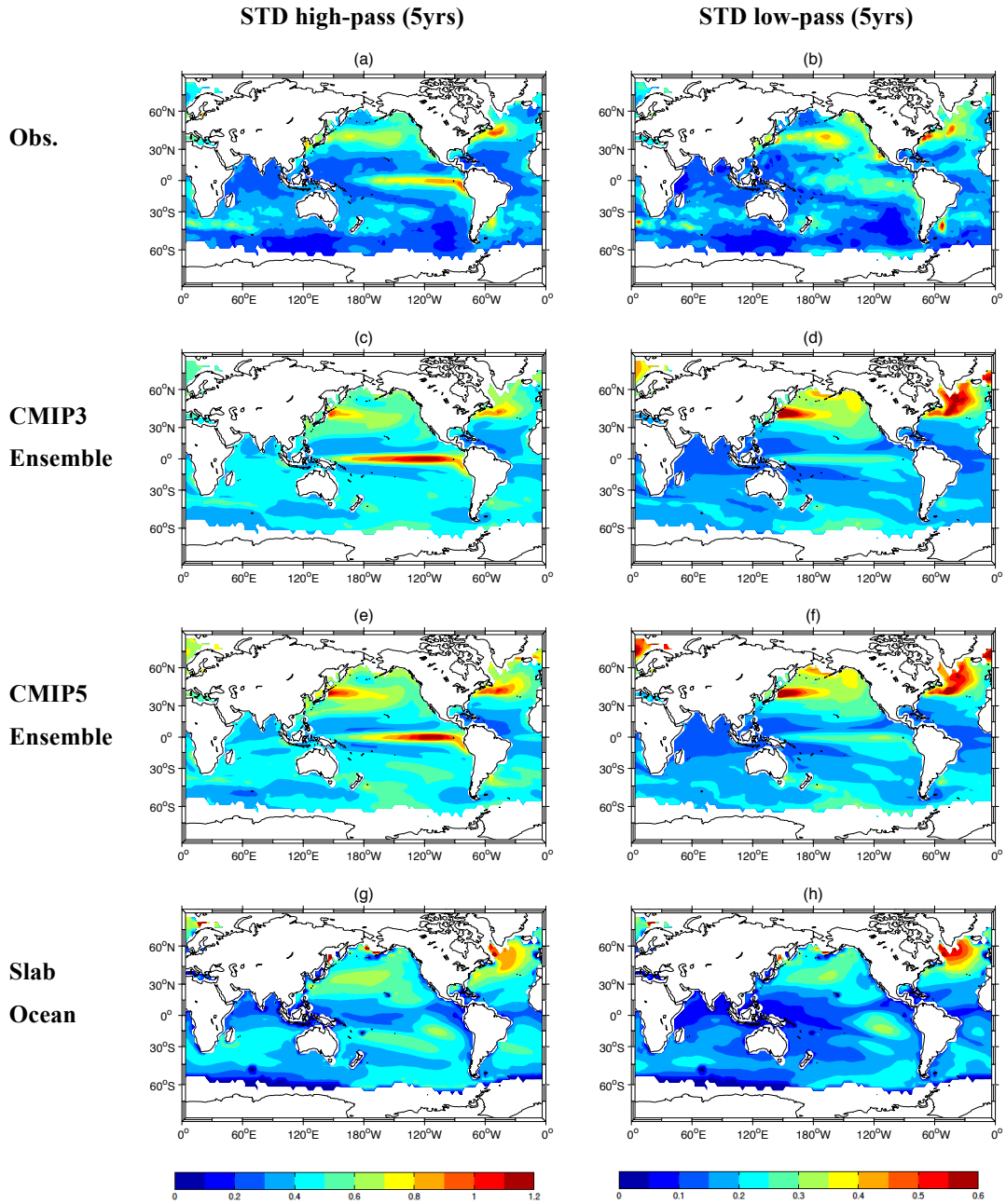


Fig. 2.5 Standard deviation fields of SSTA for (a-b): HadISST; (c-d): CMIP3 ensemble mean; (e-f): CMIP5 ensemble mean; (g-h): slab ocean experiment result. (a,c,e,g): after high-pass filter; (b,d,f,h): after low-pass filter.

2.4. Comparison of the Eigenvalue (EV)-spectrum

In this section we present the main results of this analysis, which is based on the comparison of the $pe_i^{A \rightarrow B}$ values (referred as EV-spectrum below) of the SST

variability in different ocean basins. We will define SST variability on two different time scales to highlight potential differences in the variability modes.

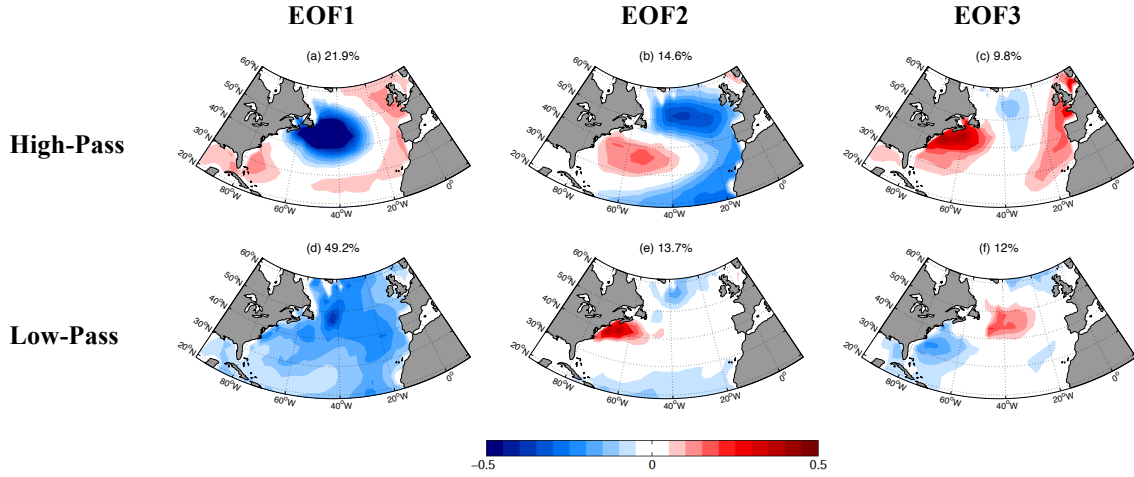


Fig. 2.6 First three leading EOF patterns of observed SSTA in the North Atlantic for (a-c): after high-pass filter; (d-f) after low-pass filter.

First we like to illustrate that the EOF-modes in the high-pass and the low-pass SST variability are indeed different. Fig. 2.6 shows the different EOF-modes structures on high-pass and low-pass scale in the North Atlantic. The following is noted here:

- The spatial patterns are quite different between the two time scales. The high-pass, for instance, reveals three tri-pole modes from EOF-1 to EOF-3. However, none of them is strongly related to the leading EOF-modes of the low-pass modes.
- The eigenvalues of the low-pass modes are much larger than their counterpart of high-pass ones. Subsequently $N_{spatial}$ is much larger for the high-pass SST ($N_{spatial} = 10$) than for the low-pass SST ($N_{spatial} = 3$). Thus the high-pass SST has more complex variability modes than the low-pass SST.

Similar findings can be made for all domains, but the EOF-modes of the different time scales may be more similar in the other domains than they are in the North Atlantic.

We start the main analysis with a more comprehensive discussion of the North Pacific to illustrate the method. We then compare all model simulations with the observed EOF-modes for all ocean basins. The analysis is then repeated by pairwise comparisons of the CMIP model simulations to evaluate the uncertainties within the model ensemble members.

2.4.1 North Pacific

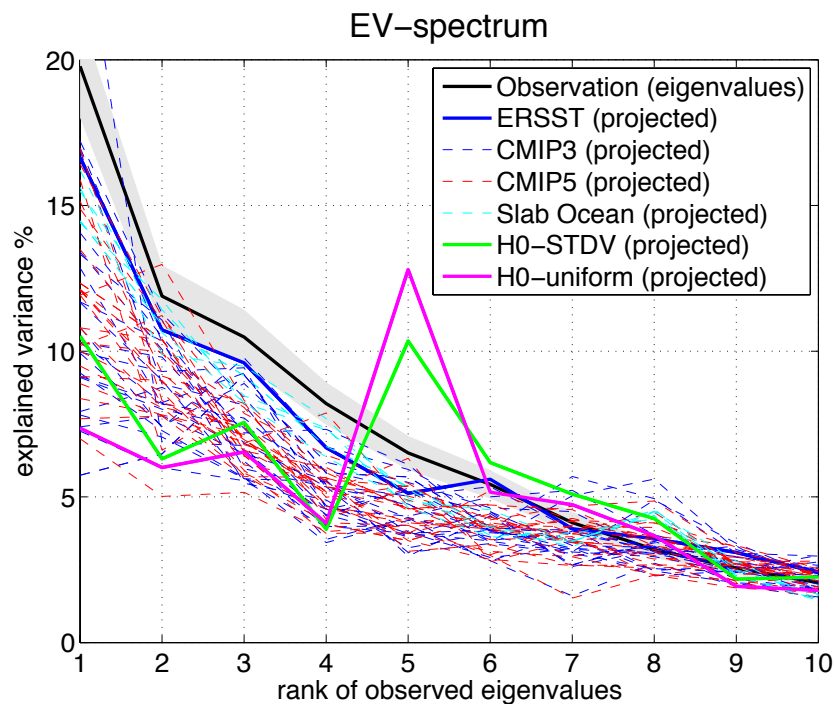


Fig. 2.7 Eigenvalue spectrum of the observed leading EOF-modes in the North Pacific as in Fig. 3a, but compared with the PEV values for all CMIP models, the Slab Ocean simulations and the null hypotheses. The shaded area marks the uncertainty interval of the eigenvalues after North et al. (1982).

Fig. 2.7 shows the EV-spectrum of the observed high-pass SSTA in the North Pacific region together with the projected $pe_i^{A \rightarrow B}$ values for all CMIP models and the four different null hypotheses references. A few points should be noted here:

- ERSST is close to the observations (HadISST) as they are basically the same observed data. The differences are mostly within the sampling uncertainties. However, there is some indication that the two data sets are not totally in agreement.
- All the models and null hypotheses underestimate the first PC of observations, namely the Pacific Decadal Oscillation (PDO) pattern (e.g. Mantua et al., 1997) and most of the other leading modes.
- The deviations of the individual models from the observed EV-spectrum are much larger than expected by the sampling uncertainties δe_i . The slab ocean simulation is closer to the observations than most models.
- The deviations of $H0_{STDV}$ are about as strong as of most of the CMIP model simulations. However, the deviations of $H0_{uniform}$ appear to be larger than those of most CMIP models. The $H0$ curves both have a peak at the EOF-5. This is due to the similarity of the observed EOF-5 with a basin wide monopole (not shown), which is the leading mode in isotropic diffusion (both $H0_{STDV}$ and $H0_{uniform}$).

The results of the EV-spectrum are quantified by the $RMSE_{EOF}$ values for the high-pass monthly mean SST as shown in Fig. 2.8a on the x-axis and for the low-pass SST on the y-axis. In addition to what we have already concluded above for the high-pass SST modes we should note the following points:

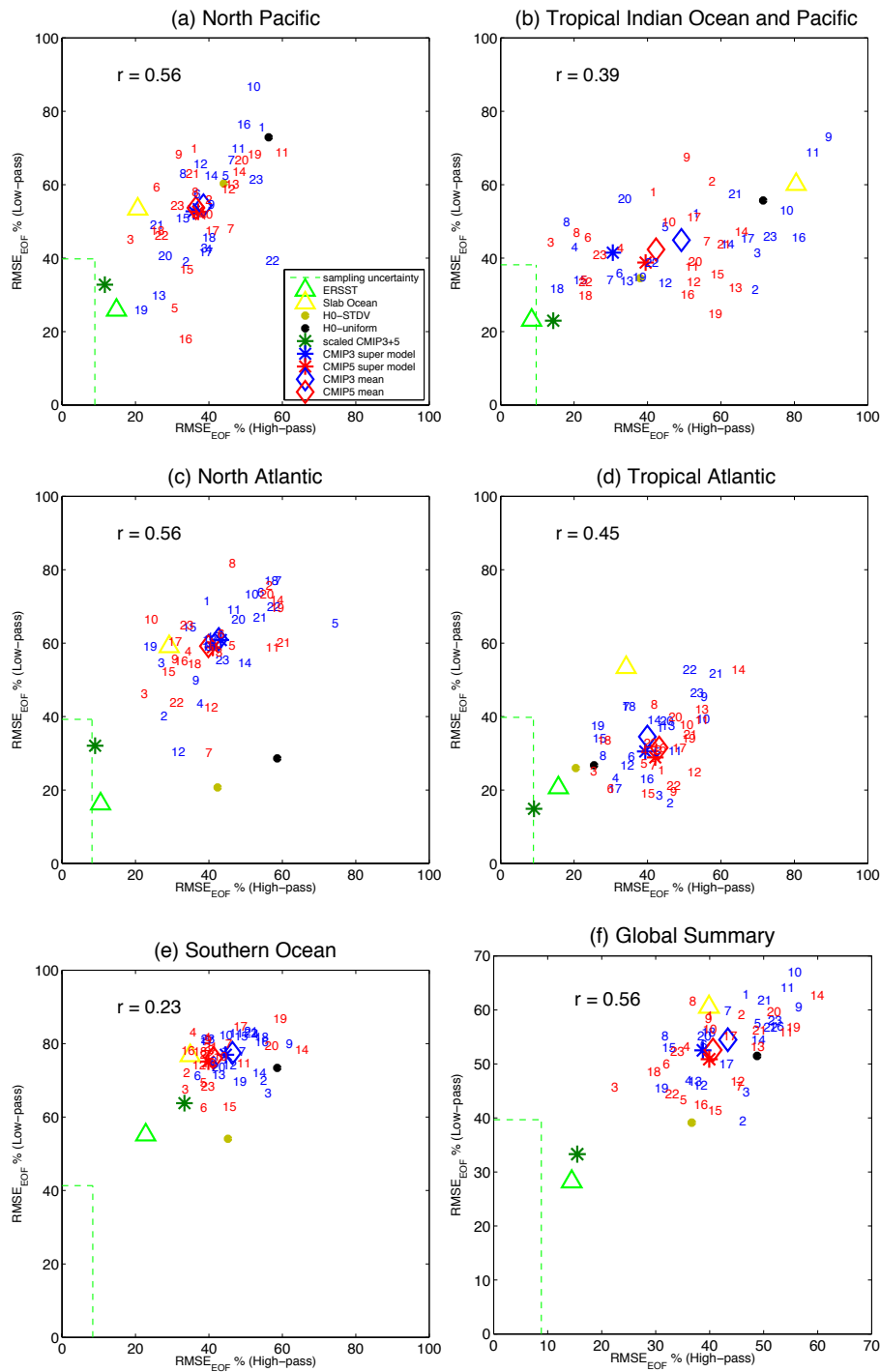


Fig. 2.8 RMSE_{EOF} values relative to the observations for high-pass and low-pass EOF-analysis of (a): North Pacific; (b): Tropical Indian Ocean and Pacific; (c): North Atlantic; (d): Tropical Atlantic; (e): Southern Ocean; (f): Global summary. Blue numbers are CMIP3 models and red numbers are CMIP5. Diamonds represents the average position of the CMIP models. Blue and red stars are the results of the CMIP3 and CMIP5 super models, respectively. The green star is the result of the CMIP3+5 super model scaled with observed eigenvalues. The letter “r” shows the correlation coefficient of the RMSE_{EOF} values between two time scales based on models only.

- The ERSST is close to expected sampling uncertainties for both time scales. Although, this indicates that the two observational data sets have good agreements in this domain, it has to be noted here that the two data sets contain the same samples (same observations). Thus, an even better agreement should have been possible.
- The model errors relative to the observations are in the range of 30% to 80% of the eigenvalues. These errors are substantial.
- The RMSE_{EOF} values for the different time scales in Fig. 2.8a have a mostly linear relationship with a correlation coefficient 0.6 indicating that in this region the models show similar performance for high-frequency and low-frequency variability. However, there are also significant deviations from the linear relationship, which indicates that some models are performing good on one time scale but not as good on the other time scale.
- Most models seem better than the $H0_{\text{uniform}}$; however, half of the models are not as good as the $H0_{\text{STDV}}$ hypothesis.
- The slab ocean simulation is closer to the observations than most models in the high-pass variability, but is about average for the low-pass variability.
- The mean position of the CMIP3 models is close to that of the CMIP5 models, implying similar skill in this region, but most of the outliers with very large deviations are in the CMIP3 ensemble.

We pick out a few models to illustrate how the modes of variability in some models deviate from those observed. In Fig. 2.9 we show the leading modes of the two models that deviate the most (HadCM3 and BCM2.0), the two models closest to the observations (MRI-CGCM2.3.2 and CCSM4) and the CMIP3 and CMIP5 super models in the North Pacific modes comparison. The following is noted here:

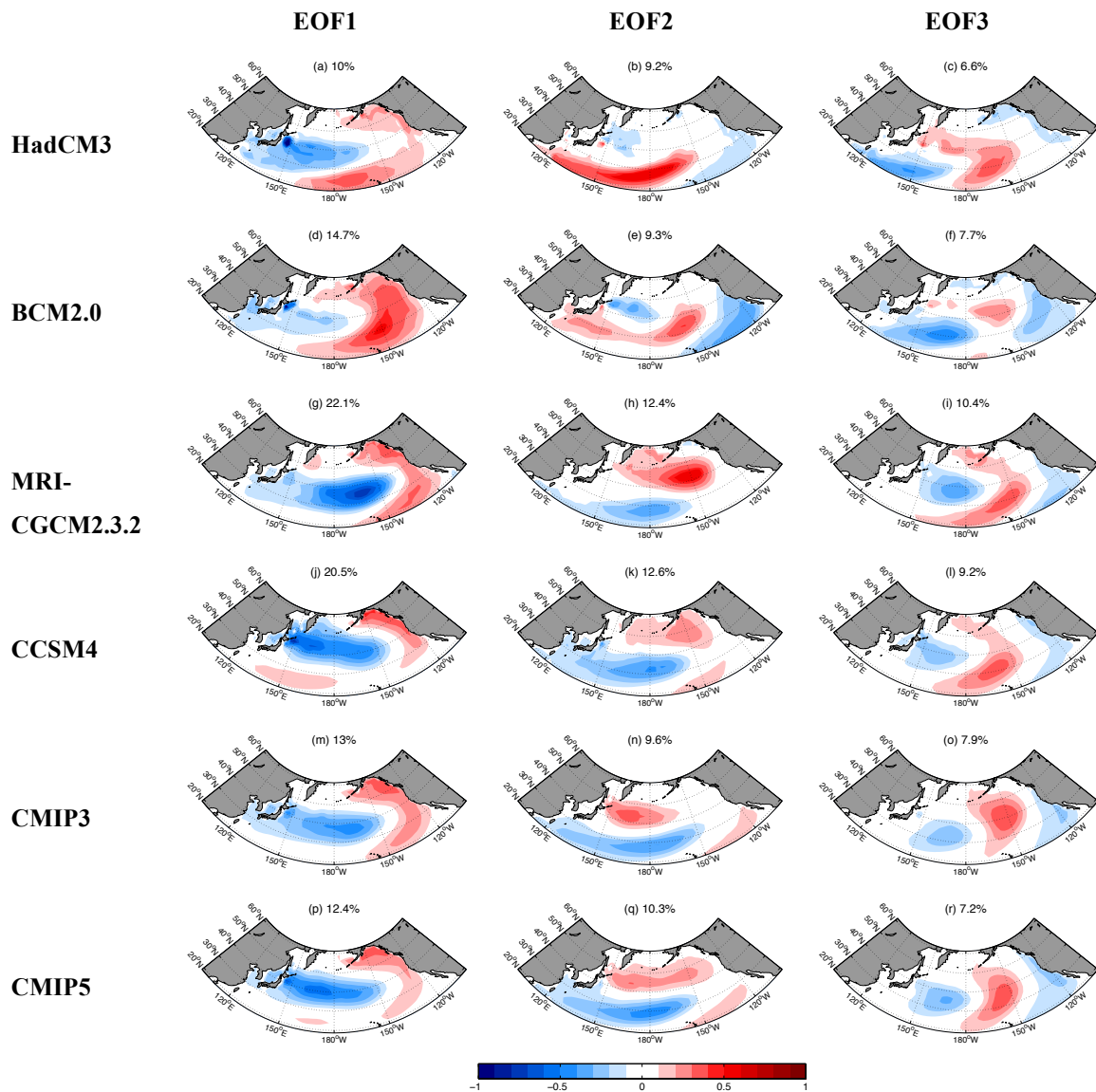


Fig. 2.9 Leading EOF-modes as in Fig. 2.2, but for a selection of model simulations.

- The two models that deviate the most both show leading EOF-modes that are somewhat different in structure from the observed. For instance, they tend to have the negative anomaly centres for the PDO-like mode (EOF-1) more to the west and more focused on a small region than in the observed PDO (EOF-1). Further, the eigenvalues of EOF-1 are much smaller than observed.
- The two models closest to the observations show leading EOF-modes that are similar in structure to the observed and that have similar amount of explained variance.

- The modes of the super models are very similar to the observed and have very smooth structures with no strong localized features. They tend to explain less variance than observed. The reduced variance of the leading modes relative to the observed, and to what individual models show, reflects the fact that the super models are based on ensembles of individual models that have different localized structures (modes), which leads to less explained variance of the leading modes.

2.4.2 Uncertainties in the SST modes in the global oceans

The analyses are now extended to all other ocean domains. To summarize, we also average the results and get the global summary of the $RMSE_{EOF}$ diagram in Fig. 2.8f. The results show a number of interesting aspects. We start the discussion with a focus on the individual domains, starting with the tropical Indo-Pacific domain (Fig. 2.8b):

- On the high-pass time scales the spread in the quality of the models is very large. Some models are close to the observed modes, but most models are quite different from the observed modes. On the low-pass time scale the skills of models are more similar and many models are as close to the observed modes as expected from sampling uncertainties.
- The slab model is quite different from the observed modes on the high-pass time scale and the longer time scale. The El Nino dynamics dominate the modes of the Indo-Pacific domain and these dynamics are not simulated in the slab model, which may explain why the slab model is quite different from the observed modes.

- The simple Null hypothesis $H_{0\text{STDV}}$ performs better than most models, but the $H_{0\text{uniform}}$ hypothesis clearly deviates more than most models and is very different from the observed structure.
- The CMIP3 ensemble has much more outliers, in particular on the shorter time scale, than the CMIP5 ensemble.

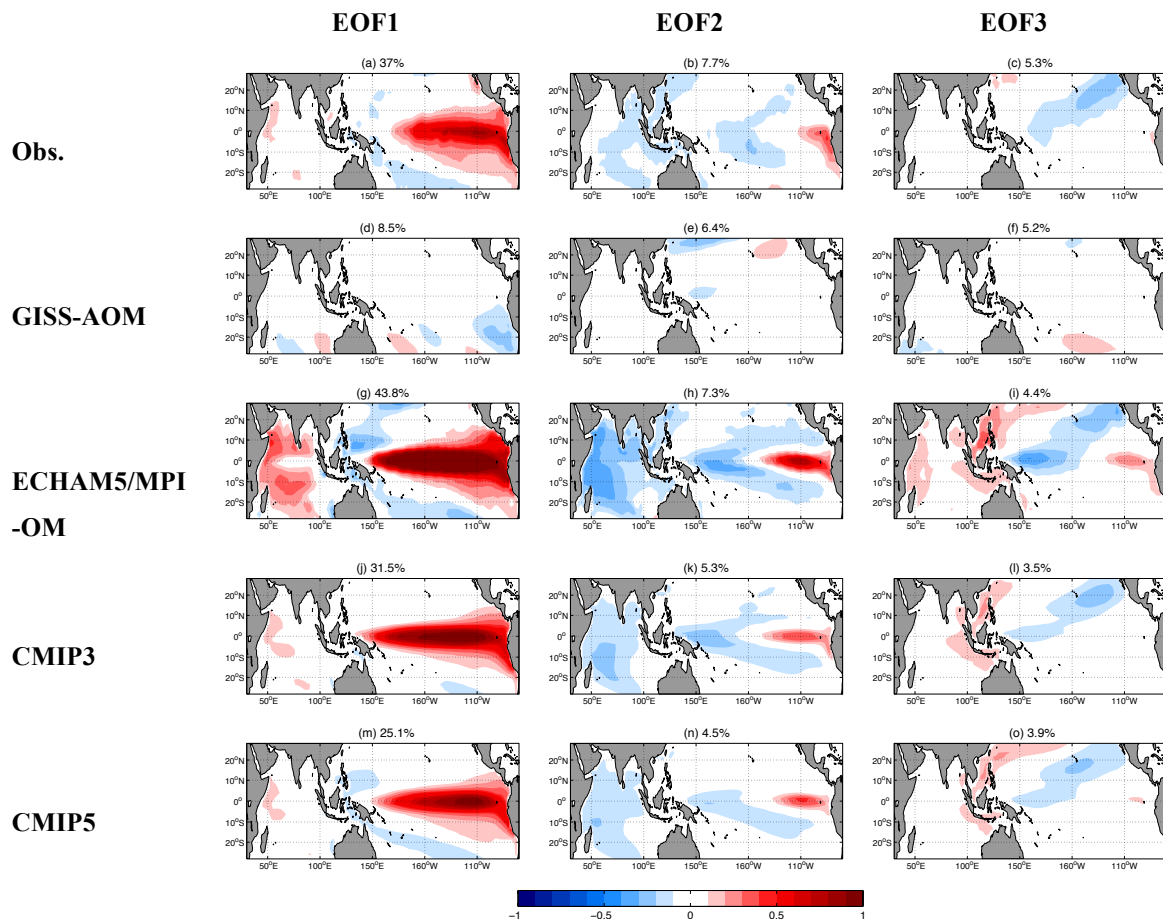


Fig. 2.10 First three leading EOF patterns, as in Fig. 2.9, but of high-pass SSTA in the Tropical Indian Ocean and Pacific for a selection of model simulations and observations. In addition to the observations, the CMIP3 and CMIP5 super models, the models with the largest (GISS-AOM) and smallest (ECHAM5/MPI-OM) RMSE_{EOF} value are shown.

Similar to the North Pacific domain, we picked out a few models to demonstrate the differences of the modes (Fig. 2.10). The model GISS-AOM that deviates the most shows no El Niño pattern. The model ECHAM5-MPI-OM, which is closest to the observed, as well as CMIP super models all display ENSO pattern and Central-Pacific

El Niño pattern (Kao and Yu, 2009) on the leading two modes, close to the observation.

In the North Atlantic the picture is quite different (Fig. 2.8c):

- The most remarkable feature is that both simple null hypotheses are closer to the observed modes than most of the CGCM simulations especially on long-term scale. First of all this is due to the fact that the observed modes in the North Atlantic are indeed more similar to the simple null hypotheses than they are in the Indo-Pacific domain. But still it indicates that the CGCM simulations have substantial problems in simulating these simple modes of variability. This conclusion appears to be quite different to what Jamison and Kravtsov (2010) conclude from their analysis of the leading modes in the North Atlantic. However, when we evaluate their Fig. 10-12 we would assume that the quantitative and objective error values $RMSE_{EOF}$ based on their analysis results should be similar to ours.
- The agreement with the observed modes is better on the shorter time scale than on the longer low-pass time scale. This is the opposite of what we see in the Indo-Pacific domain.
- The slab model performs better than any of the CGCM simulations on the high-pass time scale and still better than many models on the longer time scale.

There is no substantial difference in the performance of the CMIP3 and CMIP5 ensembles. Fig. 2.11 again shows several models for comparison in the North Atlantic.

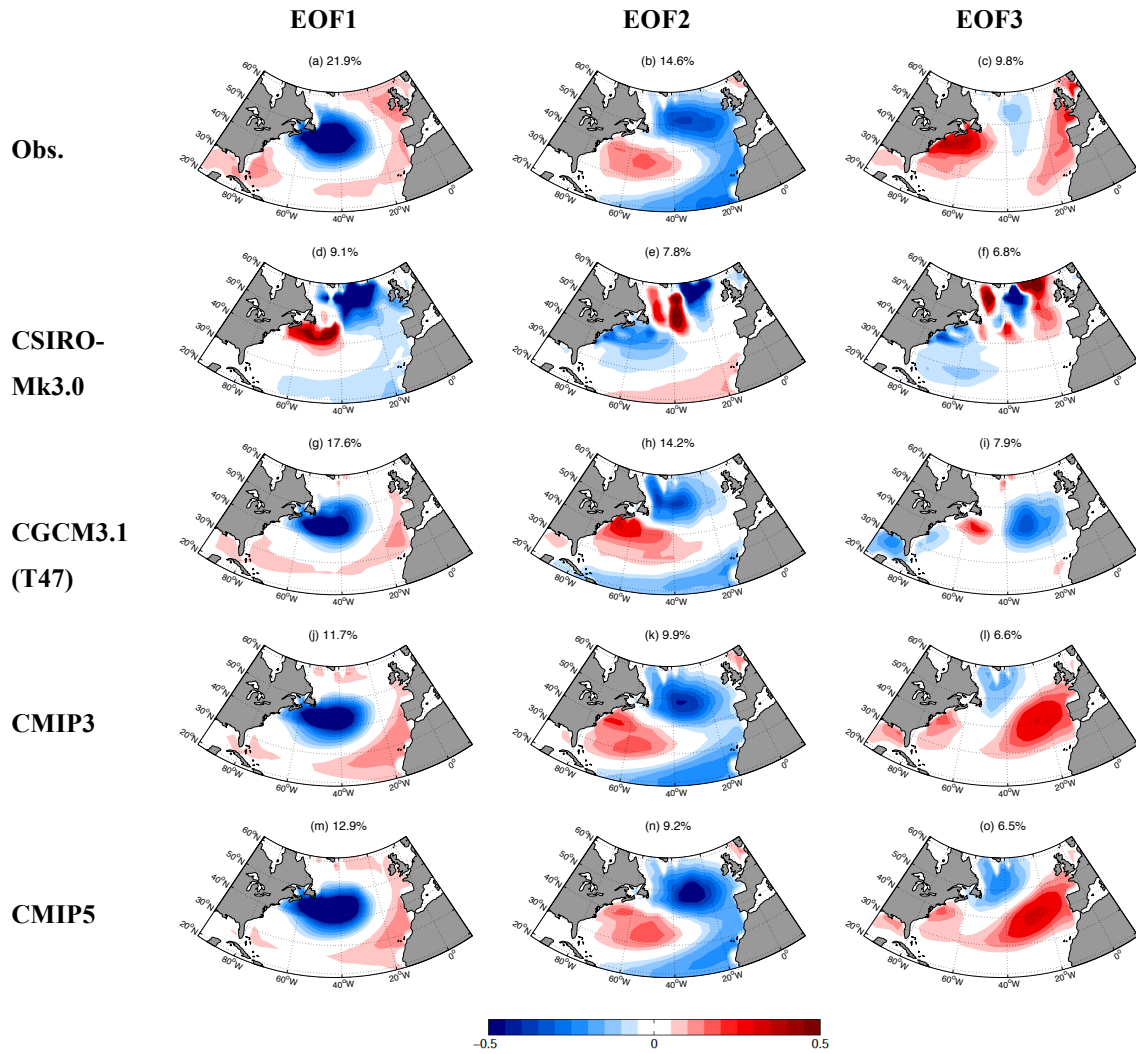


Fig. 2.11 First three leading EOF patterns, as in Fig. 2.9, but of high-pass SSTA in the North Atlantic for a selection of model simulations and observations. In addition to the observations, the CMIP3 and CMIP5 super models, the models with the largest (CSIRO-Mk3.0) and smallest (CGCM3.1 (T47)) RMSE_{EOF} value are shown.

The tropical Atlantic has again some interesting features (Fig. 2.8d). Fig. 2.12 shows the modes of some models in this domain.

- Notable is that the CGCM simulations are on average closer to the observed modes on the longer and also on the shorter time scales than in any other domain. On the longer time scale this domain actually seems to be the only domain where the CGCM simulations are mostly in agreement with the observed modes.

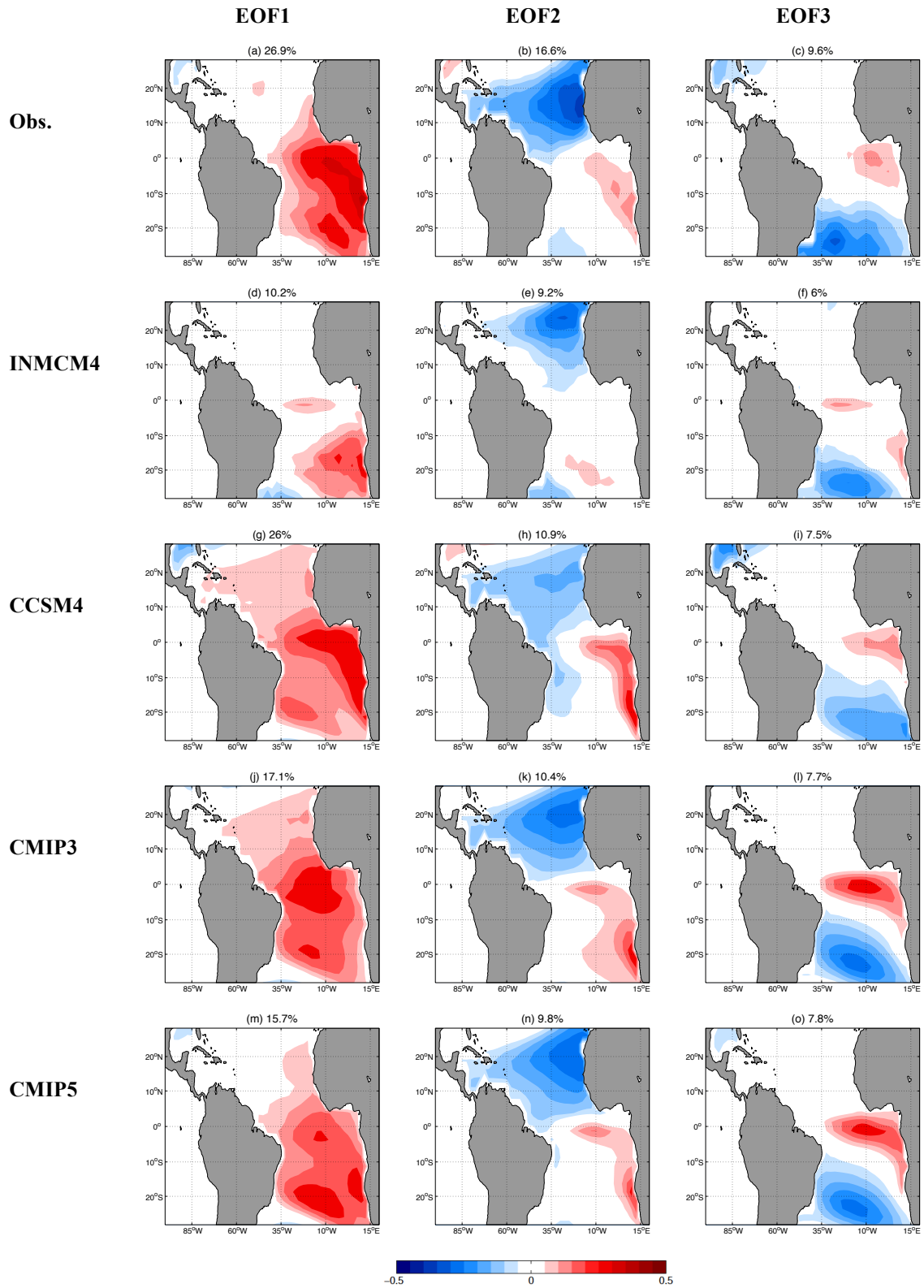


Fig. 2.12 First three leading EOF patterns, as in Fig. 2.9, but of high-pass SSTA in the Tropical Atlantic for a selection of model simulations and observations. In addition to the observations, the CMIP3 and CMIP5 super models, the models with the largest (INMCM4) and smallest (CCSM4) $RMSE_{EOF}$ value are shown.

- The CMIP5 simulations show a clear improvement over the CMIP3 simulations for the longer time scale, which is more than in any other domain. This is even more remarkable considering the already good fit to the observations in the CMIP3 simulations and also considering the much better performance than in any of the other domains.
- The slab model is closer to the observations than most CGCM simulations on the high-pass (5 yrs) time scale, but deviates more than all models on the longer time scale.
- Both the H_{0STDV} and the $H_{0uniform}$ hypotheses are very close to the observations on both time scales and closer than most of the CGCM simulations. This indicates that knowing the SST STDV field and assuming a multi-pole deconstruction, as it follows from an isotropic diffusion process, would already explain most of the SST variability in this domain.

Finally, the Southern Ocean (Fig. 2.8e):

- This domain shows the overall largest deviations from the observed modes, with all models disagreeing with the observations substantially.
- There appears to be no substantial difference between the CMIP3, CMIP5 and the slab simulations.
- Similar to the North Pacific both null hypotheses are substantially different from the observed modes on both time scales. However, the H_{0STDV} hypothesis is closer to the observed modes than any CGCM simulation on the longer time scale and closer than most on the shorter time scale.

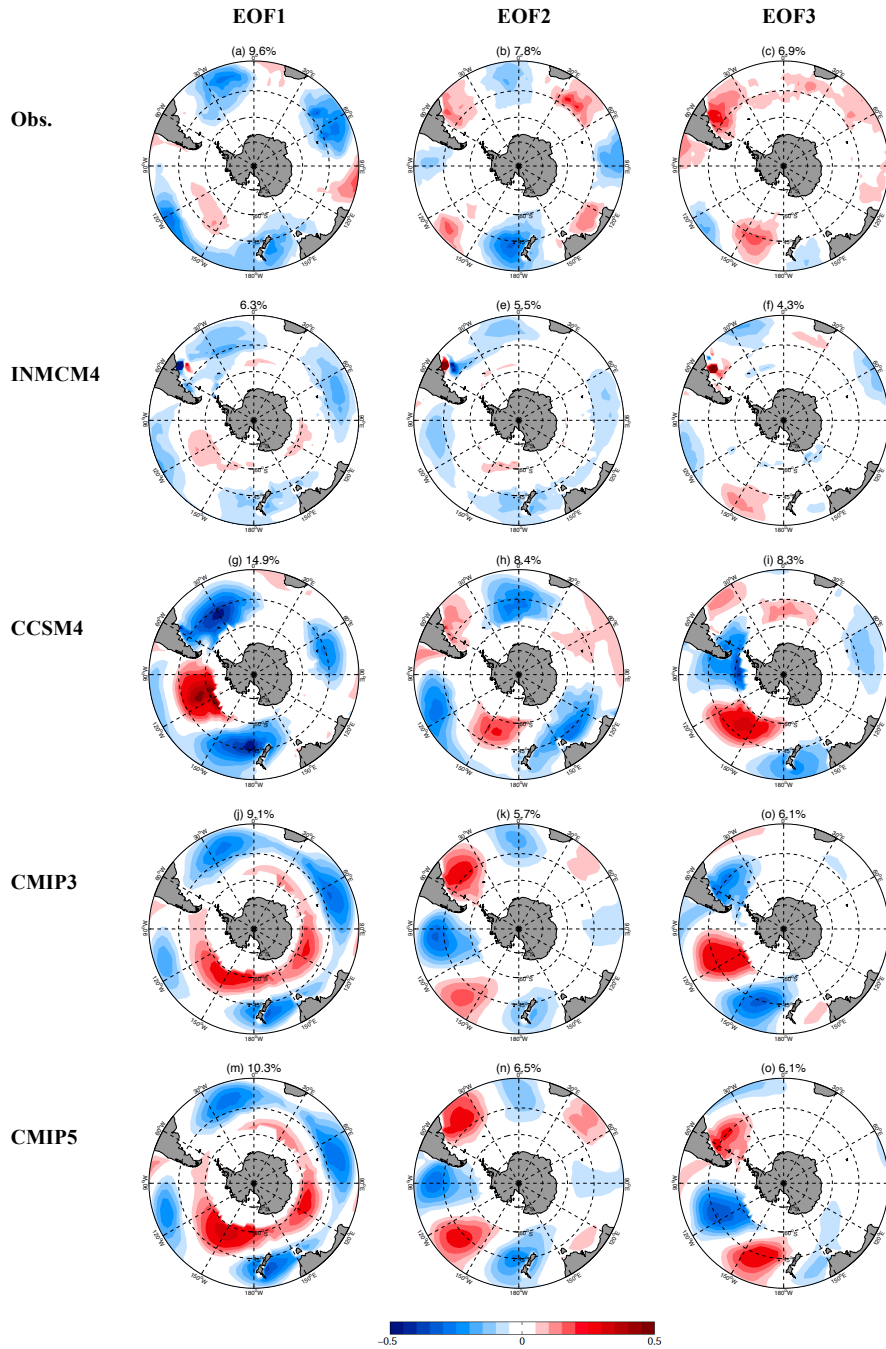


Fig. 2.13 First three leading EOF patterns, as in Fig. 2.9, but of high-pass SSTA in the Southern Ocean for a selection of model simulations and observations. In addition to the observations, the CMIP3 and CMIP5 super models, the models with the largest (INMCM4) and smallest (CCSM4) $RMSE_{EOF}$ value are shown.

The Southern Ocean is a special domain for its sparse in-situ observation, which introduces non-negligible uncertainties of observed reference. The modes comparison (see Fig. 2.13) is essentially different to other domains, as we can't find too much

similarity here between the leading modes of observed and the CMIP super models especially on EOF1. The Southern Ocean is also one of the largest domains; it involves the more complex extra-tropical dynamics (larger $N_{spatial}$; see Fig. 2.14) and interactions with sea ice, which may explain the large disagreement to some part.

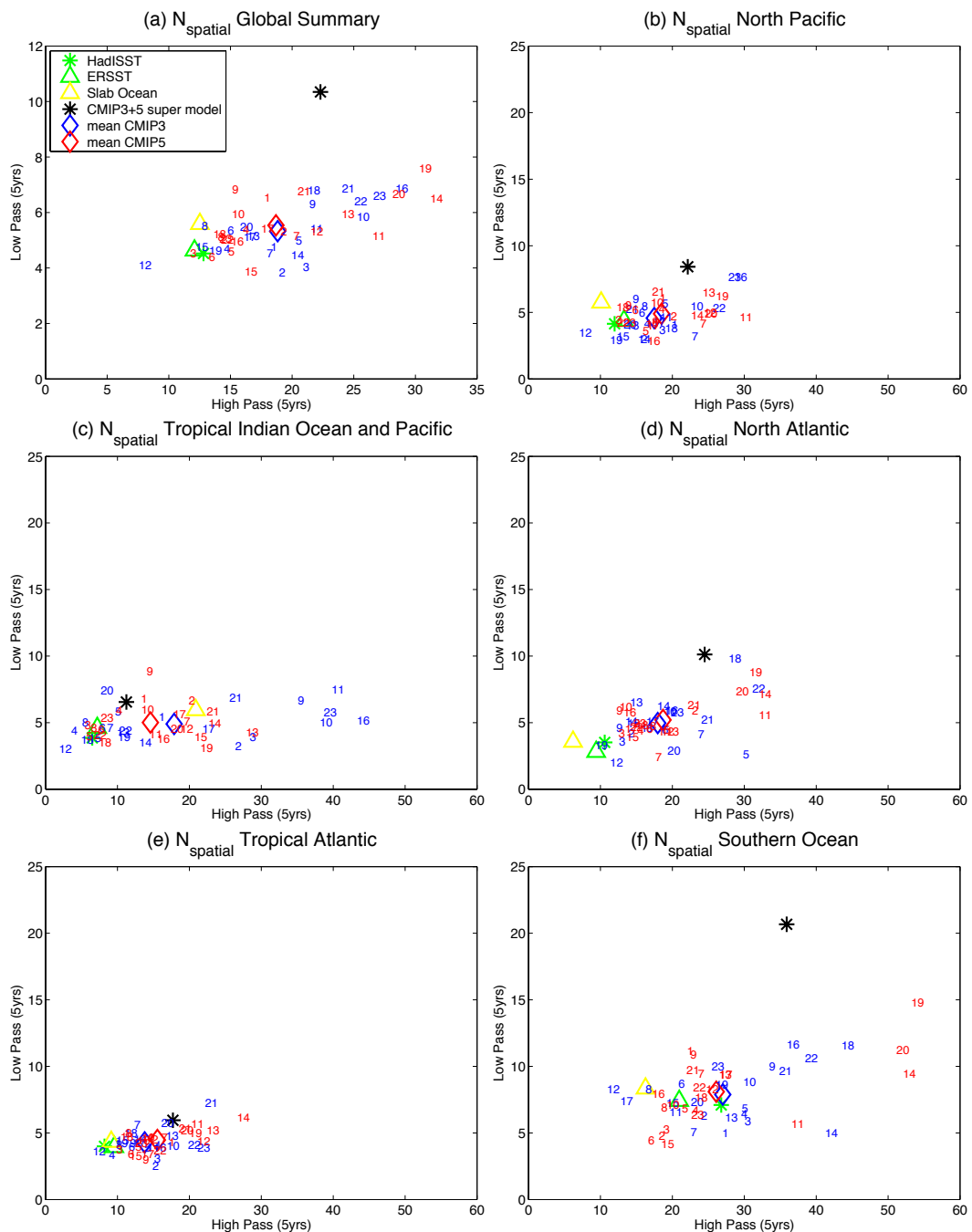


Fig. 2.14 $N_{spatial}$ values for high-pass and low-pass EOF-analysis of SSTA in (a): Global summary; (b): North Pacific; (c): Tropical Indian Ocean and Pacific; (d): North Atlantic; (e): Tropical Atlantic; (f): Southern Ocean.

The summary of all individual domains (Fig. 2.8f) shows the average skill of the models:

- First of all we note that the models skills on the short and longer time scales are roughly linearly related with a correlation of 0.6. Models that are close to the observed modes on the shorter time scale tend to be close to the observed modes on the longer time scale as well.
- Basically all models show significant deviations in the spatial structure from the observed modes. These deviations are in the order of 50% of the eigenvalues on the leading modes. This means they in average under-/over-estimate some of the leading modes by a factor of 1.5/0.5, which is a substantial error.
- In the global average some models are clearly much closer to the observed modes (e.g. the CCSM4 model is closest) than others and some models substantially deviate from the observed modes (e.g. all the CMIP3 GISS models). However, the spread in the global average is not as big as in the individual domains, indicating that models that have big $RMSE_{EOF}$ in some domains often have smaller $RMSE_{EOF}$ in other domains.
- The CMIP5 ensemble appears to be slightly closer to the observed modes than the CMIP3 ensemble on both time scales. However, the super model modes are very similar in their structure and skill relative to the observed modes.
- The slab simulation is of similar skill on the shorter time scale, but has less skill than most models on the longer time scale. Nevertheless, on both time scales the slab simulation is not consistent with observations ($RMSE_{EOF}$ is larger than expected by sampling uncertainties).

- The simple $H0_{STDV}$ hypothesis is in average closer to the observed modes than any CGCM simulation on the longer time scale and closer than most simulations on the shorter time scale. Even the $H0_{uniform}$ hypothesis is better than many models. This suggests that knowing the $N_{spatial}$, the domain geometry, the SST STDV field (most importantly) and assuming a modal structure resulting from isotropic diffusion could already describe the observed spatial structure of SST variability better than most of the CGCM simulations.

The above analysis has shown that the CMIP model simulations have substantial errors in simulating the observed spatial structure of SST variability. A closer look at the leading EOF-modes of the model simulations (not all shown, but some are shown in Fig. 2.9~2.13) reveals why the models differ from the observations:

- First, we see that $N_{spatial}$ is larger than observed in most CMIP models and for all domains and on both time scales, (see Fig. 2.10). It is also larger than in the slab simulation. This suggests that the simulated leading modes of variability explain in average less variance than observed and are on smaller spatial scales (the patterns are more localized) than observed. This is also seen by visual inspection of the leading modes of all the model simulations (not shown).
- Further, we note that the patterns of the leading modes in the model simulations are often different from those observed. They are often quite localized patterns of scales much smaller than the domain size. The observations also do have such localized modes, but these are often at different locations than in the models and are of different structure and smaller

amplitude. Thus, the models produce a double error: They simulate significant localized structures at the wrong locations and with the wrong structure and subsequently miss the observed localized structures at the right locations and with the right structure. The simple null hypotheses and the slab simulation do not have these localized structures and therefore do not have these double errors.

Additionally, it is noticeable that the super model ensembles do not perform significantly better than most of the models. This is quite different from many other inter-model comparisons (e.g. seasonal forecasting skills or mean state errors), where the ensemble mean outperforms the individual models (e.g. Tebaldi and Knutti 2007, Reifen and Toumi 2009, Santer et al. 2009; Knutti et al., 2010). The modes of variability or the spatial structure of internal SST variability does not average out to be more realistic in an ensemble super model. If models have different modes of variability, then the super model will have all of these modes, but each with a smaller eigenvalue, which increases $N_{spatial}$ of the ensemble super model (see Fig. 2.14).

However, we can illustrate that the ensemble super model is indeed improving compared to most individual models if we replace the eigenvalues in eq. (2) against observed eigenvalues. These scaled values are shown in Fig. 2.8. They are much closer to the observed spatial structure than most models. Even if we replace the eigenvalues of all models against observed eigenvalues, which clearly decreases the $RMSE_{EOF}$ values of most models, the ensemble super models still demonstrate smaller $RMSE_{EOF}$ values than the majority of the individual models, while the CMIP5 super model is a bit closer to the observations than its counterpart of CMIP3 (not shown). It illustrates that the leading patterns in the ensemble super model are indeed

realistic, but the relative explained variance of each mode is underestimated by the ensemble super model due to the artificial diversity in the individual models.

Finally, we also discuss the similarity in the two different observations:

- For most domains there is a relative good agreement between the ERSST and the HadISST data sets on both time scales. This indicates that we have some relative good confidence in the spatial structure of SST variability in these domains.
- The best agreement is in the North Atlantic, which seems to be consistent with the larger database existing in this relatively well-observed domain.
- Strong disagreement exists in the Southern Oceans. Here, the spatial structure of the observed SST variability is very uncertain. On the longer time scale the uncertainties in the leading modes are in the order of 40-60% of the eigenvalues, which is a substantial uncertainty. Again, this seems to be consistent with the lack of sufficient observations in this domain.

2.4.3 Comparison between models

In the above section we evaluated the models against the observations, which revealed some substantial differences of the model's spatial structures in SST variability relative to the observed. We also noticed that the leading modes of the CMIP3+5 super model have much smaller explained variance as the observed modes, illustrating a larger diversity of modes in the model ensembles relative to the observed. This indicates that the models have strong differences in the spatial structures in SST variability between each other. These model-to-model differences are quantified by repeating the above analysis by pairwise comparison of the EOF-

modes in the CMIP3 and 5 ensembles.

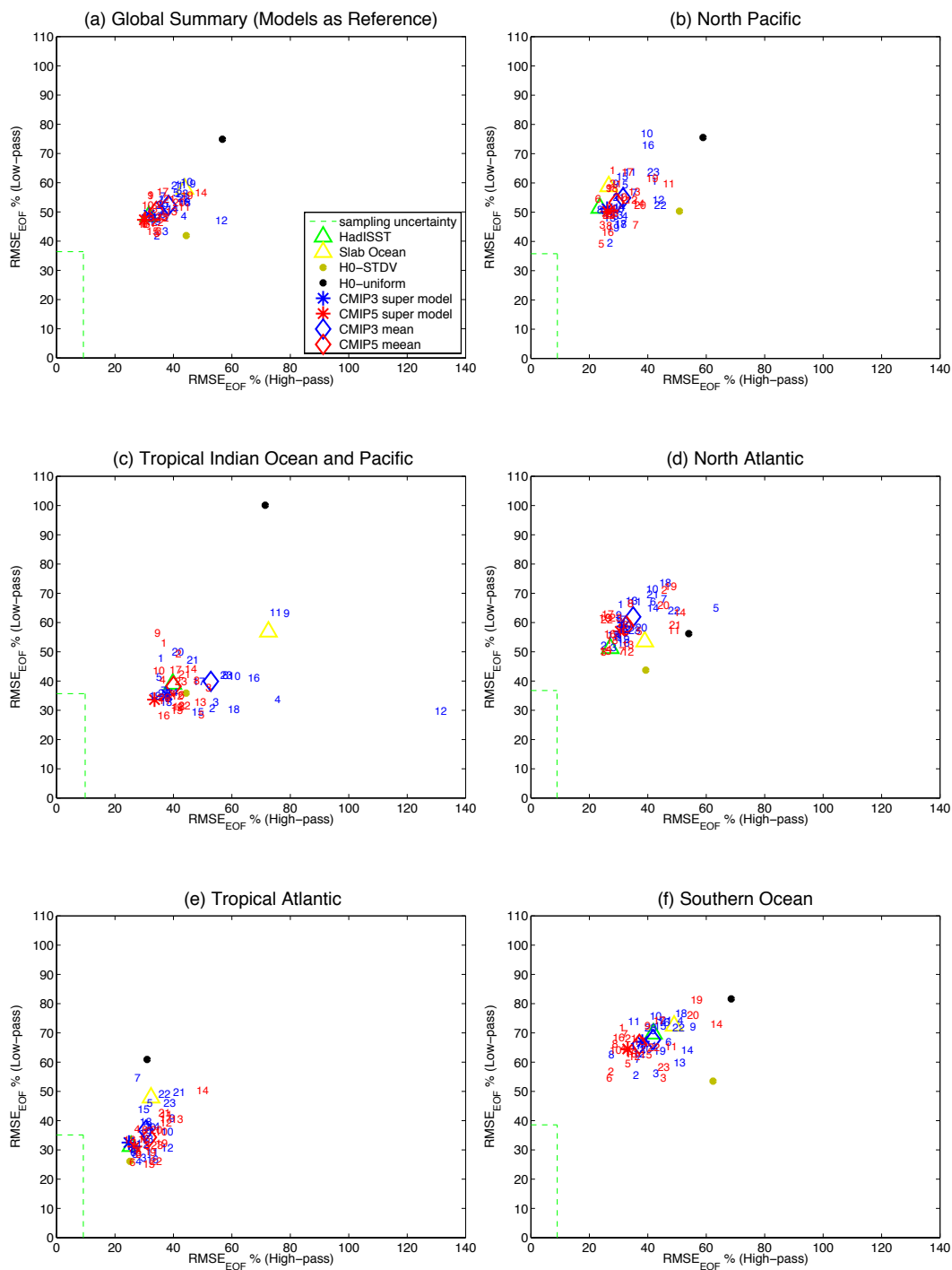


Fig. 2.15 Mean $RMSE_{EOF}$ values of pairwise model comparisons for high-pass and low-pass EOF-analysis in (a): Global summary; (b): North Pacific; (c): Tropical Indian Ocean and Pacific; (d): North Atlantic; (e): Tropical Atlantic; (f): Southern Ocean.

Fig. 2.15 shows the $RMSE_{EOF}$ values as in Fig. 2.8, but for the average of all pairwise

comparisons between all CMIP3 and 5 models. Thus, the reference modes in these comparisons are the EOF-modes from each of the CMIP3 and 5 models. Here small $RMSE_{EOF}$ values suggest small differences in the spatial structures in SST variability of the model relative to the spatial structures in SST variability of all the other models and vice versa for large $RMSE_{EOF}$ values. The following features are noted in this comparison:

- All models show $RMSE_{EOF}$ values larger than expected from sampling uncertainties ($RMSE_{EOF}(\delta e_i)$). Thus, the models substantially disagree with each other in terms of the spatial structures in SST variability. The errors are in the order of 40-60% of the eigenvalues.
- The largest model internal spread is in the North Atlantic and the Southern Ocean. This is similar to what we found in the comparison with the observations.
- In global average the model-to-model spread is similar in all models, indicating that there is no model that is closest to all the other models.
- The CMIP5 models tend to be slightly closer to all the other models than the CMIP3 models on both time scales and for all domains.
- In the tropical Indo-Pacific domain several CMIP3 models have substantially larger $RMSE_{EOF}$ values than most of the other models. This suggests that these models poorly represent the ENSO pattern and are indeed quite different from the overall model ensemble on the monthly mean scale.

2.5. Summary and Discussion

In the study presented here we evaluated the skill of the CMIP3 and CMIP5 models in

simulating the observed spatial structure of SST variability on interannual and decadal time scales. This comparison was based on a quantitative and objective comparison of the leading EOF-modes in the five major ocean basins (tropical Indo-Pacific, North Pacific, tropical and North Atlantic and the Southern Ocean) with the observed EOF-modes and those of simplified null hypotheses. The study illustrated a number of interesting aspects in the skill of the model simulations, but also about the observed spatial structure of SST variability. For the observed spatial structure of SST variability we list the following main findings:

- By comparing the observed modes with those of the simple isotropic diffusion null hypothesis we can note that for most domains and both time scales the observed spatial structure of SST variability is significantly different from isotropic diffusion. Thus, the observed modes of variability have non-trivial structure in particular on the monthly mean time scale in the tropical Indo-Pacific and Atlantic and on both time scales in the North Pacific and Southern Ocean. The longer time scale of the tropical and North Atlantic are, however, remarkably similar to the simple large-scale multi-pole modes of the isotropic diffusion process.
- The effective numbers of spatial degrees of freedom ($N_{spatial}$) are between 5-10 for most domains on the monthly mean time scale and smaller (<5) on the longer 5yrs time scale. The Indo-Pacific, which is the largest domain, has the smallest $N_{spatial}$, whereas the Southern ocean, which is similar in size to the tropical Indo-Pacific domain, has the largest $N_{spatial}$ on both time scales, marking the most complex spatial structure in SST variability.
- The comparison of the two observational datasets suggests that the modes of SST variability are relatively well known for most domains, but not for the

Southern Ocean. Here the uncertainty in the SST modes is quite substantial, even in two datasets that contain the same observations.

We start the summary and discussion of the model results with some positive findings:

- Some models have a quite realistic spatial structure of the SST variability in some domains at some time scales. In particular this is the case on the monthly mean time scale in the tropical Pacific and also (for some models) in the North Pacific. On the longer 5yrs time scale most models simulate the tropical Atlantic and Indo-Pacific SST variability with quite realistic spatial structure. The good performance of these models in these domains is in particular notable, as these models also outperform the simple null hypotheses, suggesting they indeed simulate non-trivial spatial structure of SST variability.
- The CMIP5 ensemble does show some improvement over the CMIP3 ensemble. The most significant improvements are seen in the two tropical domains. In the tropical Atlantic the CMIP5 ensemble as a whole is shifted towards more realistic variability on the longer time scale and in the tropical Indo-Pacific the CMIP5 ensemble has improved on both time scales, but mostly by a lag of very ‘bad’ models from CMIP3 and not by an improvement of the ‘best’ models from CMIP5.
- The modes of the CMIP3+5 super ensemble scaled by the observed eigenvalues are quite close to the observed modes and overall are closer to the observed spatial structure than any individual model. Thus the super ensemble of all the models gives the representation that is closest to the spatial structure of the observed SST variability.

- The global summary of the RMSE_{EOF} for all domains in Fig. 8f can be considered the synthesis of the models skills in simulating natural SST variability. In this synthesis the CCSM4 turns out to be the best performing model. The CCSM4 model is performing relatively well in each individual domain.

The most important findings of this study are, however, the substantial limitations that the CMIP3 and CMIP5 model ensembles have in simulating the spatial structure of SST variability:

- Most CMIP models in most domains on both the monthly mean and the 5yr running mean time scales have less skill in simulating the spatial structure of SST variability than the simple isotropic diffusion (red noise) null hypothesis $H_{0\text{STDV}}$. And in many cases they have less skill than the Slab Ocean simulation. The tropical Atlantic region is the only region in which the CMIP ensembles perform as well as the $H_{0\text{STDV}}$ null hypothesis on the longer time scale.
- The models largely overestimate the effective number of spatial degrees of freedom (N_{spatial}) in all domains and in particular on the shorter time scale. Thus, the models produce more complex spatial structures in the SST variability, with more localized smaller scale patterns.
- The models do not only disagree largely with the observations, but also with each other. The mismatch between the models is as big as the mismatch with the observations. The largest uncertainties are in the North Atlantic and in the Southern Ocean on the longer time scale. Here, the mismatch between models is larger than relative to the simple $H_{0\text{STDV}}$ null hypothesis.

- Much of the disagreement between the models and the observations comes from smaller scale patterns. Often these have different locations, structures and amplitudes in the models relative to the observations or other models.

Several aspects of this analysis indicate that the models limited skill is caused by ocean dynamics, coupling processes and possible error amplification: The first piece of evidence comes from the relative good performance of the Slab Ocean simulation, which does not simulate any ocean dynamics, but performs more realistic in the simulation of the shorter time scale in the extra tropical domains than most CGCM simulations. The most remarkable difference to the CGCM simulations here is the much more realistic low $N_{spatial}$ values in all extra-tropical domains. This may indicate that the ocean and air-sea interaction simulations of extra-tropical dynamics cause significant problems. In particular, they seem to generate much more complex small-scale SST variability that is inconsistent with observations. This is also related to the second piece of evidence pointing towards problems in the simulations: The models produce too many small, localized modes of variability that are at the wrong positions with the wrong structures. Such modes do neither exist in the Slab Ocean simulation nor in the simple null hypotheses.

These localized modes, or “climate drift” can be easily found in fully coupled GCMs as the atmospheric, oceanic and coupling processes could all introduce errors and even amplify the errors from each other. Further, this result seems to be consistent with what we know from the dynamics of the atmosphere and oceans: Atmospheric meso-scale internal variability is on a much larger scale than that of the oceans. Indeed, current state-of-the-art CGCMs do not resolve oceanic meso-scale dynamics. The coarse resolution of the ocean models may potentially be one of the main

problems in the CGCMs. However, it also needs to be noted that the CGCMs need to simulate a correct mean SST climatology in order to simulate the correct spatial structure of the SST variability. In particular in the extra-tropical domains SST variability is often a reflection of variability relative to fronts in either the ocean (e.g. between different gyres) or the atmosphere (e.g. jet stream). The variability in the position or the strength of the fronts is a significant part of the extra-tropical SST variability. CGCMs that simulate the positions of these fronts incorrectly will not be able to simulate the spatial structure of SST variability correctly. Here, the Slab Ocean simulation has a significant advantage, as it has the right mean SST climatology by construction due to the use of flux correction terms. Thus it seems reasonable to assume that the CGCM simulations will improve in the simulation of the spatial structure of SST variability if they would operate at a more realistic mean ocean state. This would in particular benefit seasonal to decadal prediction schemes in which the assimilation of observed ocean states is an important aspect of the overall skill of the predictions.

Chapter 3

Basic Long-term Modes in the Southern Ocean

The content presented in Chapter 3 was submitted as the following paper:

Wang G, Dommenges D (2015) The leading modes of decadal SST variability in the Southern Ocean in CMIP5 simulations. *Climate Dynamics*.

Declaration for Thesis Chapter 3

Declaration by candidate

In the case of Chapter 2, the nature and extent of my contribution to the work was the following:

Nature of contribution	Extent of contribution (%)
Data analysis. Writing and preparation of the manuscript. Main author of the manuscript. 75% contribution	80%

The following co-authors contributed to the work. If co-authors are students at Monash University, the extent of their contribution in percentage terms must be stated:

Name	Nature of contribution	Extent of contribution (%) for student co-authors only
Dietmar Dommenges	Co-author of manuscript	

The undersigned hereby certify that the above declaration correctly reflects the nature and extent of the candidate's and co-authors' contributions to this work*.

Candidate's Signature		Date 27/10/2015
------------------------------	---	---------------------------

Main Supervisor's Signature		Date 27/10/2015
------------------------------------	---	---------------------------

In this chapter, the leading modes of Sea Surface Temperature (SST) variability in the Southern Ocean on decadal and even larger time scales are analysed using Coupled Model Intercomparison Project 5 (CMIP5) model simulations and observations. The analysis is based on Empirical Orthogonal Function (EOF) modes of the CMIP5 model super ensemble. We compare the modes from the CMIP5 super ensemble against several simple null hypotheses, such as isotropic diffusion (red noise) and a Slab Ocean model, to investigate the sources of decadal variability and the physical processes affecting the characteristics of the modes.

3.1. Introduction

The Southern Ocean (SO), for its large heat and carbon capacity, plays a critical role in the Earth climate system (e.g. Sabine et al. 2004; Séférian et al., 2012). There are evidences that decadal and even longer variability exists in the SO, such as tree rings in Tasmania (Villalba et al, 1997, Cook et al. 2000) and increase of the Antarctic sea ice extent (e.g., Cavalieri and Parkinson 2008; Comiso and Nishio 2008).

However, due mainly to sparse observations, the long-term climate variability of the SO has not been studied extensively especially on the larger scale as its Northern Hemisphere counterpart. For the Sea Surface Temperature (SST) variability, most research focus on the remote response to the El Nino/Southern Oscillation (ENSO) (e.g. Karoly 1989; Kidson and Renwick, 2002; Mantua and Hare, 2002). The Rossby wave teleconnection patterns in the Southern Hemisphere atmosphere, known as the Pacific South America (PSA) patterns, transport the ENSO climate anomalous signals from the tropics to high southern latitudes (e.g. Mo and Higgins, 1998; Renwick, 2002; Turner, 2004). Another important factor in the SO is the Southern Annular Mode (SAM), which could be defined as the leading EOF pattern of sea level pressure

(SLP) at 20~70°S and is approximately zonally symmetric, but out of phase between middle and high latitudes (Kidson, 1988; Karoly, 1990; Thompson and Wallace 2000; Simmonds and King, 2004; Jones et al. 2009). The SAM affects the westerly circumpolar flow, then further influences the circulation, temperature distribution, mixed layer depth and heat capacity in the ocean via the Ekman pumping effect (e.g. Boer et al. 2001; Cai and Watterson, 2002; Fyfe, 2003). Recent studies suggest that a quasi-decadal variability exists in the SAM (Yuan and Li, 2008; Yuan and Yonekura, 2011).

Within the deeper subsurface SO, the intrinsic variability is closely related to the Antarctic Circumpolar Current (ACC). The baroclinic instability originates within the thermocline of the ACC (O’Kane et al., 2013; Monselesan et al., 2015), and further results in positive feedbacks between meso-scale eddies and the ACC mean flow (Hogg and Blundell, 2006). On even longer-term variability the Southern Ocean centennial variability is possibly caused by deep ocean overturning circulation changes, as discussed in model based studies (e.g. Latif et.al, 2013).

Further, a number of modes in the atmosphere-ocean system have been identified in the Southern Hemisphere, such as the Trans-Polar Index (TPI, Jones et al, 1999), Antarctic Circumpolar Wave (ACW, e.g. White and Peterson, 1996; White et al., 2004; White and Simmonds, 2006) and South Pacific subtropical Dipole (Morioka et al., 2013). They might also exhibit decadal variations, which are still unclear (e.g., Simmonds, 2003; Yuan and Yonekura, 2011).

The length of observational records and limitations of models restrict our understanding of the long-term variability in the Southern Ocean. Besides, most previous studies focus on the modes from the atmosphere rather than from the ocean,

mainly because of the relative abundance of the atmospheric data. However, as the significant heat content of the SO, the ocean itself should have more influence on the decadal and even longer variations. In this study presented here we will base our SST variability analyses within SO on the empirical orthogonal function (EOF) modes in the model simulations and observations, and get the basic SST modes in SO on the low frequency as well as their features and influencing factors. We will also compare the leading modes of variability against simple null hypotheses such as isotropic diffusion (red noise) and atmospheric forcings only (Slab Ocean simulation), to test the factors that influence the generation and proposition of the modes (see Dommenget, 2007 and Wang et al. 2015; also see Chapter 2).

The chapter is organized as follows: firstly, section 3.2 presents the data used. Section 3.3 evaluates the consistency of CMIP5 simulations in the Southern Ocean. The main results of this study are shown in Section 3.4. Here the leading modes in the Southern Ocean and their features are presented and analysis of the sources of the modes and the factors affecting their main characteristics are presented. Finally a summary and discussion are provided in section 3.5.

3.2. Data, model simulations and methods

The observed global monthly mean SSTs are taken from the NOAA Optimum Interpolation Sea Surface Temperature (OISST) V2 from 1982 to 2004, which are based on in-situ and satellite observations (referred as “observations” below, Reynolds et al., 2002). Hadley Centre Sea Ice and SST data set (HadISST, Rayner et al., 2003) was chosen as an auxiliary.

Our analysis focuses on the long-term internal natural variability, therefore the scenario of CMIP5 “pre-industrial control” (PiControl) is used for the following study for its relatively long output without anthropogenic forcing influence. 10 CMIP5 models (Table. 3.1) are selected from the CMIP5 datasets (Taylor et al., 2012), as they represent all the models having at least 500 years continuous simulation and all the variable outputs needed for the analysis in this paper. We take 500 years from each model and concatenate the SST anomalies (computed for each model individually) to generate a CMIP5 super model with 5000 years of data to provide a synthesis. This kind of super model has been shown to be more similar to the observed modes than individual models (Bayr and Dommenges, 2014; Wang et al., 2015; also see Chapter 2). We will further verify the super model performance in section 3.3.

Table 3.1 List of CMIP5 models

Number	Originating Group(s)	Country	Model
1	CSIRO and BOM	Australia	ACCESS1.0
2	CSIRO and BOM	Australia	ACCESS1.3
3	National Center for Atmospheric Research	USA	CCSM4
4	Canadian Centre for Climate Modelling and Analysis	Canada	CanESM2
5	Geophysical Fluid Dynamics Laboratory	USA	GFDL-CM3
6	Geophysical Fluid Dynamics Laboratory	USA	GFDL-ESM2G
7	Hadley Centre for Climate Prediction and Research / Met Office	UK	HadGEM2-ES
8	Institut Pierre Simon Laplace	France	IPSL-CM5A-LR
9	Meteorological Research Institute	Japan	MRI-CGCM3
10	Beijing Climate Center	China	bcc-csm1-1

We also use a 500 years long simulation of an atmospheric GCM coupled to a simple Slab Ocean to compare against the CMIP5 models. This model is comprised of the UK Meteorological Office Unified Model general circulation model with HadGEM2 atmospheric physics, a Slab Ocean model with a 50m-layer thickness and prescribed sea ice climatology. A flux correction scheme is used to force the model SST to closely follow the Hadley Centre Sea Ice and SST data set (HadISST) SST climatology (for more details see Chapter 2).

All data sets (models and observations) were interpolated to a common 2.5° latitude \times longitude grid and linearly detrended to remove the global warming signal and/or climate drift prior to the analysis.

The concept of the data set SST mode comparison is based on Dommenget (2007) and Bayr and Dommenget (2014), and has been applied in a similar way to the SO SST modes in Chapter 2.

Apart from the EOF projection method above, we also use the distinct EOFs (DEOFs) to estimate the patterns that describe the largest differences in explained variance between two data sets A and B (Dommenget, 2007), which are found by pairwise rotation of the EOF-modes to maximize the leading e_i^A values relative to the $pe_i^{A \rightarrow B}$ iteratively (Dommenget, 2007, Bayr and Dommenget, 2014). Each DEOF mode has two explained variance values. One is the explained variance in dataset A, $dev_i^{A \rightarrow B}(A)$, and the other the explained variance in B, $dev_i^{A \rightarrow B}(B)$. The DEOFs patterns are ordered by the difference between $dev_i^{A \rightarrow B}(A)$ and $dev_i^{A \rightarrow B}(B)$. Therefore, the first DEOF mode, $DEOF_1^{A \rightarrow B}$, would represent the pattern that explains more variance in A than in B, and this difference should be the largest among all DEOF patterns. Thus, DEOFs is a simple way to illustrate the largest differences between two datasets demonstrating significant differences in terms of spatial patterns, however, they may have some limitations in the interpretation similar to those of EOF patterns (for more details see Dommenget, 2007).

3.3. Model Evaluation

Chapter 2 showed, in an evaluation of the SST modes for CMIP5 historical runs in the Southern Ocean, that all models differ significantly with the HadISST modes with the

uncertainties in the order of 40-60% of the eigenvalues. The study also illustrated larger inconsistency of the model with each other via pairwise model comparison. However, the super model ensemble showed better agreement with the observation, suggesting that it has spatial modes similar to the observed and should be more suitable for further data analysis. To verify the reliability of the models in the study here, especially the super ensemble, we will do a similar evaluation, but for the CMIP5 PiControl simulations against the OISST data.

Fig. 3.1 shows the leading modes of Southern Ocean monthly mean SST anomalies (south of 30°S) to get a first impression of how similar model simulations and observations are. Each EOF pattern is multiplied by the root of its own eigenvalue for consistency so that the amplitude of all patterns is in the unit of Kelvin. There are clear similarities between the observed and the CMIP5 super ensemble. They both have the annular mode as the EOF-1, with the similar structure: maximum anomaly amplitude in the South Pacific and the out-of-phase zonal anomalies around 30-45°S (Fig. 3.1a and d). The CMIP5 super ensemble also has a similar wave train like EOF-3 as observed (Fig. 3.1c and f). However, the EOF-2 in CMIP5 is more like a wave-3 pattern along 60°S with two weak troughs (Fig. 3.1e) while differently the observed EOF-2 composes of 4 waves (Fig. 3.1b).

The Slab Ocean results (Fig. 3.1g-i) illustrate more differences with much larger eigenvalues compared to observations and CMIP5 data. Its EOF-1 (Fig. 3.1g) shows similar wave-3 structure as CMIP5 EOF-2, but the two weak troughs get much stronger in the Slab Ocean simulation south to Africa/Australia. Another wave-3 pattern also exists within the Slab Ocean EOF-2 (Fig. 3.1h) and its anomaly centres in the Pacific are in the same location as the annular mode (EOF-1) in CMIP5 and the

observed. Last but not least, Slab Ocean has a similar wave-like EOF-3 as its counterparts but with lower latitude centres.

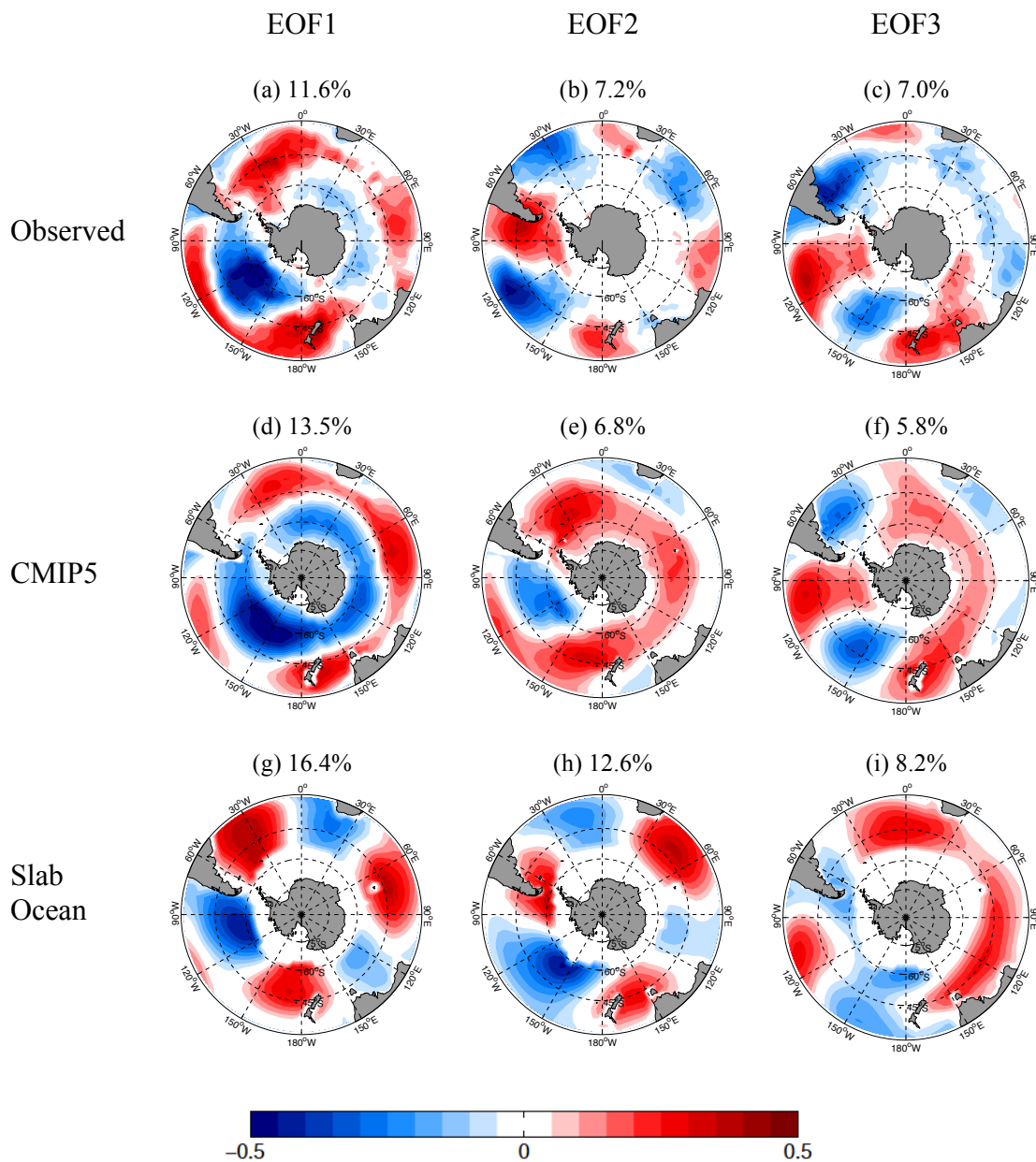


Fig. 3.1 First three leading EOF patterns of detrended monthly SSTA in the Southern Ocean for (a-c): Observation (OISST); (d-f): CMIP5 super model; (g-i): slab ocean experiment. The values in the headings of each panel are the explained variances of each EOF-mode.

To quantify the differences among data sets, Fig. 3.2 presents the $RMSE_{EOF}$ with OISST as reference on the x-axis and all models as references on the y-axis. The

values on the y-axis are the mean $RMSE_{EOF}$ of all pairwise comparison with all individual models as references.

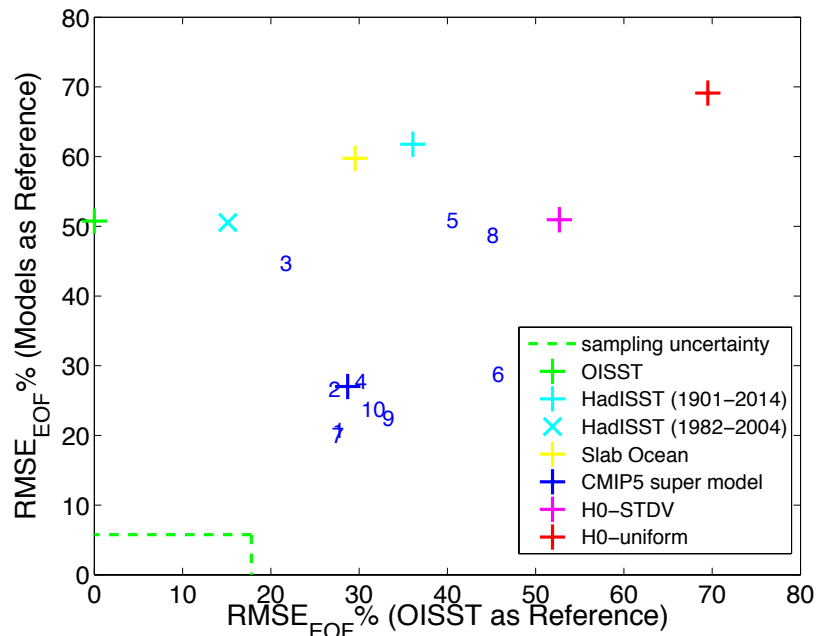


Fig. 3.2 $RMSE_{EOF}$ values distribution relative to the observations (x axis) and mean $RMSE_{EOF}$ values of pairwise comparisons to all CMIP5 model simulations (y axis) for monthly SSTA EOF-analysis in the Southern Ocean. The sampling uncertainty is based on North et al. (1982) and Wang et al (2015).

OISST and HadISST for the same period (1982-2014) agree well with each other, since the two observational data sets contain the same observations. However, the HadISST data for the much longer period (1901-2014) disagrees with the OISST data substantially. This is most likely due to the sparse observations prior to the 1980s. The relative errors of most models are ranging from 20% to 45% of the eigenvalues, which are substantial and similar as the difference between Slab Ocean and the observed (29%). The CMIP5 super model performs better (28%) than most models and has by construction much longer statistics than any individual model, which suggests that the super model is the best data set for the following analysis.

For the model pairwise comparison, most models are in the range of 20% to 50%, while the observed has larger bias of 50%~65%. This indicates that models have

strong differences and disagreements in the spatial structures between each other. Again the super model is better than most individual models with an error of 26%, implying the model ensemble should be a good substitution of an individual model.

The slab ocean shows substantial difference relative to the fully-coupled models (60% error), which suggest that the dynamics of the CMIP5 models are significantly different than in the slab ocean model. Additionally, we introduce two categories of isotropic diffusions representing homogeneous spatial red noise processes (refer as $H0_{\text{uniform}}$) and spatial red noise with known standard spatial deviation pattern (refer as $H0_{\text{STDV}}$) (see Dommenges 2007 and Wang et al. 2015 for details). Both these simple stochastic models are farther away from the observations than any individual model, suggesting that the SST modes in the Southern Ocean are indeed related to more complex dynamics than assumed in the simple null hypotheses.

3.4. Leading Modes in the Southern Ocean

In this section we present the main results of this analysis, the leading modes in the Southern Ocean and possible factors for their generation and propagation. As a start Fig. 3.3 firstly depicts the standard deviation (STDV) of annual mean SST anomalies from OISST, CMIP5 ensemble mean and Slab Ocean simulation. The OISST has maximum variation south to Africa, around New Zealand and in the middle of South Pacific. The CMIP5 runs simulate most of the observed structures of the STDV distribution successfully, but underestimate the variability for the most active areas and tend to have stronger fluctuation within the sea ice region around Antarctic. The spatial structure of the STDV in the slab ocean simulation is too smooth, but with similar overall amplitudes. The regions around the sea ice border have by construction no SST variability, as the model has prescribed sea ice climatologies.

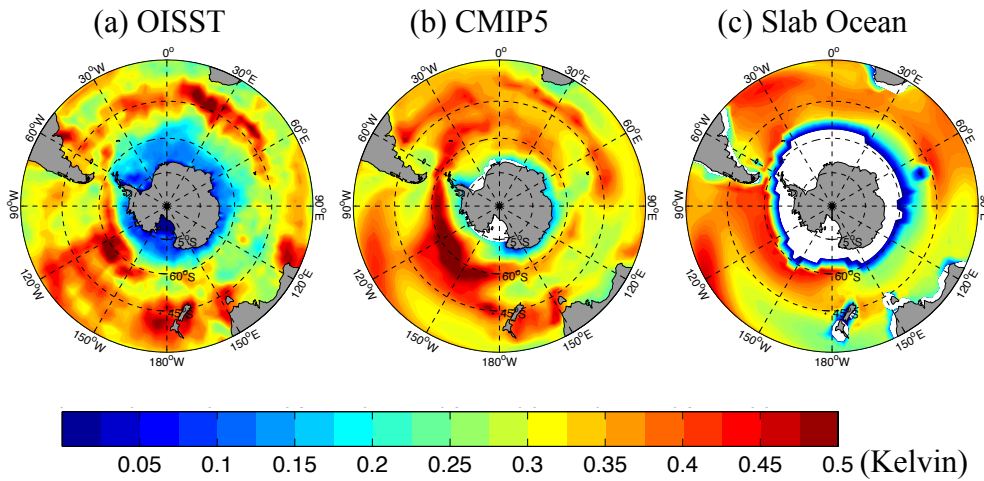


Fig. 3.3 Standard deviation fields of annual mean SSTA for (a): OISST; (b): CMIP5 super model; (c): Slab Ocean experiment result.

Fig. 3.4 shows the fraction that the long-term SST variability (>10 years) contributes to the total annual mean variation based on the CMIP5 super model ensemble. Note that most of the high latitude oceans are dominated (>60%) by low-frequency variations, while in the tropics it contributes less than 30%. In the Southern Ocean, the long-term signal is stronger in the higher latitudes and in the Indian Ocean it appears to reach from the south-west to north-east, while one branch reach the south of Australia and the Tasman Sea.

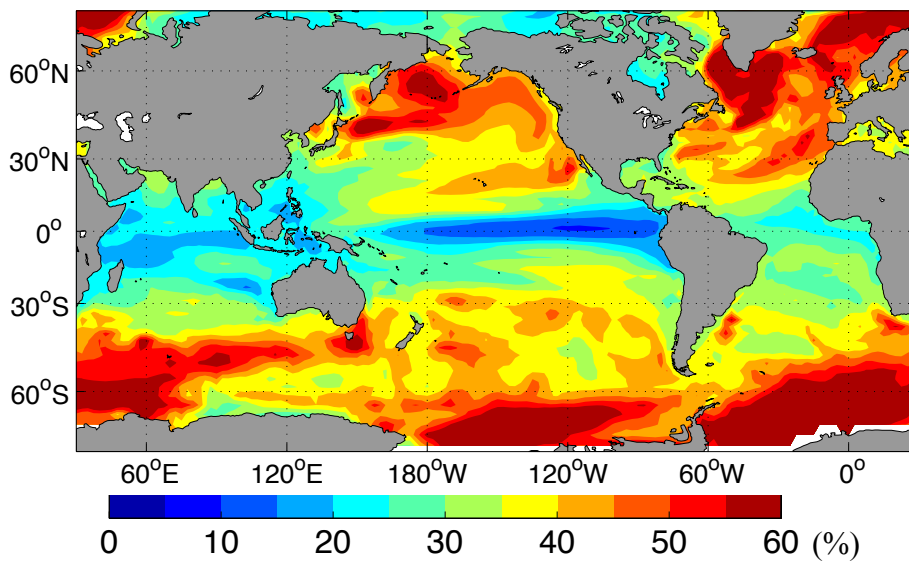


Fig. 3.4 The relative contribution of Long-term (> 10 years) variability to the total of annual mean variations based on the CMIP5 super model.

The leading modes of SST variability in the CMIP5 super model on different time scales including monthly mean, annual mean and 5 years running mean are shown in Fig. 3.5 based on EOF-analysis. A few characteristics can be noted here:

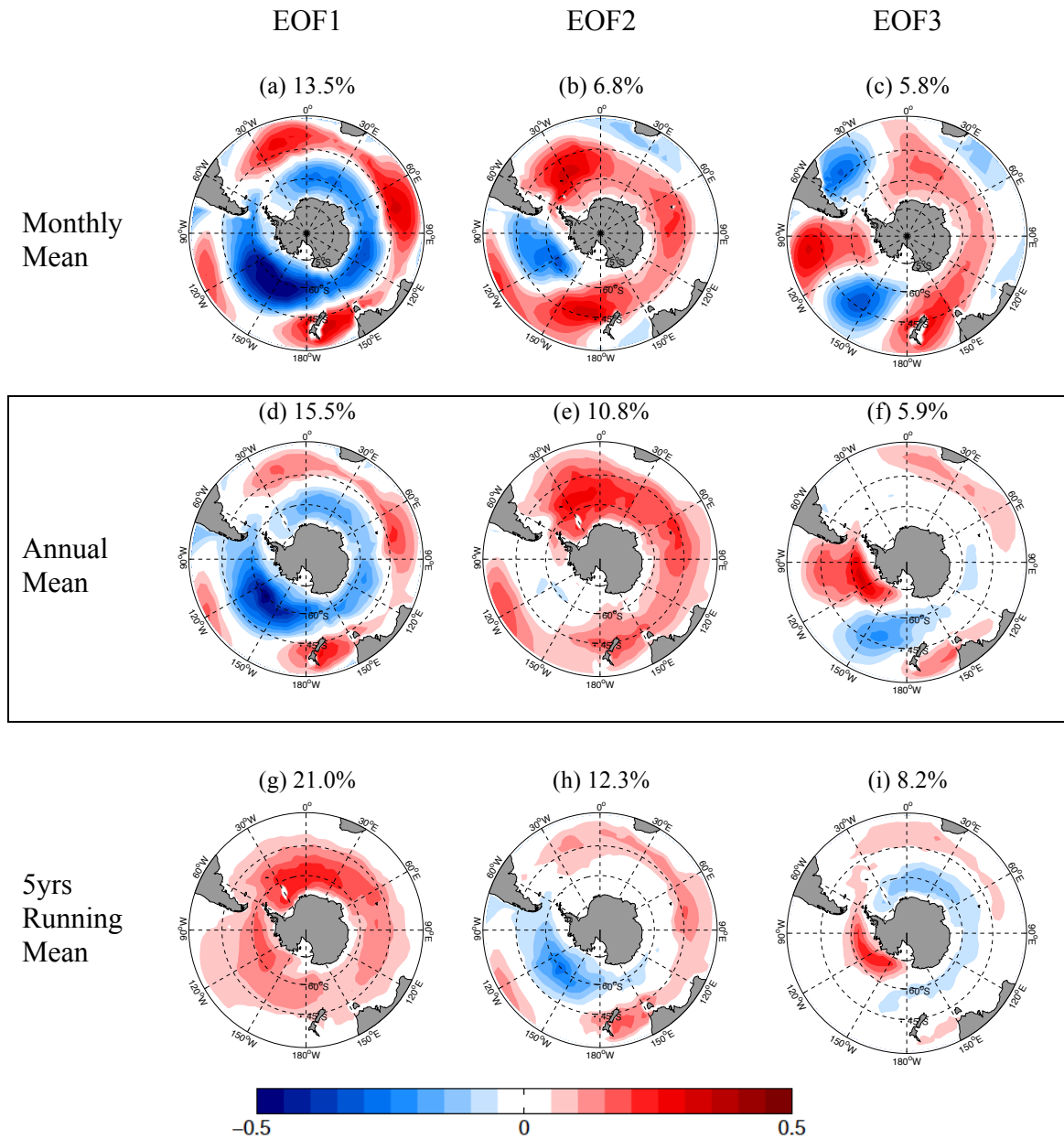


Fig. 3.5 First three leading EOF patterns of CMIP super model SSTA in the Southern Ocean for (a-c): monthly mean; (d-f): annual mean; (g-i): 5 years running mean. The values in the headings of each panel are the explained variances of each EOF-mode.

- The three leading modes on the monthly mean time scale all together explain only about 26%, which indicates a fairly large number of spatial degrees of freedom ($N_{\text{spatial}} = 27$, see Bretherton et al., 1999 for the definition). This N_{spatial} here is larger than in most other ocean basins (Wang et al. 2015) and thus indicates the complexity of the SO SST variability. On the longer time scales the relative importance of the leading modes increases, with more than 40% explained by the three leading modes. This indicates that on the longer time scales the leading modes of SST variability become larger in spatial scale and the SST variability overall becomes less complex ($N_{\text{spatial}} = 13$ for 5yrs running mean).
- The monthly mean EOF-1 corresponds to EOF-1 on annual mean and EOF-2 on 5 years running mean. All three of them illustrate the annular structure with the maximum anomalies in the Pacific, corresponding to the region with large SST STDV in Fig. 3.3b. The relative importance (eigenvalue) of this pattern appears to be strongest in the annual mean SST variability. It becomes less important on the longer than 5yrs time scales.
- The EOF-2 of monthly mean, as described above (Fig. 3.1), is a wave-train like pattern with three clear crests, which is much more pronounced in the slab ocean simulation (Fig. 3.1g). When it comes to annual mean time scales (EOF-2 in Fig. 3.5e), the troughs become much less conspicuous and the crest in the Southern Atlantic intensified while the other two crests get much weaker. The corresponding pattern on the even longer time scale (EOF-1 in Fig. 3.5g) has the no more signature of the three-wave structure and it leaves a monopole pattern. Thus it appears that the atmospheric three wave pattern forcing is very clear in the slab ocean simulation and then transforms into a

basin wide monopole pattern in the dynamical ocean simulations of the CMIP5 super model ensemble on longer decadal time scales. The eigenvalue of this mode is increasing as the time scale gets longer from 7% to 21% and it becomes the leading pattern on the 5yrs running mean analysis, implying that this pattern is more dominant on decadal scale.

- The EOF-3 pattern does not seem to change much over the varying time scales. The time series of EOF-3 has strong correlation with its counterpart on the different time scales ($r > 0.7$), implying all the EOF-3s belong to basically the same mode and its temporal variation is well kept, however, its spatial pattern gradually transform from wave-train pattern to a dipole structure in the Pacific on the annual mean scale with anomalies moved to the higher latitudes. The dipole pattern further fades as the pole in the west Pacific weakens on the longer time scale.

In the following analysis we will focus on the annual mean modes, as we are mostly interested in long time SST variability. The power spectra of the leading annual mean EOF-modes are illustrated in Fig. 3.6. For comparison with the slab ocean simulation we project the CMIP5 annual mean EOF-modes onto the slab ocean data to estimate the time series that these patterns would have in the slab ocean simulation. The power spectra of these time series are shown in for Fig. 3.6 comparison. Thus we here consider the slab ocean as being a simple red noise test as discussed in the stochastic climate model by Hasselmann (1976). The theoretical red noise power spectrum is fitted to the slab ocean power spectrum in Fig. 3.6. A number of interesting characteristics can be noted in these power spectra:

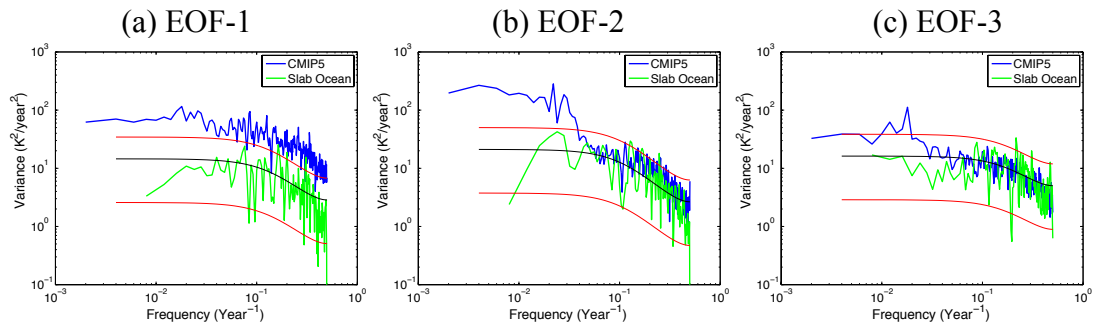


Fig. 3.6 Spectrum of the time series of the three leading EOF-modes of the CMIP super model annual mean SSTA (as in Fig. 3.5d-f). The power spectrum of the time series resulting from the projection of these patterns onto the slab ocean simulation SSTA variability are shown for comparison. The black line is a red noise fit to the slab ocean time series and the red lines mark the 95% confidence interval relative to the red noise fit of the slab ocean simulation.

- All three CMIP5 super ensemble modes have more variability on the longer time scales than the slab ocean simulations. Thus it indicates that in all three modes ocean dynamics may be key in producing the long time SST variability.
- The EOF-1 mode has a very similar shape of the power spectrum in both the CMIP5 super model and the slab ocean, but the CMIP5 super model power spectrum shifts higher up, indicating it has more variance on all time scales.
- The EOF-2 mode has a very interesting time scale behaviour that deviates from a red noise power spectrum quite substantially. It appears to be similar in amplitude and time scale behaviour to the slab ocean for interannual until about decadal time scales. But on multi-decadal time scales the CMIP5 super model SST variability starts to increase again by about an order of magnitude for the centennial time scales. Thus the EOF-2 mode has a two-step power spectrum, with an interannual to decadal level of variance and a second higher up level of variance on the multi-decadal to centennial time scales.
- The EOF-3 mode has a similar indication of increased variance on the longer time scales compared to the slab ocean, but it is not as strong and it seems to have a more pronounced time scale (peak) at around 50yrs periods.

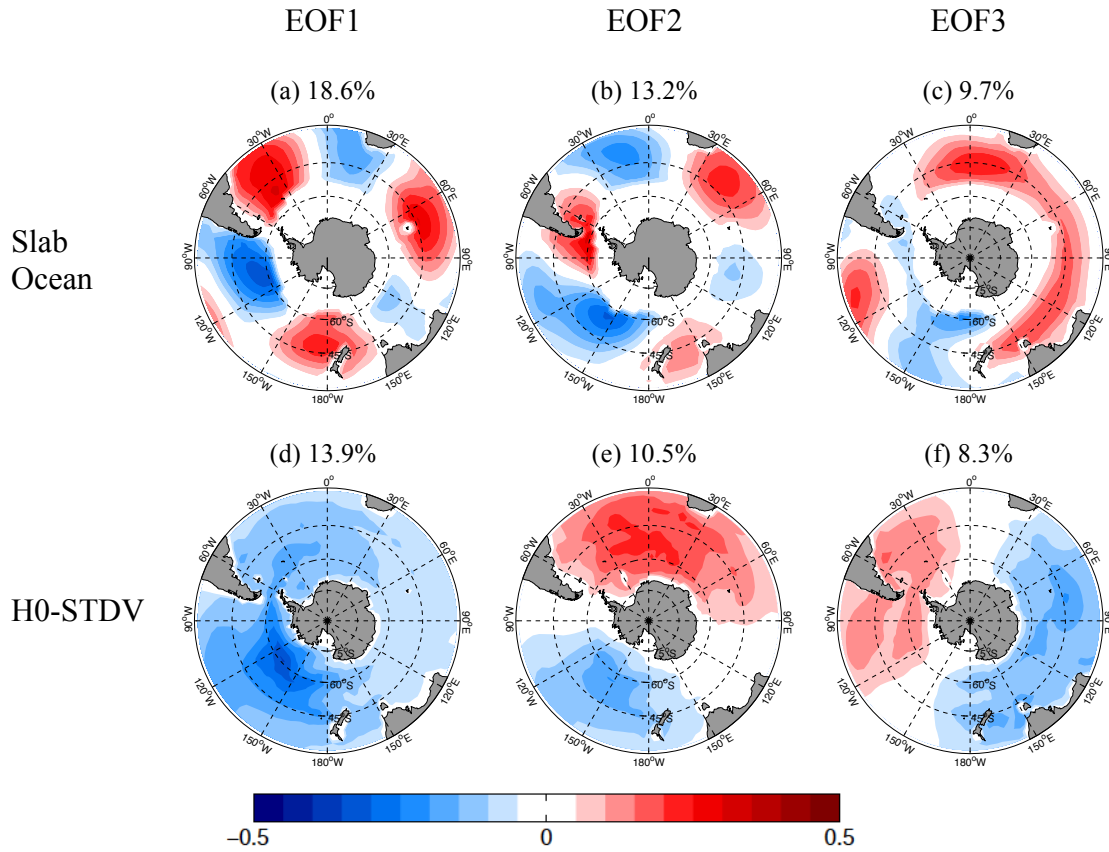


Fig. 3.7 First three leading EOF patterns of detrended annual mean SSTA in the Southern Ocean for (a-c): Slab Ocean; (d-f): H0-STDV null hypothesis. The values in the headings of each panel are the explained variances of each EOF-mode.

To further explore the origin of the spatial structures of the leading modes we take a closer look at the leading modes in the Slab Ocean simulation and in the simple spatial red noise patterns H0-STDV (see Fig. 3.7). The leading modes of the slab ocean simulation are dominated by the wave number three shapes that are forced by the atmospheric wave trains. The patterns also show no substantial changes from monthly mean (Fig. 3.1g-i) to annual mean time scales, suggesting that the patterns are present on all time scales. The simple spatial red noise H0-STDV EOF-modes are a hierarchy of multi-poles (Fig. 3.7d-f), starting with a monopole (largest scale), followed by dipoles with increasing complexity (see Dommenget 2007 for a more

detailed discussion). These multi-pole modes are centered on the regions of large SST STDV (see Fig. 3.3b).

The modes of the Slab Ocean simulation and H0-STDV stochastic null hypothesis are clearly different to CMIP5 super model ones. The DEOF modes shown in Fig. 3.8 further quantify these differences. The DEOF modes represent the modes that in the comparison between the CMIP5 super model and the Slab Ocean simulation or H0-STDV stochastic null hypothesis are most dominant in the CMIP5 super model (see methods section for details on the DEOF-modes).

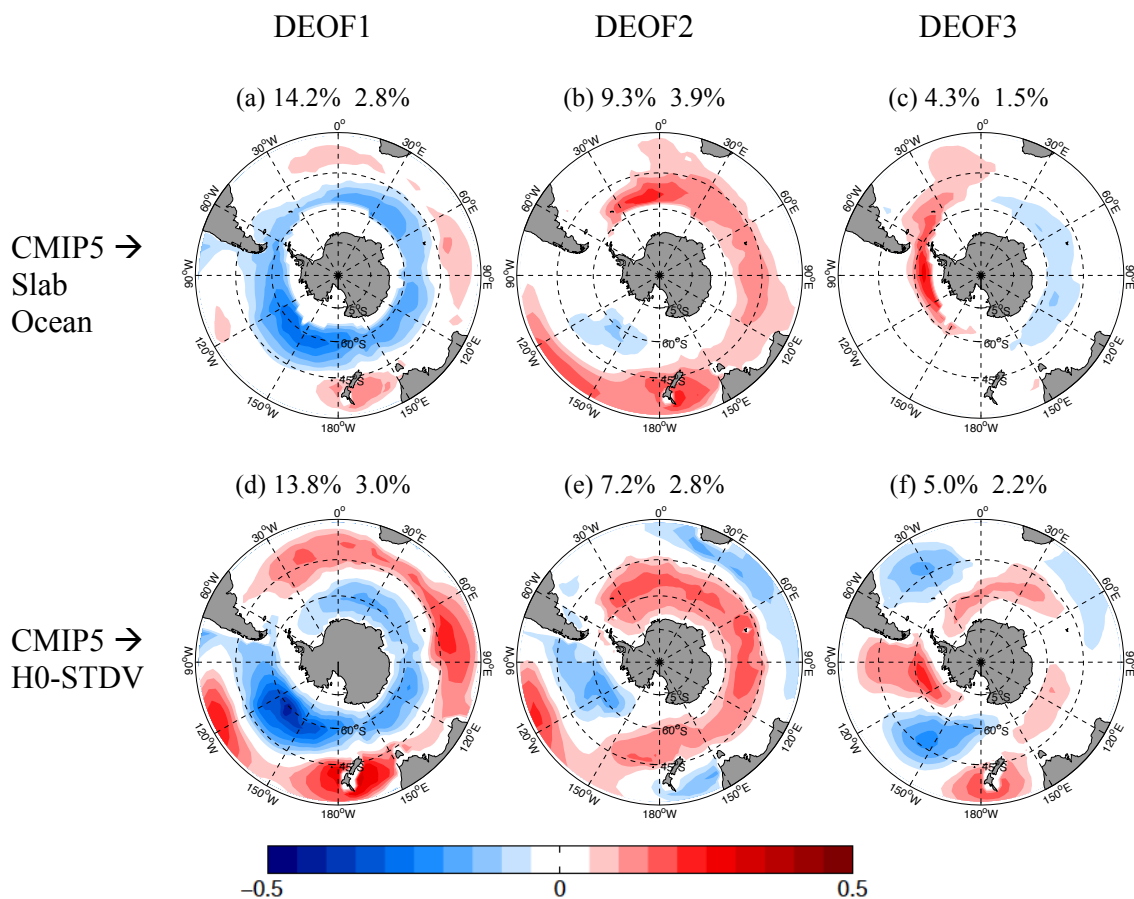


Fig. 3.8 (a-c): Leading DEOF patterns of annual mean SSTA CMIP5 projection to Slab Ocean; (d-f): Leading DEOF patterns of annual mean SSTA CMIP5 projection to H0-STDV. The headings show the explained variances of the DEOF-modes in the CMIP5 super model (first value) and the slab ocean simulation or H0-stdv null hypothesis (second value), respectively.

Most of the leading DEOF modes duplicate the leading CMIP5 modes in Fig. 3.5d-f, suggesting that the Slab Ocean and red noise H0-STDV process do not produce these leading modes with enough variance. This is also consistent with the comparison of the power spectra in Fig. 3.6, where we found that the slab ocean power spectrum of EOF-1 was much weaker than in the CMIP5 super model. One exception is the DEOF-3 for the Slab Ocean (Fig. 3.8c). This DEOF mode is not similar to the CMIP5 EOF-3 and is more concentrated around Antarctica.

In summary of this first part of this analysis we can say that we have three leading modes of SST variability on the interannual and long time scales, which all three are fairly different in either their patterns or in their amount of variance from a simple red noise integration of atmospheric forcings. Thus all three modes are likely to involve ocean dynamics to create the pattern or at least the amount of variance. In the following we want to discuss the characteristics of these modes a bit more in detail. However, it will be beyond the scope of this work to fully explain the physical mechanisms of all three leading modes.

3.4.1 Mode 1: The Annular Mode

The first annual mean mode is described as the annular mode, which is also the leading mode within monthly mean analysis and has a similar structure as the SAM. Besides, the strong anomalies of the mode in the Pacific suggest it is related to ENSO as well. The SAM index (difference in the normalized monthly zonal-mean sea level pressure between 40°S and 65°S, Gong and Wang, 1999) leads the time evolution of this mode by about one month and the Niño 3.4 SST index (average SST anomaly in the region of 5°N to 5°S, 170°W to 120°W) leads by several months (Fig. 3.9). Thus we have two important atmospheric teleconnections that drive this mode. The global

monthly mean SSTA correlation with Niño 3.4 and SAM indices are also shown in Fig. 3.10. Both the correlation distributions in the Southern Ocean show similar spatial structure as this annular mode itself. However, obviously the correlation focuses within the South Pacific domain in the Southern Ocean when correlated with ENSO, while the SAM correlation is extended to the entire ocean.

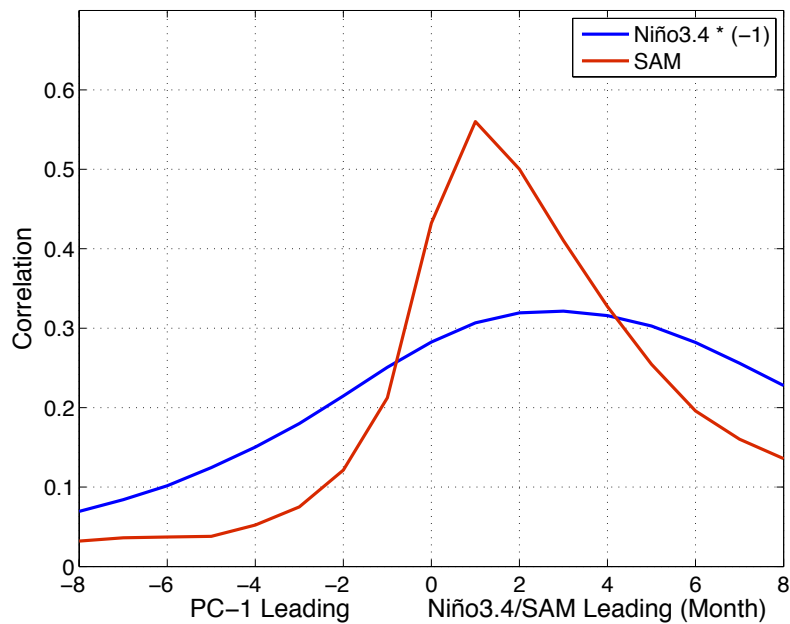


Fig. 3.9 Lead-lag correlation between Niño3.4/SAM and monthly mean PC-1 time series of CMIP super ensemble. Note that the correlation with Niño3.4 is multiplied by minus one to be positive.

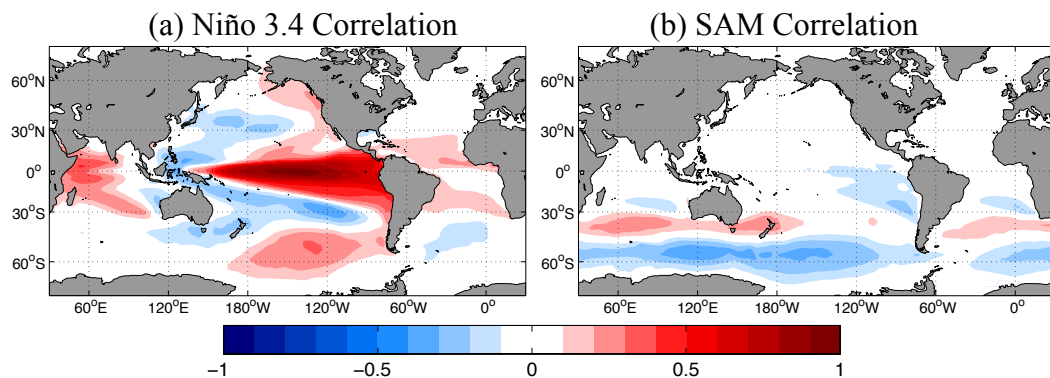


Fig. 3.10 (a): Monthly SSTA correlation with Niño 3.4 in CMIP5 super model; (b): same as (a) but for the correlation between SSTA and SAM index.

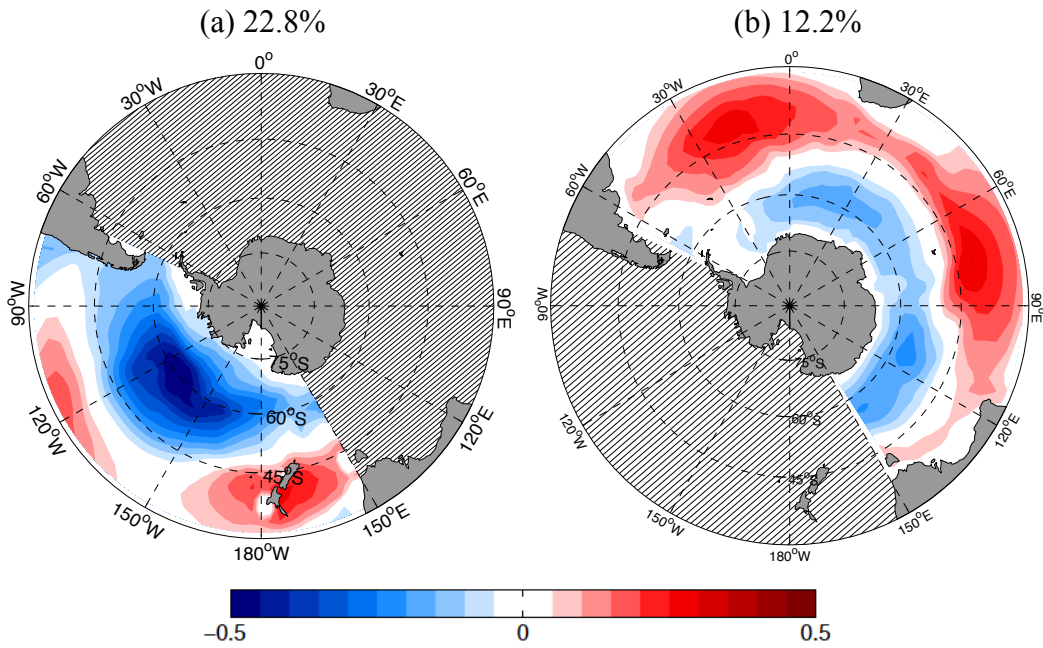


Fig. 3.11 (a): CMIP5 super model EOF-1 of annual mean SST in South Pacific; (b): EOF-2 of annual mean SST in South Atlantic and Indian Ocean. The values in the headings of each panel are the explained variances of each EOF-mode.

To further discuss these two effects separately, we divide the Southern Ocean into two regions, namely the Pacific part (150°E to 60°W) and the Atlantic-Indian part (rest of the SO), and compute the respective EOF modes for the CMIP5 super model (see Fig. 3.11). The corresponding spatial patterns (EOF-1 for the South Pacific sector and EOF-2 for the Indian-Atlantic domain) are almost identical to the Southern Ocean pattern (EOF-1 in Fig. 3.5d). The correlation between the time series of Southern Ocean pattern and Pacific one (pattern in Fig. 3.11a) is 0.9, and it is 0.7 between entire ocean time series and Atlantic-Indian Ocean counterpart (pattern in Fig. 3.11b); but it is only 0.5 for the two separated region comparison.

We construct a simple linear model for the variability of these EOF time series based on ENSO and SAM influences:

$$H_n = \alpha H_{n-1} + \beta Nino34_n + \gamma SAM_n + f \quad (3.1)$$

,where H_n is the value of the time series in the n^{th} year in the CMIP5 models, α is the memory of the ocean, β and γ are the linear forcing coefficients for normalized Niño3.4 and SAM indices, respectively. f is the residual. Thus, larger absolute value of β (γ) represents stronger impact from ENSO (SAM) on the temporal variability. The results of a least squared fit to the CMIP5 super model data are listed in Table. 3.2. As expected, ENSO shows strong influence in the Pacific and limited impact for the rest of the domain. SAM has almost the same influence on both individual regions. For the entire basin, the impacts of these two phenomena are comparable to each other and also to the ocean memory. The reconstructed time series H_n has strong correlation ($r = 0.8$) with the Southern Ocean EOF-1 time series and it basically reproduces the spatial structure of EOF-1 (see Fig. 3.12). Similar results are also found within the observation ($\beta = -0.54$, $\gamma = 0.31$ for OISST annual mean EOF-1 in the SO). Thus, this annular mode is driven by ENSO and SAM.

Table 3.2 Parameters of linear regression model for annual mean EOF-1 time series discussed in the text.

	α (Ocean Memory)	β (Niño 3.4)	γ (SAM)
Pacific EOF-1	0.42	-0.69	0.19
Southern Ocean EOF-1	0.38	-0.37	0.25
Atlantic-Indian Ocean EOF-2	0.30	-0.06	0.25

In this context it is interesting to note that the slab ocean simulation has much less variance in this mode (see Figs. 3.6a and 3.8a), although it is forced by the SAM. ENSO is not simulated in the slab ocean simulation, but it is unlikely that this is the main reason why the mode is much weaker in the slab ocean simulation. Both SAM and ENSO mostly affect the Southern Ocean via the variation of zonal winds and thus by wind induced mixing (e.g. Sallée et al., 2010; Screen et al., 2010). But wind mixing does not exist in the slab ocean simulation. The relation to wind forcing is also

highlighted by the fact that the main node of EOF-1 is around the 60°S to 40°S latitudes band, which is also where the SAM pattern has its maximum sea level pressure gradients and thus the strongest wind stress forcings.

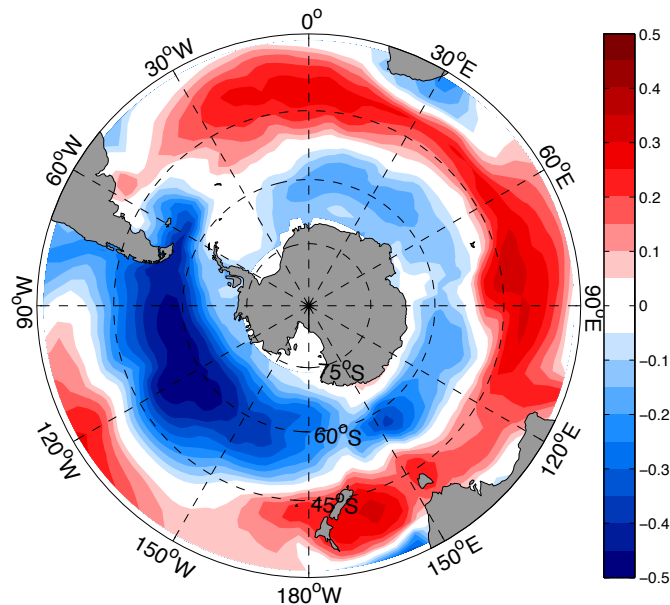


Fig. 3.12 Correlation between a reconstructed SSTA PC-1 time series and SSTA of the CMIP5 super model on annual time scale. See text for details on the reconstruction model.

3.4.2 Mode 2: Basin wide monopole mode

We name the annual mean EOF-2 the basin wide monopole mode as its anomalies expand with the same sign over the entire SO domain on longer scales. This kind of spatial structure is more apparent on even longer time scale (10 years running mean to 50 years running mean) as shown in Fig. 3.13. The eigenvalues are increasing with longer time scales indicating the increasing importance of this mode for longer time scales. Thus, this pattern, as the leading pattern on interannual scale already, becomes more dominant on decadal and multi-decadal scales, which is consistent with the internal centennial variability (Martin et al., 2013; Latif et al., 2013).

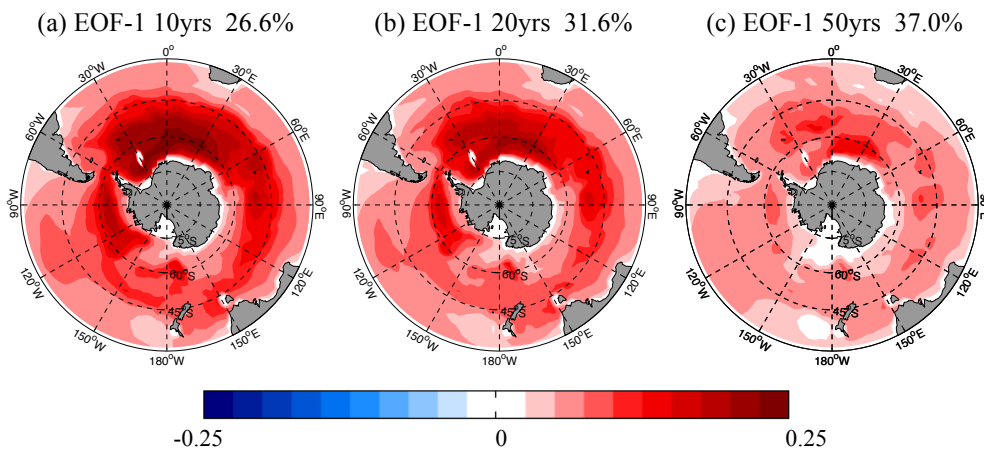


Fig. 3.13 EOF-1 of SSTA in Southern Ocean of the CMIP5 super ensemble for (a): 10 years running mean; (b) 20 years running mean; (c) 50 years running mean. The values in the headings of each panel are the explained variances of each EOF-mode.

This pattern, as mentioned in the previous sections, originates from a wave number three wave-train prototype pattern in the slab ocean EOF-1 without ocean dynamics. Thus it is forced from the atmospheric heat flux forcing at least partially. Fig. 3.14 shows the correlation of the time series of EOF-2 with the geopotential height at 500hPa. The three wave crests can be recognized in the atmosphere and the nodes are well collocated with the nodes of the SST pattern (Fig. 3.5b).

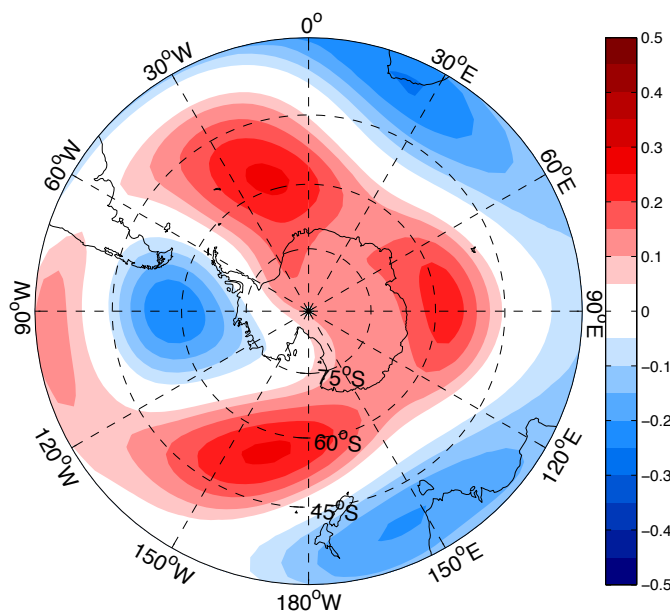


Fig. 3.14 Correlation between SSTA PC-2 time series and 500hPa geopotential height anomaly of the CMIP5 super model on monthly time scale.

To further analyse the relation of the SST to the atmosphere and the subsurface ocean we create an SST index based on the three crests boxes (0-30°W, 40°S-60°S for Box-1; 60°-90°E, 40°S-60°S for Box-2 and 160°E-170°W, 40°S-60°S for Box-3) and make the boxed averaged value as a SST proxy index for this mode. The SST index has a correlation of 0.9 with the annual mean EOF-2 and thus illustrates that the EOF-2 mode is indeed mostly the variability in these three regions combined. The 500hPa geopotential height index of the same boxes leads the SSTA index by about one month (see Fig. 3.15a). Thus, the atmospheric internal wave-3 structure is a forcing of this SST pattern.

In the CMIP5 super model it appears that the pattern transforms from the wave-3 structure on the shorter monthly mean time scales to the basin wide monopole mode pattern on the decadal and longer time scales. In the Slab Ocean simulation this development does not happen and the SST variability keeps the wave-train structure on the longer time scales (Fig. 3.1g and Fig. 3.7a). This is also reflected in weaker power spectrum for this mode in the slab ocean simulation (Fig. 3.6b). This suggests that the ocean dynamics may be the essential factor responsible for the mode transformation and power spectrum increase on multi-decadal and longer time scales.

The vertical structure of this mode in the upper ocean may give some indication of its nature. For this we take a look at the lag-lead correlation between the SST mode index and the ocean temperature at different depths, and we look at the pattern of the in phase (zero lag) correlation between the SST mode index and the ocean temperature at different depths (see Fig. 3.15).

The SST evolution appears to lead the subsurface temperature evolution on all layers and signal generally gets weaker the deeper we go (Fig. 3.15a-b). However, it is

interesting to note that the correlation in 500m depths is larger than in the upper ocean layers when the SST is leading by more than two years. It is also interesting to note that the patterns transform slightly from a monopole at the surface to an annular dipole structure at 500m depth (Fig. 3.15c).

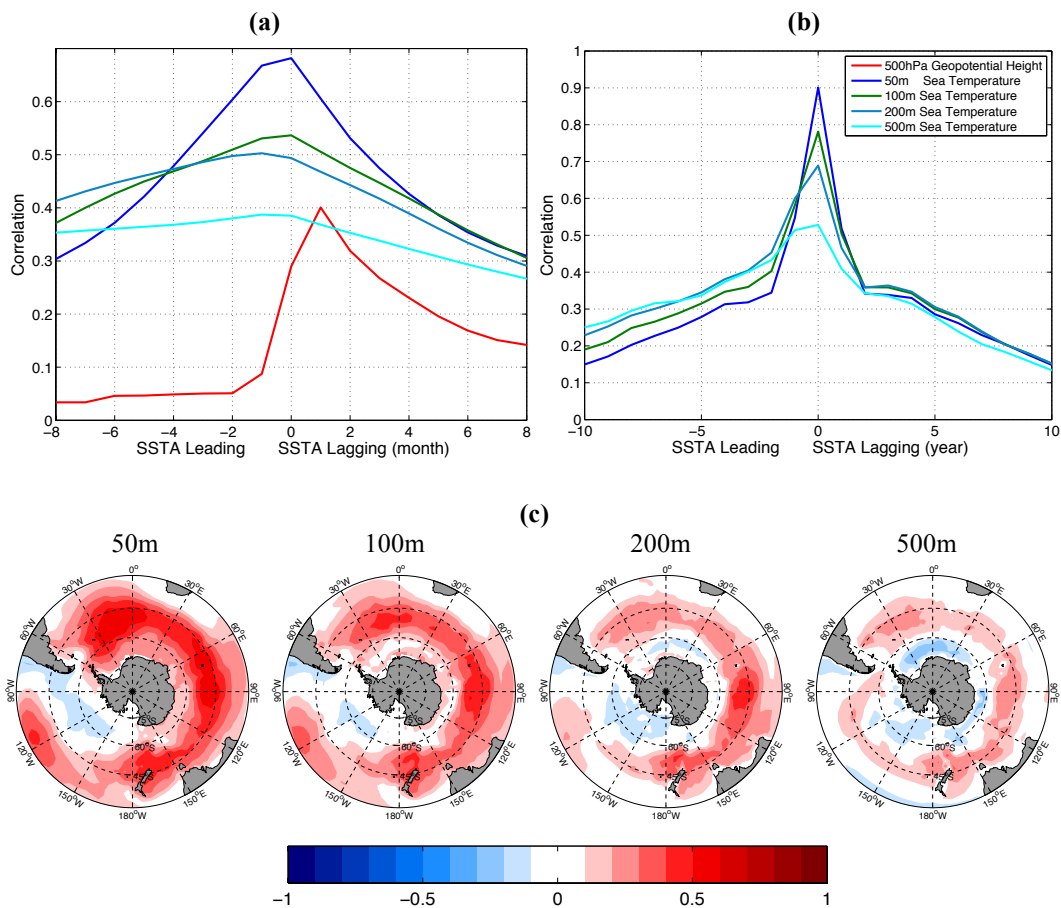


Fig. 3.15 Lead-lag correlation for box-averaged indices for the monopole mode between SSTA and 500hPa geopotential height/subsurface ocean temperature anomalies. (a): Lead-lag correlation on monthly time scale; (b): same as (a) but for annual time scale; (c): Correlation between SSTA PC-2 time series and subsurface ocean temperature of the CMIP5 super model on annual time scale.

3.4.3 Mode 3: Dipole Mode in the South Pacific

The EOF-3 is a dipole in the South Pacific on annual mean scale (shown in Fig. 3.5f). It also starts from a zonal wave pattern shown in Fig. 3.5c on shorter time scale, but the wave pattern is out of phase with that of EOF-2. The anomalies in the Atlantic and

Indian Ocean get weaker on longer time scales, while the pattern gets transformed gradually and more focuses within the Pacific on annual mean time scale. The western pole in the South Pacific also loses its strength on longer time scales, making this pattern concentrate around Antarctica (Fig. 3.5i). To illustrate that this pattern is indeed mostly in the Pacific sector of the SO we again look at the EOF-modes of the Pacific region (EOF-2 as shown in Fig. 3.16). This EOF-2 mode of the South Pacific has a correlation of 0.95 with the annual mean time series of Southern Ocean EOF-3.

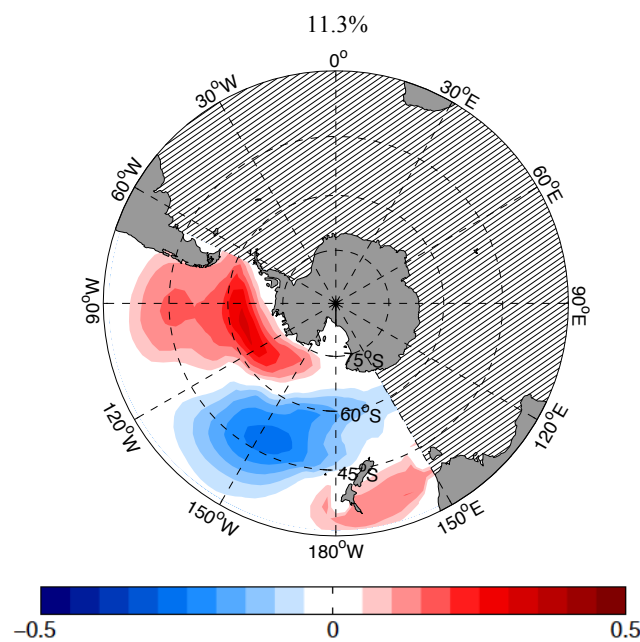


Fig. 3.16 EOF-2 of CMIP5 super model SST in the South Pacific for annual mean analysis. The value in the heading is the explained variance of this EOF-mode.

For the further analysis we simplify the SST mode by a dipole index (hereafter as Index_{A-B}) over the two main centres (Box-A: 45°S-70°S, 120°W-80°W and Box-B: 45°S-60°S, 180°-140°W). This index matches the EOF-3 time series fairly well (correlation = 0.89 for annual mean analysis). Fig. 3.17 depicts the correlation between monthly SSTA Index_{A-B} and 500hPa geopotential height anomaly. Again it demonstrates another wave-3 structure, but the maximum anomalies are mostly

restricted within the South Pacific. The crests are around New Zealand, south to South America and South to Africa, and the troughs are mostly in the middle of the oceans.

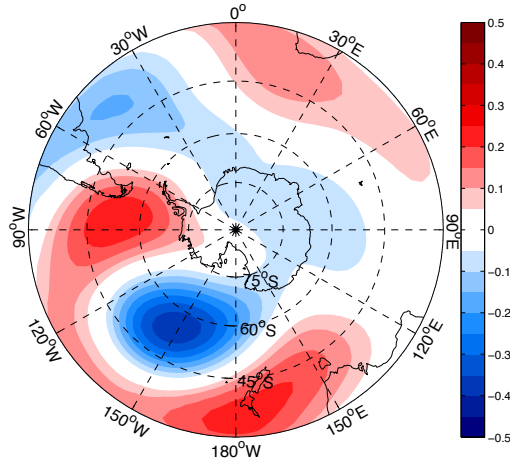


Fig. 3.17 Correlation between Box [A-B] time series and 500hPa geopotential height anomaly of the CMIP5 super model on monthly time scale.

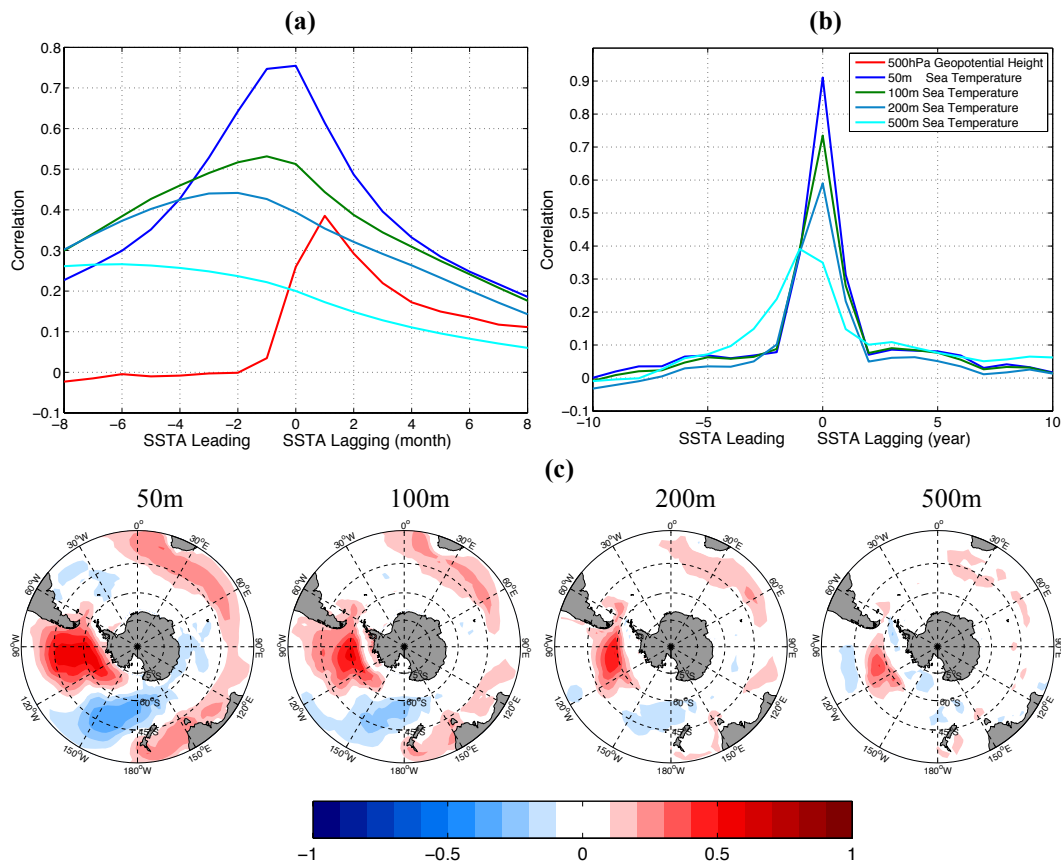


Fig. 3.18 Lead-lag correlation for Indices_{A-B} between SSTA and 500hPa geopotential height/subsurface ocean temperature anomalies. (a): Lead-lag correlation on monthly time scale; (b): same as (a) but for annual time scale; (c): Correlation between SSTA PC-2 time series and subsurface ocean temperature of the CMIP5 super model on annual time scale.

As for Mode-2 we again look at the lag-lead correlation between the SST Index_{A-B} and the ocean temperature at different depths and we look at the pattern of the in phase (zero lag) correlation between the SST Index_{A-B} and the ocean temperature at different depths (see Fig. 3.18). As expected the geopotential height variation leads the SST variability for one month, demonstrating that the atmosphere also drives this dipole mode. The SST also leads the deeper water temperature anomalies as well, but the influence decreases more rapidly with lead/lag time (Fig. 3.18b), which is consistent with the power spectrum having less multi-decadal variance than the Mode-2. However, the lag-lead relationship to the 500m depths temperature appears to be somewhat different than in Mode-2. Here the 500m depths temperature has strong correlation with the SST Index_{A-B} when the 500m depths temperature is leading, which may suggest a subsurface ocean influence on the SST Index_{A-B} on the longer time scales. The SST pattern also has some minor changes with depth (Fig. 3.18c). The western pole in the Pacific gets weaker, which might explain why the western pole also becomes unclear on the longer scale on the surface.

3.5. Summary and Discussion

In the study presented here we discussed the leading modes of SST variability in the Southern Ocean on long, decadal time scales in CMIP5 preindustrial scenario simulations. We compared the CMIP5 simulations with observations, simple stochastic null hypothesis for the spatial structure of SST variability and against a simulation with a slab ocean that does not simulate any ocean dynamics. This study illustrated a number of interesting modes dominating the Southern Ocean. We list the main findings below:

- First it is important to note that current state of the art CMIP5 simulations have large inconsistencies against the observation and with each other. Our understanding of the leading modes of SST variability is therefore still limited and is likely to have substantial biases. However, using the CMIP5 super model ensemble of all available models does have some advantage in smoothing out model biases and is therefore a good basis for the analysis of the SO SST modes.
- The SST modes of the SO are the most complex of all ocean basins (Wang et al. 2015). They have the largest effective spatial degrees of freedom of all ocean basins and the leading three EOFs only contribute 26% (monthly scale) to 42% (5 years running mean) of the total variance. It implies that higher order modes contribute to the SST variability significantly and are potentially also relevant for understanding the leading modes.
- All three leading modes found in the CMIP5 super model have distinct patterns and time scale behaviour that can not be explained by simple stochastic null hypothesis, like spatial red noise (isotropic diffusion), nor by a slab ocean dynamics. Thus all three leading modes are ocean-atmospheric coupled modes and are likely to be substantially influenced or driven by ocean dynamical processes.
- The first leading mode is described as an annular mode. It is forced by two main drivers: ENSO and SAM. ENSO mainly influences the Pacific part of the mode while SAM impacts the entire basin of the Southern Ocean. The impact of these drivers is much stronger in the CMIP5 simulations than in the slab ocean simulation, suggesting that it is mostly the wind stress forcing that drives the SST variability of this mode. This is also consistent with the

position of the main amplitudes of this mode being at the same locations as the maximum wind variability being associated with the SAM index.

- The second most dominant mode is a basin wide monopole pattern. It transforms from the atmospherically forced three-wave pattern on shorter time scales to an all basin wide mode on multi-decadal time scales. Such a transformation is not observed in the slab ocean simulation suggesting it involves ocean dynamics. A potential candidate for such a transformation could be lateral advection by ocean transport and stochastic resonance with atmospheric forcing. However, it was beyond the scope of this study to understand the details of these processes. This mode further has a very distinct time scale behaviour with a significant increase of variance from the decadal time scales to even longer centennial time scales that is very clearly distinct from the behaviour of the slab ocean simulation. Thus this mode has a lot of power on very long time scales that are strongly related to ocean dynamical processes.
- The third leading mode is a dipole structure in the South Pacific. It also originates from the atmospheric forcing of three-wave pattern, but unlike the monopole pattern its variance is not increasing as much on multi-decadal and longer time scales. However, this pattern appears to have a peak in the power spectrum, suggesting a preferred time scale of oscillation. This mode also has some weak indications of the subsurface ocean temperature leading the evolution of the SST variability on the longer (~10yrs) time scales. This indicates that this mode may be influenced by deeper ocean variability on the longer time scales. There are a few studies about dipole structures in the South Pacific, e.g. Huang and Shukla (2006), Morioka et al. (2013) and Guan et al.

(2014). However, their results actually are parts of the annular mode in north-south direction or monopole mode in the Pacific, which is not the same as this pattern.

- Another question is the possible interactions among these modes. As discussed above, the Annular Mode is partly driven by SAM. On the other hand, the strengthened westerlies caused by positive SAM above the Southern Ocean may alter the ocean circulation pattern and introduce more mixing locally (e.g. Meredith and Hogg, 2006; Boning et al, 2008). These changes might lead to the evolution of the monopole mode and dipole mode in the South Pacific, though the correlation between SAM and these two modes within CMIP5 super ensemble is unclear. Besides, the monopole mode and dipole mode, as they have similar mechanisms and wave train prototypes, might have the out-of-phase relationship. However, the lead-lag correlations are obscure in CMIP5 dataset and the interactions require further studies.

As monopole mode and dipole mode in South Pacific are mainly influenced by ocean dynamics, it is essential to understand the different effects within the ocean. The related phenomenon includes but are not limited to a different zonal wave-3 pattern (van Loon and Jenne, 1972; Raphael, 2004), the ACC advection, ocean diffusion mixing and deep ocean circulation. These factors above have close relationship with each other but are also relatively independent with their own specific period. The interactions between them should be the critical step for a deeper understanding of the modes.

Another important factor is sea ice, which also influences atmospheric circulations substantially and is capable of introducing long-term variability. The ice-sea

interaction affects the SST variability and further influences the spatial structure and temporal variation. As our slab ocean model does not create sea ice variability, the role of sea ice is not fully discussed above. Besides, it is worth reminding that though CMIP5 multi-model ensemble mean gives good climatology and seasonality of sea ice simulation, most CMIP5 historical runs presents negative trends of sea ice extent against observed sea ice increase in last three decade (Shu et al., 2015; Simmonds, 2015; Turner et al., 2015;). Model errors on sea ice trend can be related to model common biases of recent warming hiatus simulation and strong negative cycle of intrinsic variability on multi-decadal and even longer scales (Latif et al., 2013; Martin et al., 2013; Zunz et al., 2013). However, it is beyond the scope of this study to understand the details of these processes, as most of this work is to investigate decadal internal variability based on pre-industrial simulation and linearly detrended observed result without considering linear trend or global warming impact. The sea ice impact requires more detailed numerical model experiments.

Chapter 4

Factors Influencing SST

Variability in the Southern Ocean

As suggested in Chapter 3, there are three main decadal SST modes in the Southern Ocean from CMIP5 output analyses: the annular mode, the basin wide monopole pattern, and the dipole pattern in the southern Pacific. It is also found that these modes are affected by several of factors such as atmosphere forcing, ocean dynamics and possibly sea ice variation. This chapter will go through these elements and check their influences on the spatial features of the coupled variability in detail via sensitivity experiments based on a General Ocean Circulation Model. The results will help us better understand the features and the development of the long-term modes in the Southern Ocean.

4.1 Introduction

The long-term SST variability in the Southern Ocean involves air-sea-ice interactions and all these three media are likely important. In this study, we focus on these three factors in the Southern Ocean climate system and analyse their influences on decadal modes of variability.

Atmospheric forcing is the direct driver of the ocean. Generally, the ocean passively responds to dominant modes of atmospheric variability on shorter time scales (Hasselmann, 1976). For instance, in the Southern Ocean the annular mode is associated with ENSO and SAM, while the basin-wide monopole mode and the southern Pacific dipole pattern are both induced by atmospheric wave-3 patterns. On the other hand, due to its huge heat capacity, the ocean varies on interannual and longer time scales. The low-frequency variability in the ocean is then imprinted onto the atmosphere (Farneti and Vallis, 2009); thus, the atmosphere also keeps some long-term variation signals from oceanic feedback, which may influence the ocean again. These two mechanisms together consist of the large-scale air-sea interaction. We

would like to investigate the contributions of these two mechanisms by looking at the responses of the ocean to alternative atmospheric forcings.

Another important factor is ocean dynamics, which is responsible for the mode transformation and power spectrum increase on longer time scales. We have shown the contrast between the CMIP5 modes and the Slab Ocean modes in Chapter 3. Without ocean dynamics, though Slab Ocean is able to produce similar wave-train modes on the shorter scale, no homogenous-like modes with low-frequency oscillation, e.g. the monopole, could be generated. Thus, ocean dynamics transport the anomalies and transform the modes. In the Southern Ocean, SST anomalies are shown to propagate eastward in the observation, and propagation speed is similar to the zonal velocity of the ACC, suggesting that the ACC carries the SST anomalies (White and Peterson, 1996; Maze et al., 2006; Verdy et al, 2006). The transport of the anomalous signals along with ocean advection may lead to the basin-wide structures of long-term modes in the Southern Ocean.

The last element is sea ice, a fundamental factor in the Southern Hemisphere. The sea ice cover has a high albedo (60%) compared to the low albedo ocean (near 10% for high latitudes), which alters the heat exchanges between atmosphere and ocean (e.g. Hartmann, 1994; Curry et al., 1995). The existence of sea ice insulates the ocean from the cold atmosphere, and sea ice also redistributes the salinity field within the ocean through ice growth and melting (Fletcher, 1969; Walsh, 1983; Rind et al., 1995). Sea ice in Antarctic demonstrates a strong seasonal cycle. It can extend to approximately 50°S in austral winter, but roughly retreats to the Antarctic coastlines in summer. On the interannual time scale, the Antarctic sea ice edge anomaly illustrates similar variability to the SST and is strongly affected by ENSO and SAM (e.g. Carleton

1989; White and Peterson, 1996; Ledley and Huang 1997; Yuan and Martinson, 2000; Lefebvre et al., 2004; Cavalieri and Parkinson, 2008). On the other hand, sea ice growth and melting lead to the dense water mass formation and further drive deep ocean circulation (Jacobs et al., 1970; Orsi et al., 1999; Gordon et al., 2004), which may influence SST variability on decadal and the centennial scale (e.g. Latif et.al, 2013). Given the importance of the sea ice, more research is needed into the role of it on SST modes of variability.

In this chapter presented here we will base our SST variability analyses within the Southern Ocean on sensitivity experiments. The experiments will isolate some essential influences of each element in the Southern Ocean climate system and test roles of them on SST decadal modes of variability by looking at the oceanic responses.

This chapter is organized as follows: Section 4.2 introduces the ocean model we use. Section 4.3~4.5 discuss the influences of atmosphere forcing, ocean dynamics and sea ice in turn based on ocean model experiments. Finally a summary and discussion are provided in section 4.6.

4.2 The HYCOM Ocean Model

HYCOM (HYbrid Coordinate Ocean Model, Bleck, 2002) is a development on the basis of the Miami Isopycnal Coordinate Ocean Model (MICOM). HYCOM uses isopycnal vertical coordinate in the open ocean, reverts to a terrain-following coordinate (sigma coordinate) in the shallow coastal area, and to z-level coordinates in the near-surface mixed layer and unstratified seas for finer vertical resolution (Bleck, 2002; Metzger et al., 2014). The HYCOM model is selected here for Southern

Ocean study, as the hybrid coordinate is suitable to simulate the complex ocean vertical structures in this domain.

An thermodynamic sea ice model is imbedded with the ocean model, where ice grows and melts as a function of heat flux and sea surface temperature without rheology.

The basic equation is

$$\Delta T_i = \frac{F_i - F_a}{(a+b)} \quad (4.1)$$

$$\Delta H_i = -\frac{F_i}{\rho_i L} \cdot \Delta t \quad (4.2)$$

$$C_i = \begin{cases} \frac{H_i}{h_{imn}}, & \text{if } H_i \leq h_{imn} \\ 1, & \text{if } H_i > h_{imn} \end{cases}, \quad (4.3)$$

, where t represents time, T_i is the ice temperature, F_a is the atmospheric net heat flux, $F_i = a(T_w - T_i)$ is the heat flux through the ice which is proportional to the gradient between ice temperature and sea water temperature T_w . a and b are proportionality factors represent the derivatives of air and ice flux, respectively. a can be obtained from the conventional heat flux bulk formula and b usually is chosen to be the ratio of ice thermal conductivity to average ice thickness H_i . ρ_i is the density of sea ice and L is the specific latent heat of the fusion. The ice coverage C_i is simplified as the ratio of average ice thickness H_i to the minimum ice thickness h_{imn} prescribed in the model.

In the thermodynamic sea ice model, the sea ice temperature must not exceed the freezing point until the ice has melted completely (Bleck and Halliwell, 2001). No ice advection or dynamics exists within the sea ice model. As a result, sea ice can only grow or melt locally without moving. This simplification improves the integration

speed of the ocean model, however, the missing ice dynamics may introduce some errors to the model simulation.

The HYCOM experiments have a near-global domain with the latitude limit of 80°S~80°N and closed north/south boundaries, covering most of the global ocean except part of the Arctic. The bottom topography is from the ETOPO5 data. The horizontal resolution is 2.5° and hybrid coordinates are applied vertically with 22 vertical layers. We use non-local K-profile parameterization (KPP) as the boundary layer mixing scheme.

Atmospheric forcing is needed to drive the HYCOM model. Unfortunately, the atmospheric observations can hardly satisfy the requirement as they span only a few decades, not enough for the study on decadal scale. Therefore, we take a long atmospheric output record from a model simulation to force the ocean model. Since our mode results are primarily based on CMIP simulations in Chapter 3, we use long-time integrated CMIP atmospheric output to drive the HYCOM model as well. Here we pick the GFDL-CM3 model, because it is one of the few models that has a long piControl run with the output of all atmospheric variables we need. Besides, GFDL-CM3 is also one of the best models based on model evaluation results in Chapter 2 both in global summary and in the Southern Ocean only (see Fig. 2.8 and Fig. 2.15), and it demonstrates similar modes of SST variability as the CMIP super models (see Fig. 4.2).

We take the 500 years continuous monthly mean output from the GFDL-CM3 piControl scenario and get the atmospheric data including surface wind velocity, near surface air temperature, specific humidity, precipitation and surface heat fluxes. The forcing data are interpolated into the HYCOM model grids and are also used to

calculate the sensible/latent heat flux and wind stress via non-constant bulk parameterization scheme during the model integration.

The model starts from a static initial condition with Levitus climatology temperature and salinity fields (Monterey and Levitus, 1997). Firstly the model is forced climatologically for 30 years to reach the equilibrium in the ocean surface. From the 31st year, the real-time GFDL-CM3 atmospheric data starts to drive the model for 500 years as the control run (hereinafter CONTROL. See table 4.1 for abbreviations of all experiments).

Table 4.1 List of all HYCOM experiments

Experiment Abbreviation	Description
CONTROL	Control run with GFDL-CM3 atmospheric forcing
ATMOS-HIGH-PASS	5yr high-pass filter applied to the atmospheric forcing
ATMOS-NOISE	Stochastic atmospheric forcing
OCEAN-PACIFIC	Pacific sector forced by GFDL-CM3 atmospheric forcing, the other sector driven by monthly climatology forcing
OCEAN-ATLIND	Atlantic-Indian Ocean sector forced by GFDL-CM3 atmospheric forcing, the other sector driven by monthly climatology forcing
ICE-BLOCKED	Region south to 65°S are replaced with land
ICE-CLIM	open boundary at 60°S with climatology relaxation in the ocean

Here we compare the CONTROL SST simulation to the GFDL-CM3 output in CMIP5 dataset to evaluate the HYCOM model result. Fig. 4.1a-b shows the global annual mean SST distributions. Both the CONTROL and GFDL-CM3 clearly illustrate the correct meridional and zonal SST gradients, and the SST patterns are similar to each other except the CONTROL slightly overestimates the SST especially in the higher latitudes. Similarly the SST annual mean standard deviations (STDV) are shown in Fig. 4.1c-d. Here the HYCOM model simulates similar variance distribution as GFDL-CM3, but still some bias exists especially in the Southern

Ocean. The CONTROL SST has stronger variation in the southeastern part of Pacific, in the southern Indian Ocean and in the middle latitudes of South Atlantic.

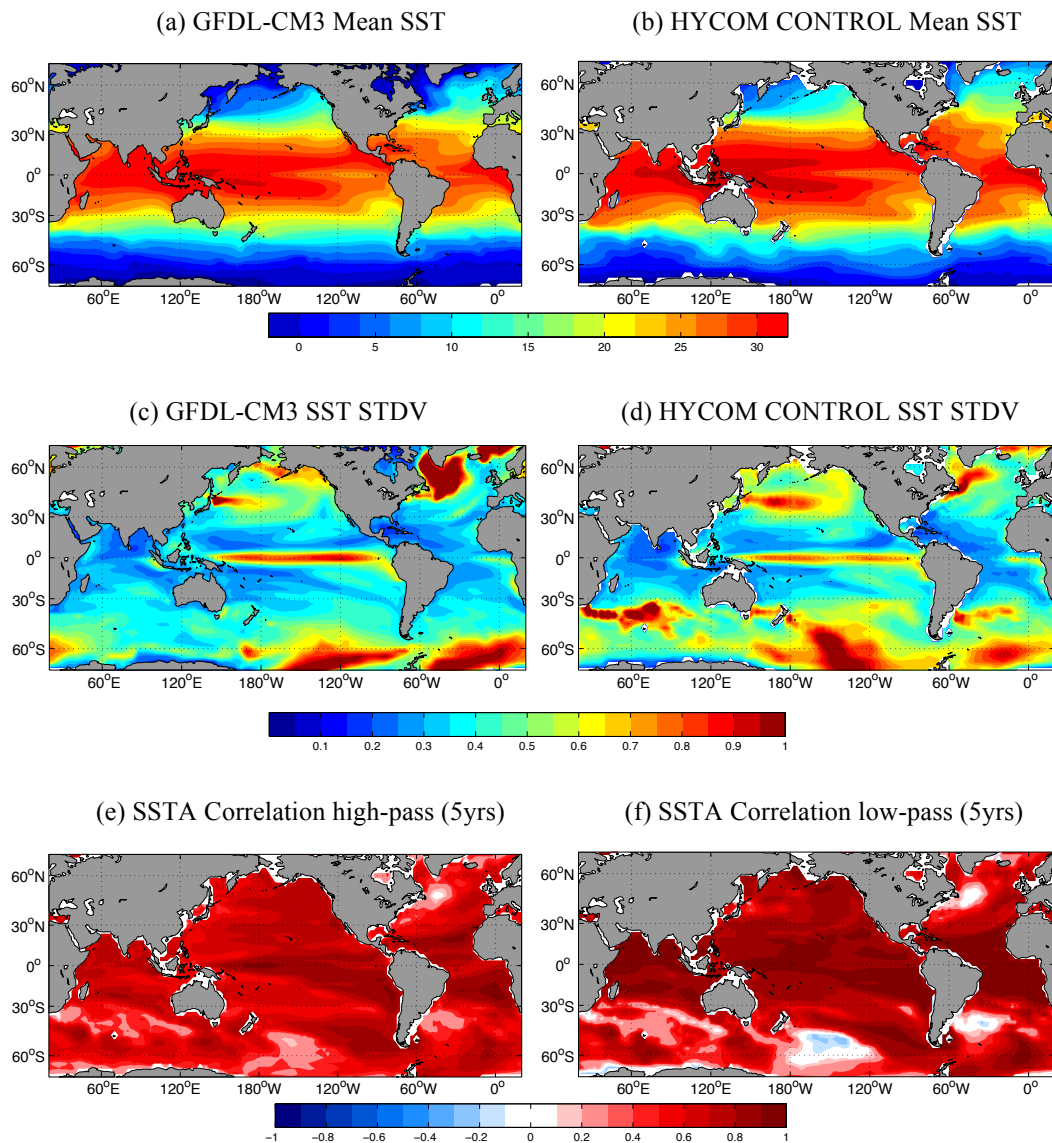


Fig. 4.1 (a) Mean field of SST for GFDL-CM3; (b) same as (a) but for HYCOM CONTROL; (c) Standard deviation field of annual mean SSTA for GFDL-CM3; (d) same as (c) but for HYCOM CONTROL; (e) SSTA Correlation between GFDL-CM3 and HYCOM CONTROL after 5yr-high-pass filter; (f) same as (e) but after 5yr-low-pass filter.

The correlations of SST anomalies are illustrated in Fig. 4.1e (for 5yr high pass filter SST) and Fig. 4.1f (for 5yr low pass filter SST). If CONTROL perfectly simulates the SST variability in GFDL-CM3, the correlations are supposed to be close to one

everywhere. For the high pass comparison, the correlation field is mostly covered by the values larger than 0.7, suggesting that the high-frequency SST variability is well reproduced in the HYCOM model. However, for the low pass comparison, similar to the STDV bias distribution, the correlation is not significant in some regions of the Southern Ocean. It is notable that these areas with larger differences are located in the path of the ACC and has strong seasonal variability of the mixed layer depth (e.g. Sallée et al., 2013). As long-term SST variability is strongly affected by the ocean internal variation and ocean dynamics, it is likely that the errors come from the bias of ACC and mixed layer depth simulations. We have also forced the HYCOM model with other CMIP5 model atmospheric outputs and got similar error in the Southern Ocean. Therefore, the errors are mostly caused by the HYCOM model itself.

Comparison of the leading EOF modes is shown in Fig. 4.2 between CONTROL and the GFDL-CM3 based on annual mean analysis. Apparently CONTROL has successfully reproduced most of the leading modes with similar spatial structures as the GFDL-CM3 ones. EOF-1s are the both annular modes but more focus on the high latitudes. Both EOF-2s shows maximum anomalies in the high latitudes Atlantic and Indian Ocean, similar as the prototype of the monopole pattern in CMIP5 super model. However, the distribution of CONTROL EOF-2 is more chaotic. It demonstrates too large amplitudes in the Southern Indian Ocean and South Pacific, associated with the SST variability simulated errors. The EOF-3s are also similar to each other, both having positive anomalies along the middle latitudes and negative anomalies in the middle of South Pacific, though again the CONTROL one tends to have stronger variability along the ACC in South Atlantic and Indian Ocean.

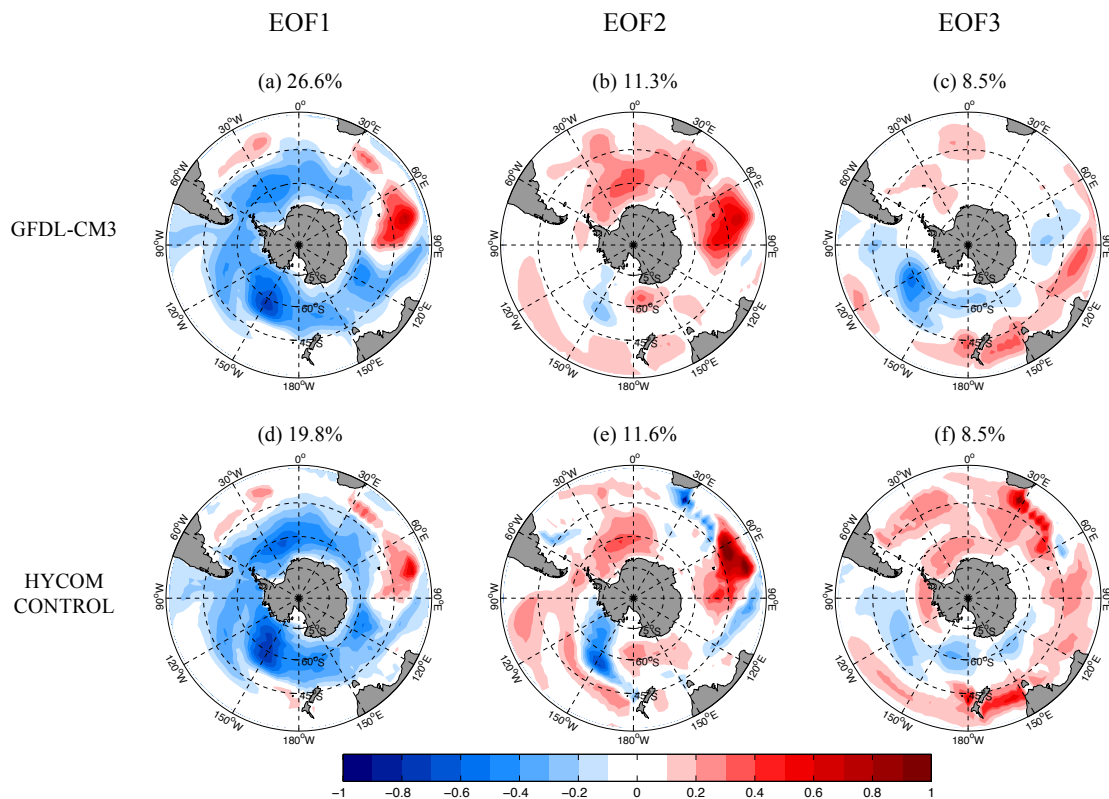


Fig. 4.2 First three leading EOF patterns of annual mean SSTA for (a-c): GFDL-CM3; (d-f): HYCOM CONTROL. The values in the headings of each panel are the explained variances of each EOF-mode.

The corresponding pairs of PC time series are also compared. The correlation between the PC-1s is larger than 0.9, while the PC-2s and PC-3s also highly correlated with correlations over 0.7 (statistically significant with 99% confidence). Thus, in spite of the mean-state SST errors, SST modes of variability are successfully reproduced in CONTROL from the GFDL-CM3. We will take CONTROL as a reference and compare it with sensitivity experiment results in the following sections.

4.3 Atmospheric forcing

In this section we test the influence of atmospheric forcing on SST modes of variability. In Chapter 3 we have discussed some impacts of the atmospheric forcing. ENSO affects the Southern Ocean especially in the South Pacific via teleconnection

and mainly exerts its impact on the annular mode. Similar effect of SAM but it influences the entire Southern Ocean domain. The wave train patterns also drive the basin-wide monopole mode and the dipole pattern in South Pacific. It is interesting to see whether the ocean can still produce similar long-term SST modes of variability with weaker or disturbed atmospheric forcing patterns. Here two experiments are applied to test the role of the atmospheric forcing.

Firstly we take the 500 years (6000 months) GFDL-CM3 output data and make the 5yr high-pass filter for each atmospheric variable. Thus, only high-frequency signals with timescales shorter than 5 years will be taken from the forcing data to drive the ocean model. This experiment is referred to as ATMOS-HIGH-PASS. After filtering, the monthly STDV of the forcing data reduced by 3%. This experiment aims to test the impact of high-frequency forcing part of the atmosphere.

Another experiment is based on random forcing (hereafter as ATMOS-NOISE). We shuffled 6000-month anomalies randomly from GFDL-CM3 and generate a stochastic forcing data set. In this manner, the new forcing data set consists of the shuffled monthly anomaly plus the monthly climatology. The spatial patterns of the atmospheric forcing are maintained but without temporal evolutions. This run is to check the influence of developments of forcing patterns in the atmosphere.

Fig. 4.3 illustrates the standard deviations of annual mean SST for ATMOS-HIGH-PASS and ATMOS-NOISE. Though the STDV spatial structures are well kept, clearly both experiments dramatically reduce the SST fluctuation globally compared to CONTROL (Fig. 4.3c-d). One interesting feature is that in the ATMOS-HIGH-PASS, the strong SST variability in the equatorial Pacific reduces significantly, implying ENSO gets much weaker in this experiment. In the Southern Ocean, the

STDV dropped by more than 20%, while the Atlantic sector becomes the most affected region and loses about 50% of the STDV. Thus, a substantial fraction of the SST variation cannot be generated in absence of the atmospheric pattern evolution or low-frequency forcing part.

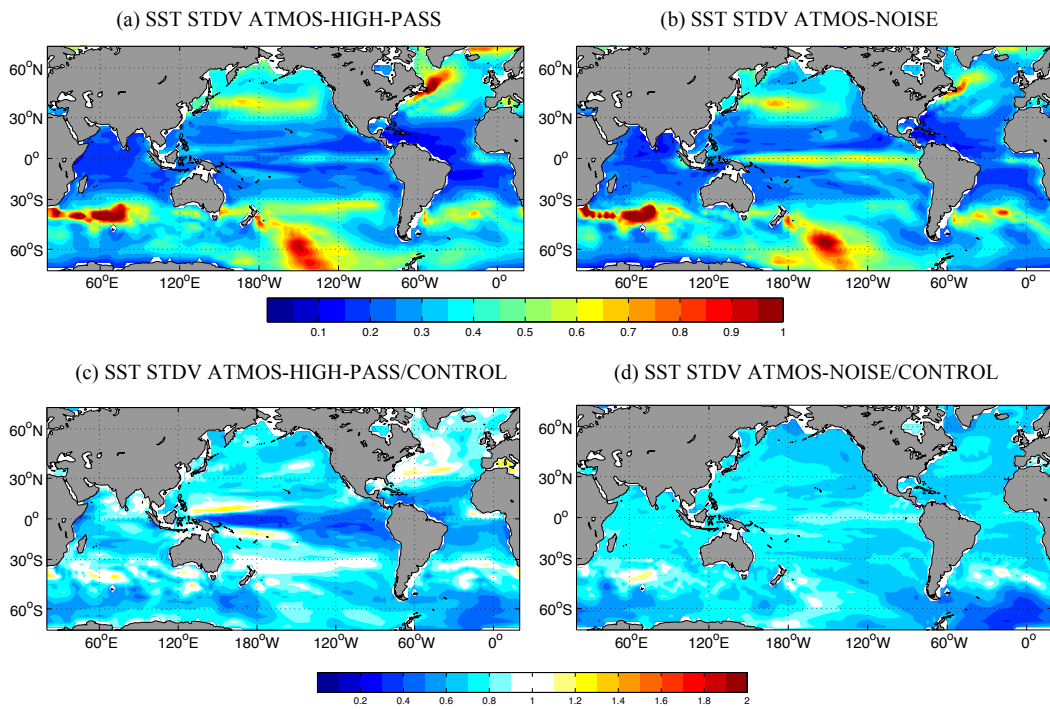


Fig. 4.3 (a): Standard deviation field of annual mean SSTA for ATMOS-HIGH-PASS; (b): same as (a) but for ATMOS-NOISE; (c): the ratio of ATMOS-HIGH-PASS to CONTROL for annual mean SSTA standard deviation; (d) same as (c) but for ATMOS-NOISE to CONTROL.

We also take a closer look at the leading EOF modes for ATMOS runs in Fig. 4.4. Generally, the ATMOS modes are weaker and more chaotic than CONTROL. Their connections to the CONTROL modes are not quite clear as the spatial structures in ATMOS modes can hardly be recognized. The ATMOS EOF-1 and EOF-2 also demonstrates large oscillation amplitudes in high-latitude Pacific and middle-latitude Indian Ocean as the CONTROL modes, however, the differences are still obvious due to the lack of basin-wide structure of the ATMOS modes. ATMOS-NOISE EOF-3 becomes a complete random wave pattern. Its counterpart in ATMOS-HIGH-PASS

illustrates similar two-band structure in South Pacific as the CONTROL EOF-3, but again its mid-latitude band does not extend to the entire basin.

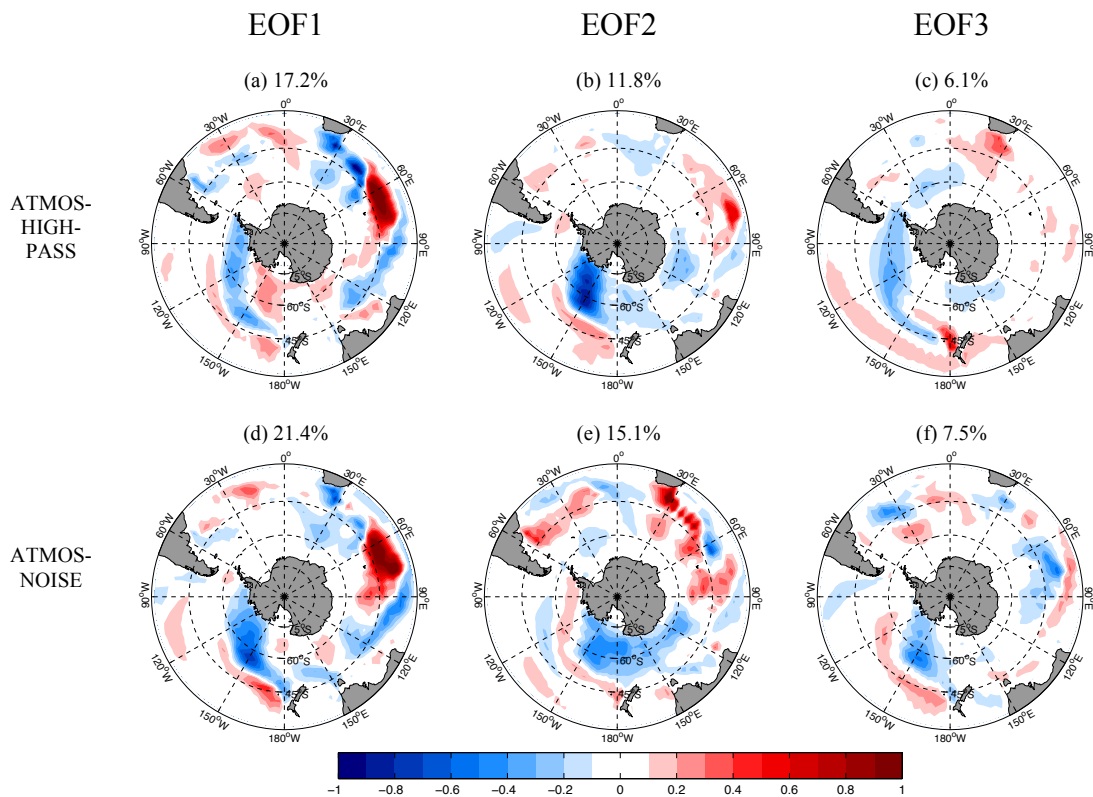


Fig. 4.4 First three leading EOF patterns of annual mean SSTA for (a-c): ATMOS-HIGH-PASS; (d-f): ATMOS-NOISE. The values in the headings of each panel are the explained variances of each EOF-mode.

The DEOF patterns are shown in Fig. 4.5 to further quantify these differences. Clearly most of the leading DEOFs duplicate the leading CONTROL modes in Fig. 4.2d-f. This suggests that the ATMOS experiments cannot reproduce the leading modes with enough variance. The exceptions are both DEOF-2. DEOF-2 for ATMOS-HIGH-PASS mostly focuses in the South Atlantic, consistent with the SST STDV reduction compared to CONTROL. ATMOS-NOISE DEOF-2 is mostly like a dipole pattern around the Antarctic, which does not appear in the leading CONTROL modes but is consistent with the further evolution of the dipole pattern in south Pacific (see Fig. 3.5i).

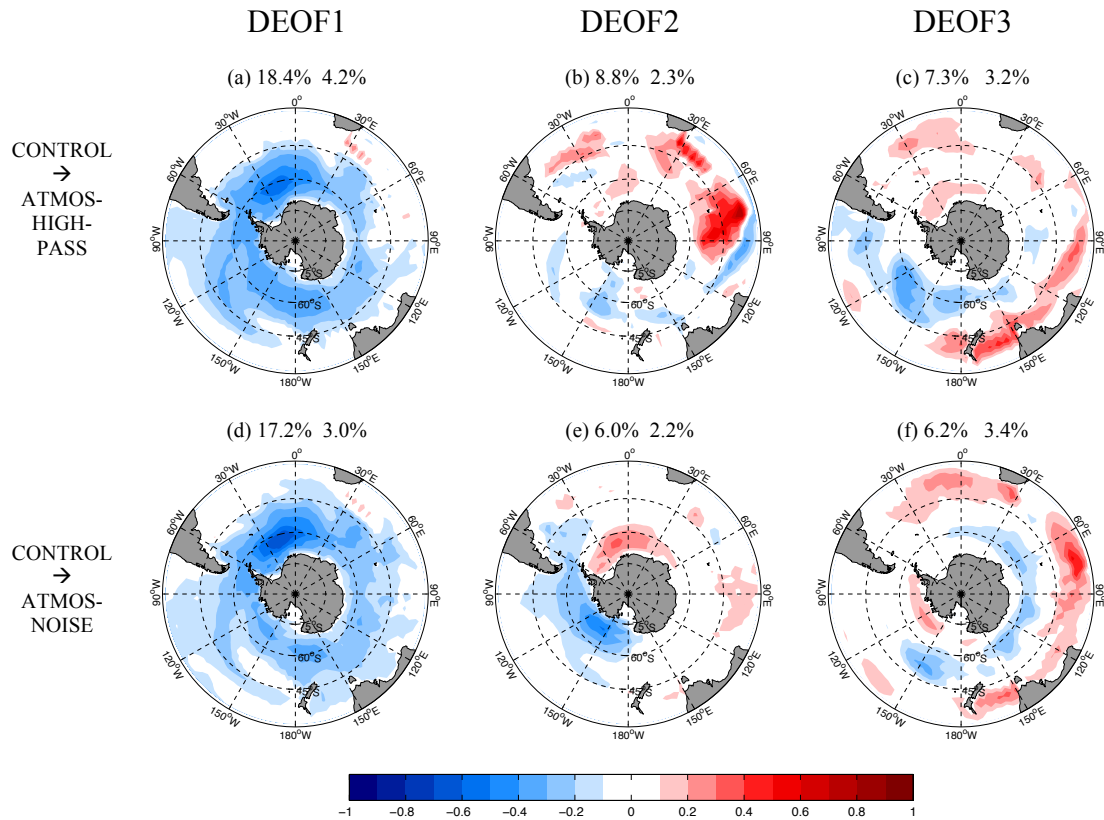


Fig. 4.5 (a-c): Leading DEOF patterns of annual mean SSTA CONTROL projection to ATMOS-HIGH-PASS; (d-f) Leading DEOF patterns of annual mean SSTA CONTROL projection to ATMOS-NOISE. The headings show the explained variances of the DEOF-modes in the CONTROL (first value) and the ATMOS-HIGH-PASS or ATMOS-NOISE (second value), respectively.

Overall, these two ATMOS experiments do not reproduce the leading modes in CONTROL. On one hand they underestimate the SST variance in the entire basin; on the other hand they cannot produce similar homogeneous-like modes. Thus, if we remove long-term variability in the atmosphere or totally disturb the atmospheric forcing signals, real coupled variability patterns will get greatly weakened or disappear.

The mechanisms are easy to understand. In the ocean model, SST is directly modulated by the surface heat flux. The adjusted latent and sensible heat flux lead SST close to the near-surface air temperature. In both ATMOS experiments, SST anomalies are damped by more turbulent surface heat flux and reduce their oscillation

amplitudes. In ATMOS-HIGH-PASS, the strong damping even significantly weakens the variability in the equatorial regions. The forcing in ATMOS-NOISE becomes stochastic and limits the development of long-term SST modes.

On the other hand, these two experiments both weaken the long-term signals in the atmospheric forcing. The low-frequency variability in the atmosphere mainly comes from oceanic feedback, which is the fundamental result of air-sea interaction. The ocean maintains the long-term variation and imprints the signals into the atmosphere, while these variations kept in atmosphere further affects the ocean again (Hasselmann, 1976). In the ocean model, these influences of the interactions are mostly prescribed in the surface heat flux input data. If these interactive signals are removed like in the ATMOS experiments, then the SST modes of variability will change dramatically. Thus, the air-sea interaction and two-way feedbacks are essential to create the modes and amplify their intensity.

4.4 Ocean Dynamics

This chapter will test the role of ocean horizontal advection, as it is likely responsible for the anomaly transport and mode transformation. The global ocean is divided into two parts: the Pacific part (120°E-60°W) and the Atlantic-Indian Ocean part (60°W-120°E). Then two parts of the ocean are driven by different atmospheric forcing schemes. One experiment (OCEAN-PACIFIC) is to drive the Pacific part with original atmospheric forcing as the CONTROL, and forces the rest of the ocean using the climatological monthly forcing data. Another experiment (OCEAN-ATLIND) is precisely the opposite of OCEAN-PACIFIC as varying forcing applies to the Atlantic-Indian Ocean part in O2. Climatology atmospheric forcing cannot introduce any long-term variability to the ocean directly; therefore, if any low-frequency anomalies exist

in the climatology-forced region, it must be transported from the varying forced region via ocean dynamical effects.

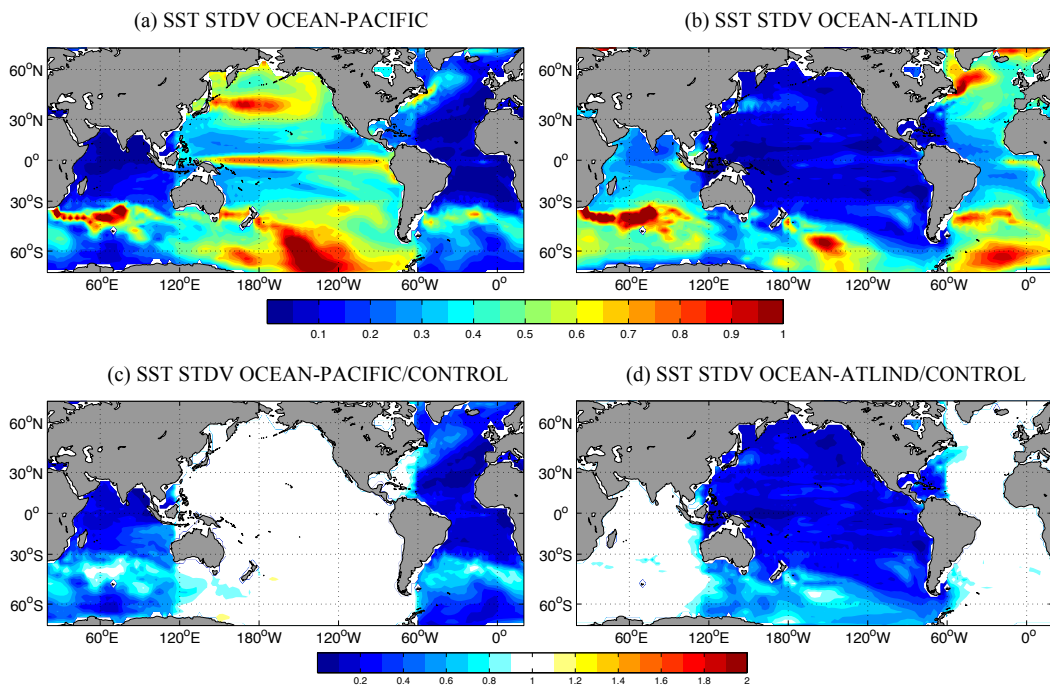


Fig. 4.6 (a): Standard deviation field of annual mean SSTA for OCEAN-PACIFIC; (b): same as (a) but for OCEAN-ATLIND; (c): the ratio of OCEAN-PACIFIC to CONTROL for annual mean SSTA standard deviation; (d) same as (c) but for OCEAN-ATLIND to CONTROL.

Again we firstly look at the annual mean STDV for these two experiments shown in Fig. 4.6. Clearly the STDV fields lose their structure in the tropics and Northern Hemisphere within the climatology-forced sectors, where STDV significantly reduces by around 90%. However, it is totally different within the Southern Ocean. The hot spot areas with large STDV still exist, e.g. South Pacific and South Atlantic, and most of the Southern Ocean is only weakened by 10% within the climatology-forced region. Thus, the ocean dynamics indeed strongly contribute as the variability transportation media in the Southern Ocean.

We further check the SST correlation with CONTROL (Fig. 4.7). To focus on the decadal variation, 5yr-low-pass filter is applied for the SST prior to the correlation.

Theoretically without external impact, the correlation in the climatology-forced region should be 0, and varying-forced sector should be 1. As might be expected, the correlation is either 0 or 1 in most regions in the tropics and Northern Hemisphere. Some exceptions exist where strong ocean currents flow through the interface, like the Kuroshio Extension area, Gulf Stream region and Indonesia Throughflow related region.

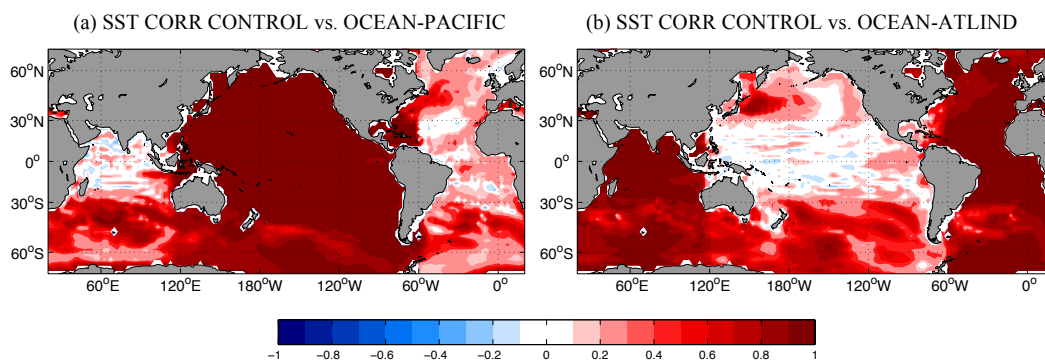


Fig. 4.7 Annual mean SST correlation after 5yr-low pass filter between CONTROL and (a): OCEAN-PACIFIC; (b): OCEAN-ATLIND.

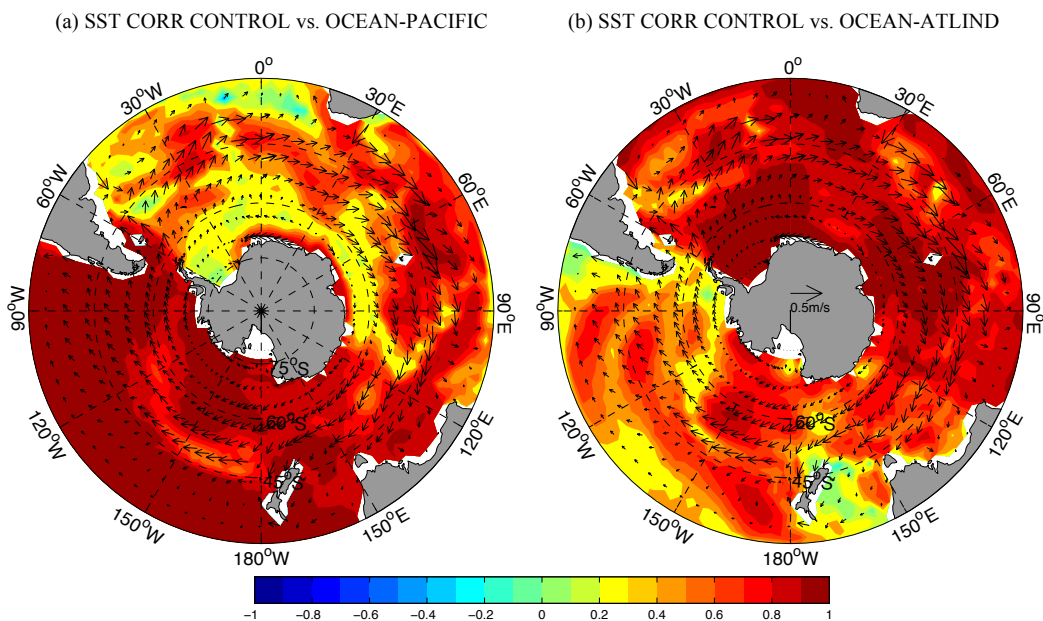


Fig. 4.8 Same as Fig. 4.7 but for extratropical Southern Hemisphere only with climatological annual mean surface current field in CONTROL run.

In the Southern Ocean we can also see the traces of the ACC clearly where it increases/decreases the correlation in the non-varying/varying-forced domain (see Fig.

4.8). Therefore, the horizontal advection acts as the main element transporting the long-term variability. The anomaly transport within the ocean connects each grid of the ocean and facilitates their coherent changes. The similar temporal variability within adjacent grids ultimately creates the homogenous-like basin-wide coupled modes.

4.5 Sea Ice

Two experiments are designed in this section to investigate the influence of sea ice on SST variability. The first one (ICE-BLOCKED) is a simulation without most sea ice domain. We replace the sub-polar ocean (South to 65°S) with solid boundary. As a result, no flux exchanges along the 65°S section interface, and most of the sea ice regions get blocked within the Southern Ocean. This experiment is to reveal how SST variability responses to the existence of sea ice.

The second experiment (ICE-CLIM) is improved on the basis of ICE-BLOCKED, as ICE-BLOCKED may significantly change the circulation pattern. The solid boundary is replaced by an open boundary at 60°S with climatology relaxation, where the temperature and salinity in the ocean is restored to the monthly climatology south to 60°S. As a result, only the seasonality is kept within the sea ice and it cannot actively produce any fluctuation longer than annual scale. This experiment can help us understand to what extent the sea ice variability influences SST variability.

Fig. 4.9 depicts the STDV in ICE-BLOCKED and ICE-CLIM, and the comparisons against CONTROL. Within ICE-BLOCKED, the impact from the missing domain spreads most of Southern Ocean with 5%~10% STDV reduction, and even to 30% in the South Pacific, but have no influence for the rest of global ocean north to 30°S.

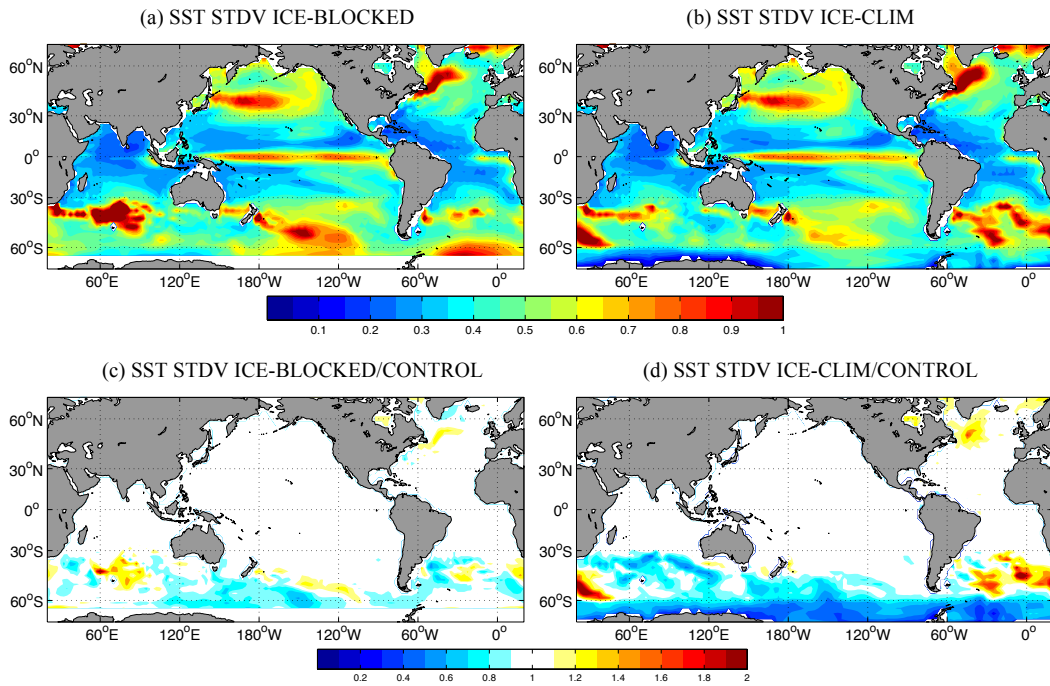


Fig. 4.9 (a): Standard deviation field of annual mean SSTA for ICE-BLOCKED; (b): same as (a) but for ICE-CLIM; (c): the ratio of ICE-BLOCKED to CONTROL for annual mean SSTA standard deviation; (d) same as (c) but for ICE-CLIM to CONTROL.

Similar is the ICE-CLIM result. It also shows the attenuation of SST fluctuation in the middle latitudes. However, the Southeast Atlantic sector has the enhanced oscillation by 10~40% within 30°S-60°S. Surprisingly corresponding STDV increase is also found in the Northwest Atlantic. The mean SST field in Southeast Atlantic is higher than CONTROL (see Fig. 4.10), suggesting less sea ice in this region leading to stronger SST fluctuation. Likely the cut off the Weddell Sea ice variability changes the ice coverage in the South Atlantic, which alters the generation of deep denser water masses, and further influences the water mass transport with Atlantic meridional overturning circulation and the sea temperature in the Northern Hemisphere.

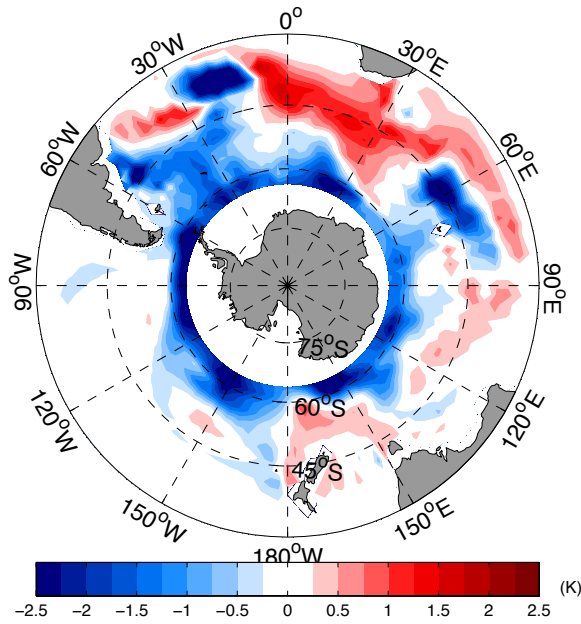


Fig. 4.10 Mean SST difference between ICE-CLIM and CONTROL.

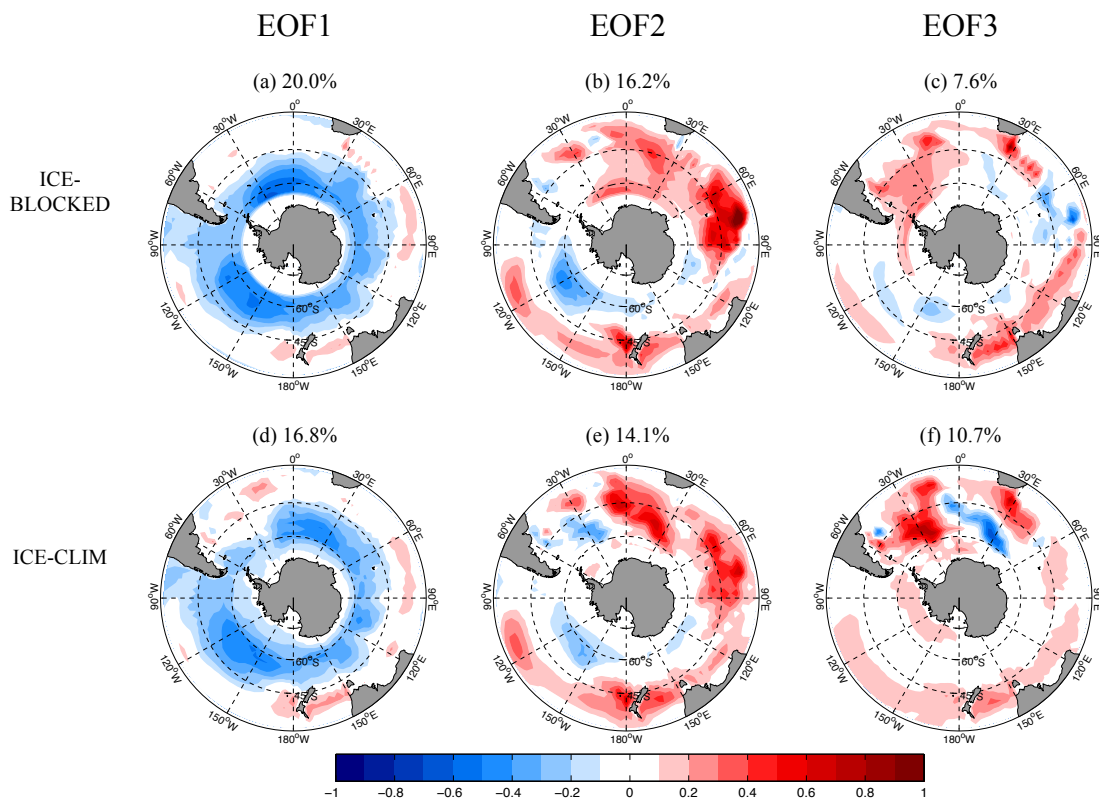


Fig. 4.11 First three leading EOF patterns of annual mean SSTA for (a-c): ICE-BLOCKED; (d-f): ICE-CLIM. The values in the headings of each panel are the explained variances of each EOF-mode.

The leading EOFs for ICE experiments are shown in Fig. 4.11. Both experiments demonstrate similar patterns as CONTROL ones and their spatial structures seem

more smoothly distributed. Both EOF-1s illustrate the annular pattern. The chaotic wave-like structure in CONTROL EOF-2 does not exist in the ICE modes, as the EOF-2s here connect the positive anomalous centres together in South Atlantic and Indian Ocean and only show a simple negative anomalous centre in the high-latitude Pacific. EOF-3s of ICE experiments are similar to the CONTROL one except ICE-CLIM one demonstrates large variation amplitude in the Atlantic, which corresponds to the ice coverage changes within that region.

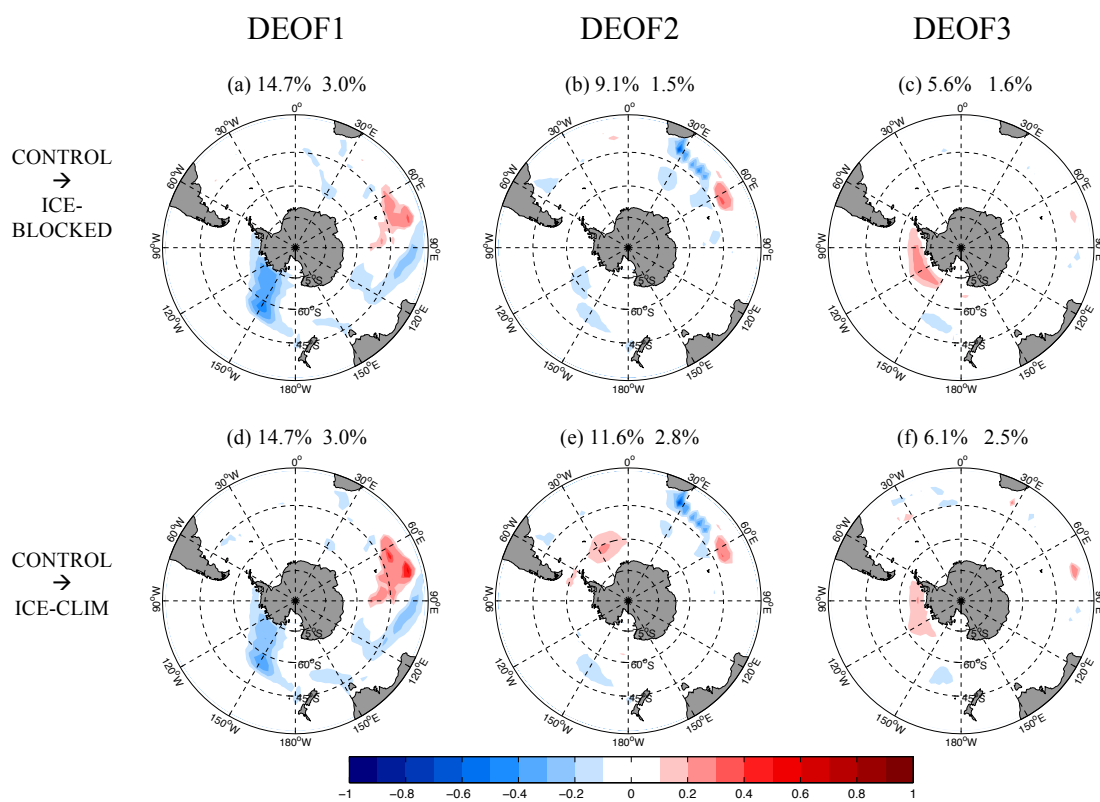


Fig. 4.12 (a-c): Leading DEOF patterns of annual mean SSTA CONTROL projection to ICE-BLOCKED; (d-f) Leading DEOF patterns of annual mean SSTA CONTROL projection to ICE-CLIM. The headings show the explained variances of the DEOF-modes in the CONTROL (first value) and the ICE-BLOCKED or ICE-CLIM (second value), respectively.

Again the DEOFs are shown in Fig. 4.12. Clearly all the DEOF patterns are much weaker compared to the amplitudes of the EOFs, implying there are no substantial

differences between ICE modes and CONTROL modes. The DEOFs mostly focus within the high-latitude Pacific, namely the wave structure in CONTROL EOF-2, where the SST variability is prescribed in the ICE runs. Other biases are mainly located within the Indian Ocean, which is likely affected by the changes of ice coverage and SST mean status there. Thus, the ICE experiments do not dramatically alter spatial structures of the SST modes.

Overall, our experiments suggest sea ice has limited influences on SST modes of variability. Therefore, though the sea ice coverage and sea ice variability are able to influence the standard deviation distribution of the SSTA, they does not substantially change the spatial features of the coupled modes of variability.

4.6 Summary and Discussion

In this chapter we discussed the influences of the climate system factors on Southern Ocean coupled variability based on sensitivity experiments. These sensitivity experiments are built on some hypotheses of weakening or separating the impacts of individual elements in the Southern Ocean climate system. We compared the SST variability and spatial structures of leading SST modes within different experiments, and tested the roles of atmospheric forcing, ocean dynamics and sea ice variability in the Southern Ocean. We list the main findings below.

- The HYCOM model is capable of simulating leading SST modes in the Southern Ocean. The CONTROL run successfully captures most features of the SST variability as the GFDL-CM3.
- The atmospheric forcing is essential for mode generation. Without low-frequency forcing or pattern evolution in the atmosphere, most SST modes

demonstrate chaotic wave-like structures and no realistic SST modes of variability can be generated. Atmospheric forcing not only induces the sea surface fluctuation directly but also intensifies the SST variability on longer time scales via air-sea interaction.

- Ocean dynamics is the main factor for mode transformation. The ocean horizontal advection transports the SST anomalies signals eastwardly along the ACC and creates the homogeneous-like spatial patterns.
- Sea ice variability does not essentially influence the mode generation or development. Without sea ice variability or sea ice region, the SST modes hardly change their spatial structures. However, the interaction between sea ice and ocean is able to affect the strength of the long-term SST fluctuation. Without sea ice variation the SST fluctuation amplitude gets smaller in most regions of Southern Ocean.

As a result, the coupled modes in the Southern Ocean are primarily influenced by atmosphere and ocean. The atmosphere acts as the direct driver and the ocean itself modulates the long-term variability, while their interactions further intensify the modes of variability. Given the complexity of the ocean dynamical processes, we only designed simple experiments like OCEAN-PACIFIC and OCEAN-ATLIND to verify the impact of ocean advection. However, the ocean dynamics in the Southern Ocean cannot be only created by ACC, while other factors may also contribute such as ocean eddies and ocean diffusion. It is difficult to separate the SST anomalous transport with ocean circulation and with other momentums.

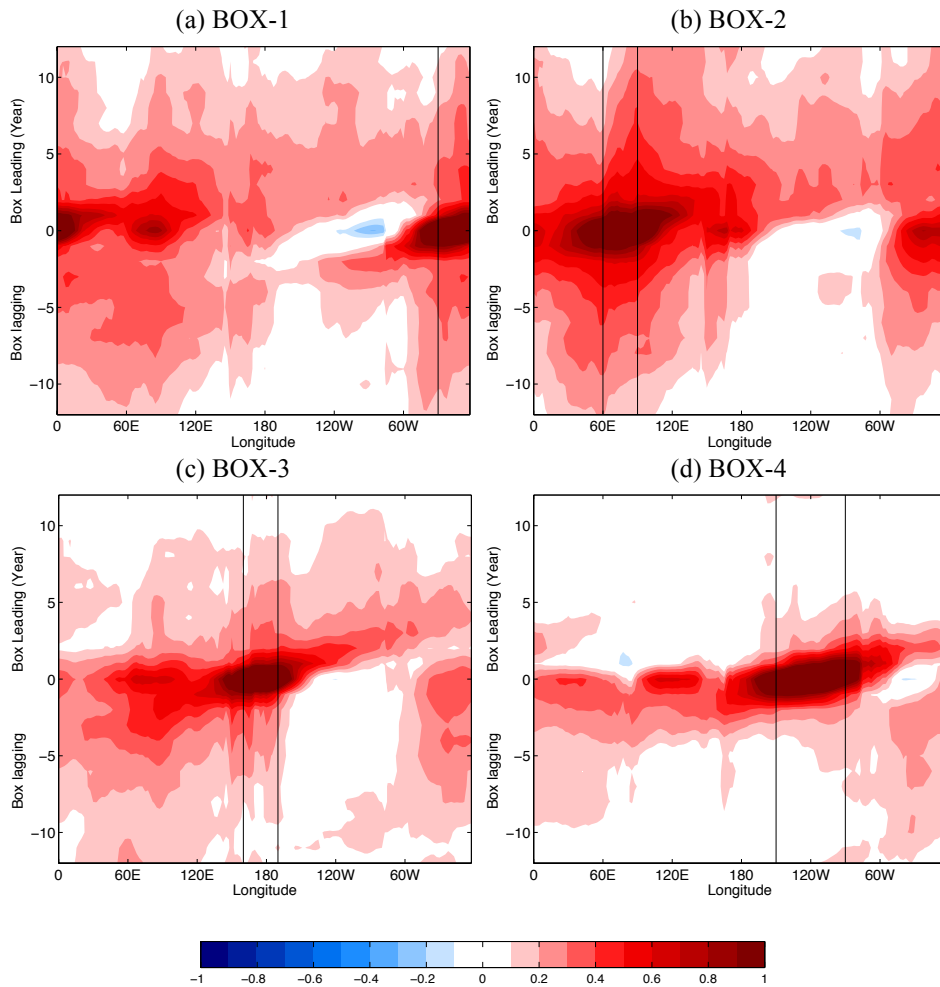


Fig. 4.13 Lead-lag correlation on annual mean sea surface temperature anomalies (SSTA) between meridionally averaged SSTA within 40°-60°S and box averaged SSTA for (a): Box-1, 0-30°W, 40°S-60°S; (b): Box-2, 60°-90°E, 40°S-60°S; (c): Box-3, 160°E-170°W, 40°S-60°S; (d): Box-4: 150°W-90°W, 40°S-60°S. The black lines show the boundaries of each box.

To further test the propagation speed of the SSTA, four boxes are chosen which correspond with the maximum anomalous centres in annual mean EOF-2 of CMIP5 super model. Fig 4.13 demonstrates the lead-lag correlation between box averaged SSTA and meridionally averaged SSTA within 40°-60°S. Clearly the box-averaged SSTA anomalies travel the globe eastward in about 4~5 years, synchronous with the ACC, suggesting most advection is dominated by the ACC.

Another problem is the HYCOM model errors. It is worth noting that the ocean model can only passively receive the forcing from the air. As a result, in the ocean model simulation, no direct air-sea interaction is included. The input atmospheric errors can be accumulated all the time, which introduces biases of the simulation. Another error source, as we have discussed, is sea ice. The imbedded Sea ice model lacks ice dynamics and cannot produce sea ice rheology. Though the temperature/salinity flux can be exchanged between water and ice, it is still not enough to explain all of the near-polar SST/salinity variation or water mass formation. The drawback of the sea ice model also decreases the accuracy of the comparisons between CONTROL and ICE runs. Thus, more complex numerical models are required for the more accurate quantitative study.

Chapter 5

Mechanism of Long-term

Variability in the Southern Ocean

We have discussed some of the temporal variability of the coupled modes in the Chapter 3. The evolutions of these modes actually demonstrate similar spectral features. The diagram in Fig. 5.1 illustrates the spectrum of annual mean monopole mode. The features can be summarized as two aspects: (1). Generally the spectrum keeps increasing as the frequency decreases, thus the low-frequency section surpasses the high-frequency variance significantly. (2) The spectrum does not exactly follow the red noise process. It increases to the interannual scale first and keeps flat on decadal scale. Then it rises up again on multi-decadal scale until it gets stable again.

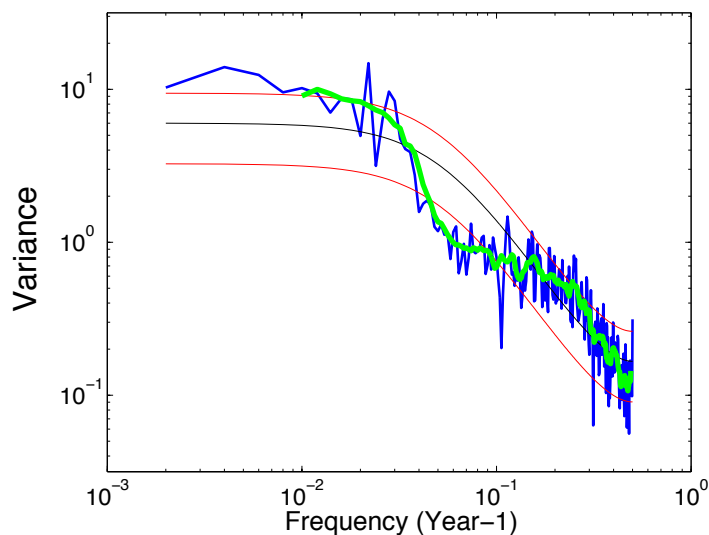


Fig. 5.1 Spectrum of normalized time series of EOF-2 of CMIP5 super model annual mean SSTA (as in Fig. 3.5d-f). The green curve is smoothed result for the blue curve after 5-point moving average. The black line is the red noise fit to the time series and the red lines mark the 95% confidence interval relative to the red noise.

These two features, for their relative low-frequency oscillating properties, are likely related to the ocean rather than atmosphere. In the internal ocean, the large heat capacity is likely leading to the strong long-term temperature variation. On the other hand, the ocean dynamics, as suggested in Chapter 4, transport the anomalous signals and possibly cause the modulation of the power spectral structure of SST variability.

In this chapter, we will focus on these two features and try to find out the their mechanisms. Section 1 analyses the impact of mixed layer heat capacity on the power spectral distribution and explain why the long-term variation is dominant in the Southern Ocean. Idealized HYCOM experiments are applied in section 2 to test the role of ocean advection on SST spectral structures. Section 3 builds a simple 1-dimensional ocean model to further verify the results in section 2. At last the section 4 provide a summary and discussion.

5.1 Mixed Layer Depth

The ocean mixed layer plays a critical role in long-term climate variability as it mediates the exchange of mass, momentum and heat between the air and sea (Mellor and Durbin, 1975). Because of the high heat capacity of water, it is a heat reservoir and acts like a flywheel, which makes the ocean gain or lose heat slowly. The deeper the mixed layer, the more heat capacity.

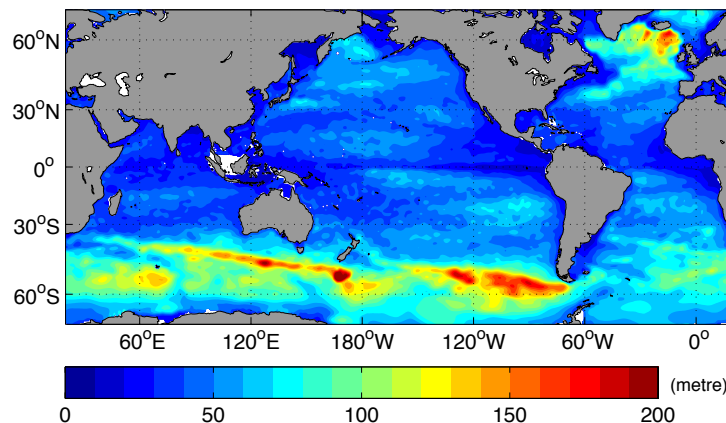


Fig. 5.2 Climatological annual mean mixed layer depth based on IFREMER/LOS Gridded Data.

Fig. 5.2 depicts the global distribution of climatological mean mixed layer depth (MLD) from Ifremer data set (de Boyer Montégut et al, 2004). Most of the deep mixed layer regions are accompanied with strong ocean currents and caused by strong Ekman pumping and mixing. In the Southern Ocean, due to the strong westerly wind

stress shear, the MLD ranges from 100m to 300m and is much deeper than the rest of the global ocean (Sallée et al., 2008; Sallée et al., 2013). The deep mixed layer may be the key element to maintain the internal long-term variability within the Southern Ocean.

To test this hypothesis, the slab ocean model experiments here are utilized to test the thermodynamical influence of mixed layer depth on SST long-term variation. We designed three experiments with different MLDs. SLAB-50 is the experiment we have shown in Chapter 2&3 with constant MLD of 50m. In experiment SLAB-200 the depth is increased to 200m everywhere in the ocean, which is around averaged value in the Southern Ocean but much larger in other regions. Experiment SLAB-CLIM has the same MLD distribution as the Ifremer climatology. Except for MLD, all experiments have same configurations and are integrated for 200 years.

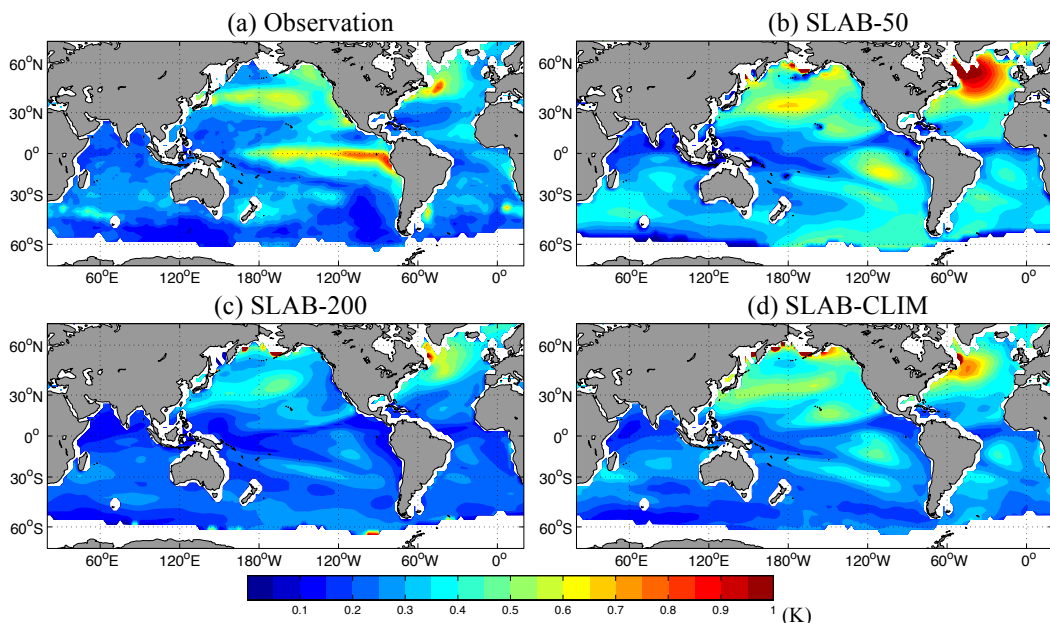


Fig. 5.3 Standard deviation field of annual mean SSTA for (a): HadISST (1901-2014); (b): SLAB-50; (c): SLAB-200; (d): SLAB-CLIM.

Firstly the annual mean SST STDV fields are shown in Fig. 5.3 for each experiment and the observation (derived from HadISST). The SLAB-50 overestimates the STDV

in most regions with the shallower mixed layer than the climatology. Especially in the Southern Ocean where the real mixed layer is deep, the amplitude of STDV in SLAB-50 is almost twice larger than the observed. SLAB-200 shows similar STDV values to the observed in the Southern Ocean but gets smaller STDV elsewhere, which is exactly opposite of SLAB-50. With the correct MLD structure, SST STDV distribution of SLAB-CLIM seems to be the closest to the observation though it overestimates the STDV along the equatorial cold tongue region probably due to the bias on ENSO variability. Thus, shallower mixed layer is associated with stronger SST STDV and vice versa, which well matches the heat capacity of ocean mixed layer. Deeper mixed layer has larger heat capacity and the well-mixed temperature within it is less likely to change.

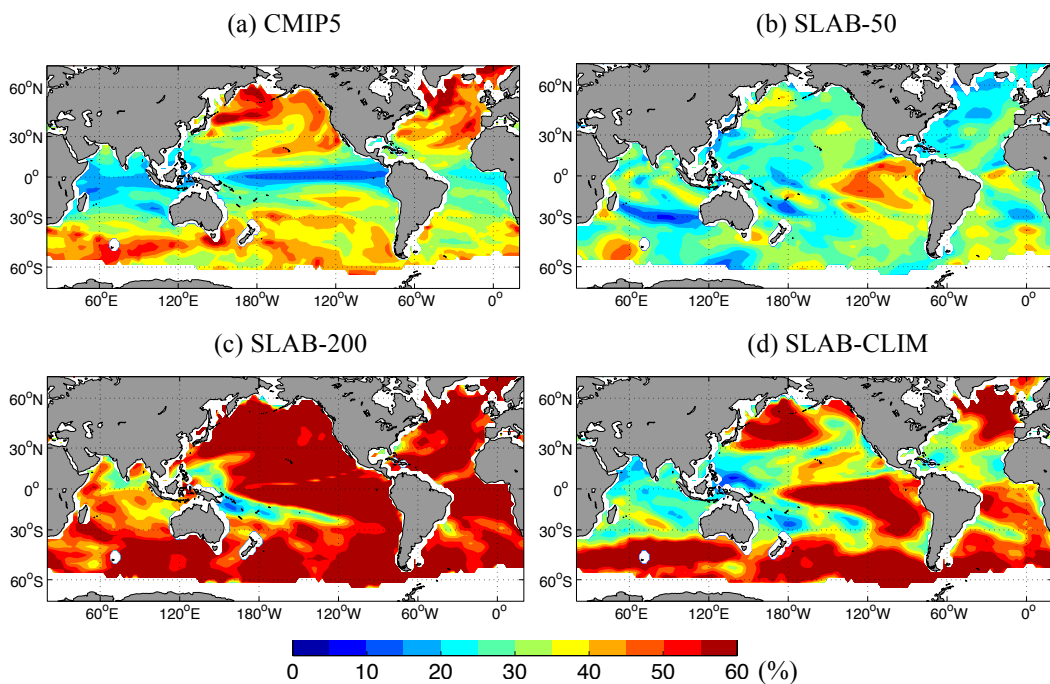


Fig. 5.4 The relative contribution of long-term (> 10 years) variability to the total of annual mean variations based on (a): CMIP5 super model (same as Fig. 3.4); (b): SLAB-50; (c): SLAB-200; (d): SLAB-CLIM

Fig. 5.4 shows the fraction that long-term variability (period longer than 10 years) contributes to the total annual mean variations based on slab ocean experiments and

CMIP5 super model ensemble. Clearly with shallower mixed layer (50m) in SLAB-50, most areas are dominated by high-frequency fluctuation as only 10%~30% variance could be attributed to long-term variation. Again SLAB-200 is just the opposite that long-term variability almost spreads everywhere and the low-frequency variation ratio is much larger than CMIP5. SLAB-CLIM demonstrates similar gradient structure as the CMIP5 super model as the low-frequency fluctuations strongly affect middle and high latitudes. Thus, deeper mixed layer can increase the ratio of low-frequency SST variability to the high-frequency part. Again this conclusion is well corresponding with the heat capacity of mixed layer.

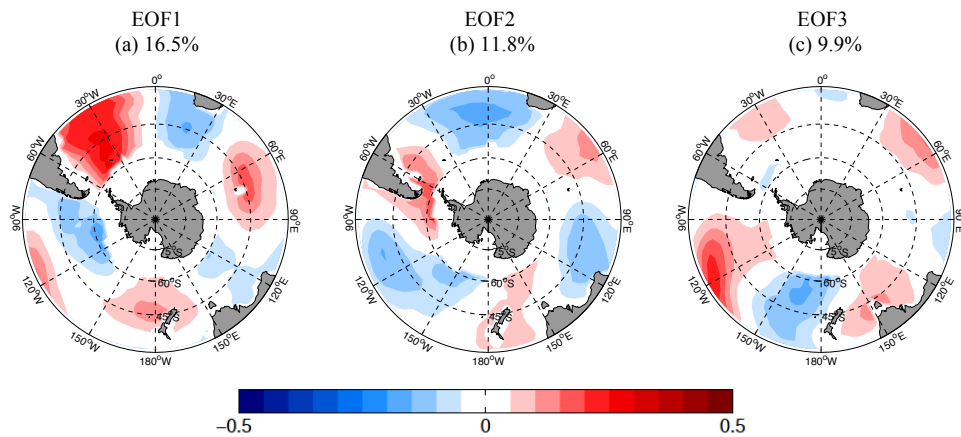


Fig. 5.5 First three leading EOF patterns of detrended annual mean SSTA in the Southern Ocean for SLAB-CLIM. The values in the headings of each panel are the explained variances of each EOF-mode.

To sum up, the near-realistic mixed layer spatial distribution is required for the correct SST variation simulation. The deep mixed layer within Southern Ocean maintains the long-term variability and enhances the low-frequency section of the SST spectrum. However, even with the real MLD in SLAB-CLIM, the slab ocean still cannot reproduce the basin-wide SST patterns. Its EOF modes still keep the wave-like structures and do not get closer to the CMIP5 ones (see Fig. 5.5). Still the ocean dynamics is needed for the formation of homogenous-like modes.

5.2 Advection Mode HYCOM Experiment

As suggested in Chapter 4, in the Southern Ocean the SST anomalies travel the globe with the ACC in 4~5 years. Similarly, the SST spectrum in Fig. 5.1 also concentrates around the period of 4~5 years. Likely SST horizontal transport maintains the power spectral structure within this time scale. In this chapter, we will test this possible causality using ocean model experiments by comparing the spectral structures with and without strong horizontal advection.

HYCOM model is utilized here for simplified experiments. The ocean domain is an idealized band-like circle limited within 55°S-45°S, like a simple representation of the Southern Ocean. The horizontal resolution is 2.5° and there are 144×5 grids in total (Fig. 5.6). Land-sea distribution is removed and ocean depth is set as constant 200m everywhere with 20 vertical layers. North and south boundaries are closed with slip boundary condition ensuring the zonal velocity will not decrease near the lateral boundaries. Experiments start with static initial condition with constant temperature of 16°C and salinity of 35 PSU (Practical Salinity Unit) everywhere.

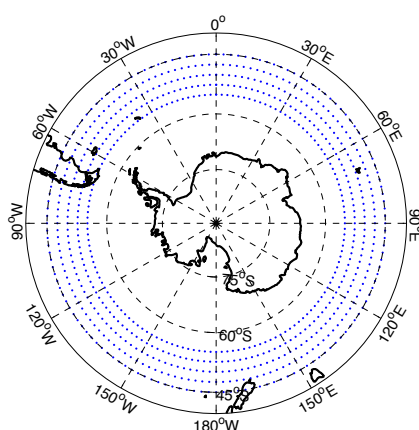


Fig. 5.6 Distribution of horizontal grids for simplified HYCOM experiments. Blue dots represent the centres of model grids.

The model is forced with simplified wind and surface net flux based on GFDL-CM3 simulation result. The control run (hereafter as H-WIND) is driven by zonally averaged climatological wind data extracted from GFDL-CM3 output. Thus, wind forcing is constant along each zonal band but has spatial variation meridionally (Fig. 5.7a). The wind forcing is removed in the corresponding sensitivity experiment (hereafter as H-NO-WIND). Therefore, no wind-driven current exists within H-NO-WIND. The same stochastic net flux forcing is applied to the two experiments. The STDV of the monthly mean net flux is 16.7 W m^{-2} , which is derived from GFDL-CM3 surface net flux anomaly at 50°S . Each experiment is integrated for 600 years and we take the last 500 years outputs for further analysis.

The main difference between H-WIND and H-NO-WIND is the existence of horizontal advection. Fig. 5.7b depicts the zonal mean sea surface velocity for two experiments. Clearly with wind forcing in H-WIND, idealized circumpolar current is simulated with averaged zonal velocity of 0.12 m s^{-1} , close to the averaged ACC speed (White and Peterson, 1996). It travels the globe in 6~7 years, longer than the period of real ACC mainly because the ACC can spread to higher latitudes. The current also demonstrates a northward component possibly due to the Coriolis effect. Without wind forcing, the surface velocity decreases to around zero in H-NO-WIND.

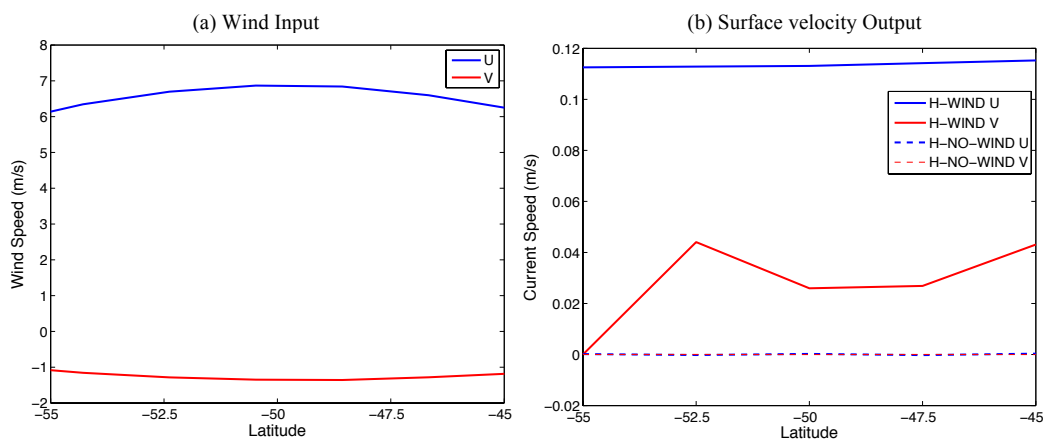


Fig. 5.7 (a) Surface wind input into H-WIND; (b): climatological zonal mean sea surface velocity for H-WIND and H-NO-WIND.

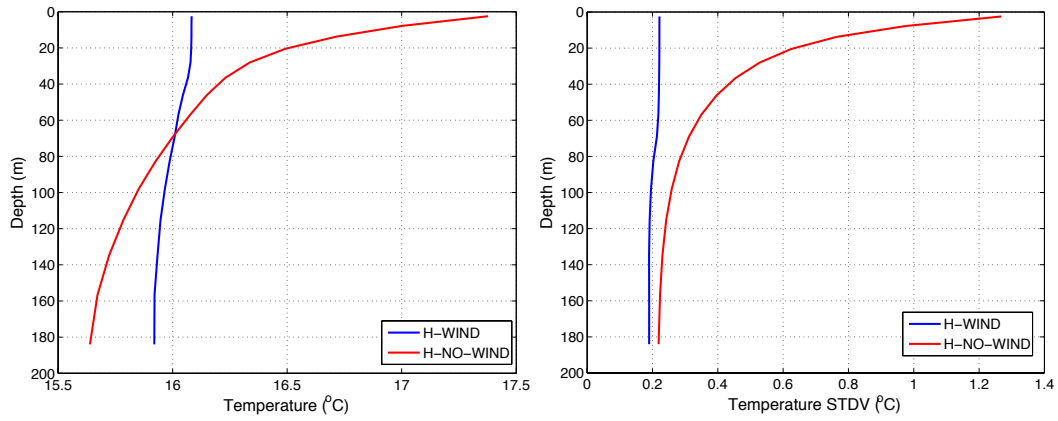


Fig. 5.8 (a): Climatological domain averaged sea temperature against depth for H-WIND and H-NO-WIND; (b): averaged standard deviation of monthly mean sea temperature against depth.

The vertical profiles of domain-averaged temperature are depicted in Fig. 5.8 for the comparison between H-WIND and H-NO-WIND. Within H-WIND, on account of the strong wind stress, the sea temperature is well mixed vertically (Fig. 5.8a), and temperature STDV tends to be uniform at every vertical level (Fig. 5.8b). Without wind forcing, H-NO-WIND demonstrates strong decreases of both temperature and temperature variability from the surface to deeper layers. At the surface, its temperature fluctuation is much larger than H-WIND due to its shallow MLD.

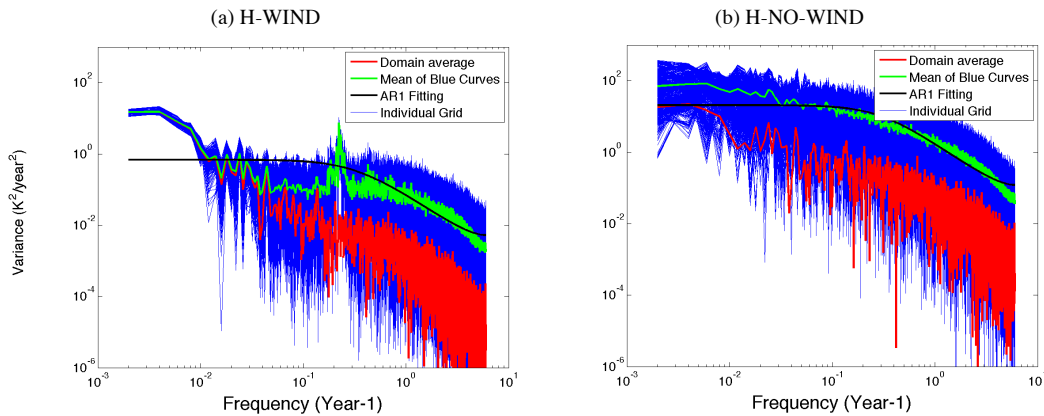


Fig. 5.9 Spectrum of monthly mean SSTA in (a): H-WIND; (b): H-NO-WIND. Red Curve is the spectrum for domain-averaged SSTA; blue curves are the SSTA spectrum for individual model grids. Green Curve is the average of all blue curves. The black line is a red noise fit to the green curves.

As expected, the spectrums of SST demonstrate different structures for these two experiments (see Fig. 5.9 and Fig. 5.10). Overall the H-NO-WIND shows much

larger spectral amplitude than H-WIND. This is because without wind-driven Ekman effect, the temperature variability of H-NO-WIND is trapped within a shallower mixed layer depth compared to the intensive vertical mixing in H-WIND. The average spectrum of all grids (green curve in Fig. 5.9b and red curve in Fig. 5.10) grows steadily and fits the red noise, implying without advection the SST variability is directly influenced by the stochastic flux and follows a simple autoregressive order one process.

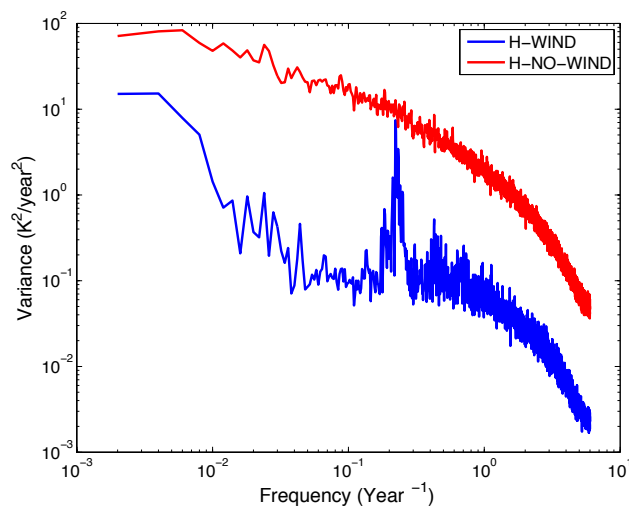


Fig. 5.10 Comparison of the averaged spectrum of all grid points SSTA in H-WIND and H-NO-WIND.

With wind forcing, the averaged spectrum increases from monthly scale to interannual scale and concentrates as a peak around 6~7 years, which well matches the propagation period of simulated circumpolar current. Then the spectrum keeps flat on the band of 10~50 years and grows again on centennial scale. This power spectral structure is similar to the CMIP5 one in Fig. 5.1, though the spectral peak in H-WIND is more obvious since the current speed and circulation period is more stable in simplified experiment. The similarity of the spectrums suggests ocean advection is the key to adjust the variability on different time scales and maintain the spectral structure of basin-wide modes.

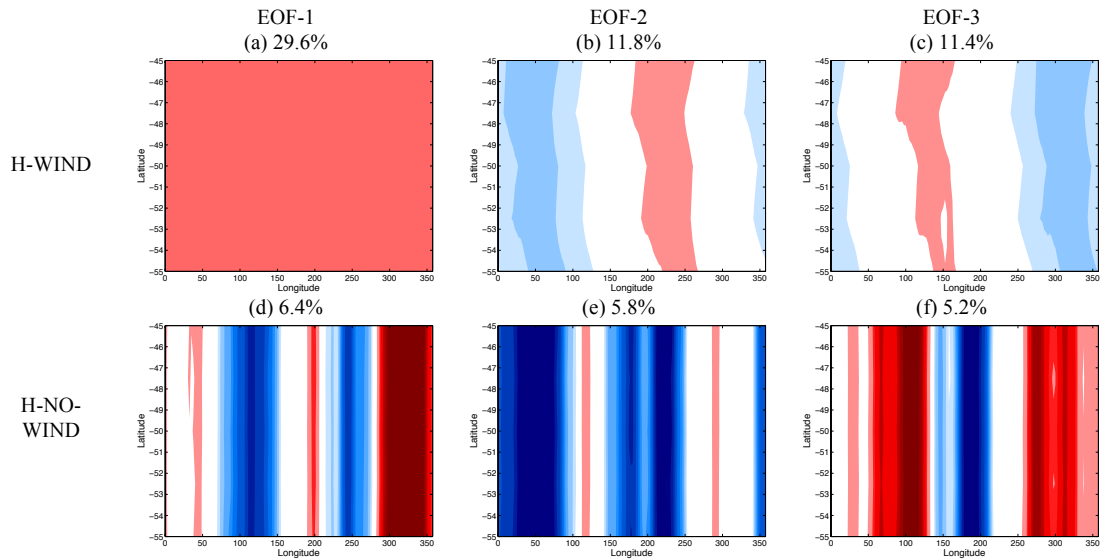


Fig. 5.11 First three leading EOF patterns of monthly mean SSTA for (a-c): H-WIND; (d-f): H-NO-WIND. The values in the headings of each panel are the explained variances of each EOF-mode.

Further the leading EOFs of monthly mean SSTA are examined in Fig. 5.11. With ocean advection, the patterns are relatively simple in H-WIND. The leading EOF pattern is a homogenous mode, which also well corresponds with the basin-wide monopole mode in CMIP5 super model. The power spectrum of its PC time series also matches the spectral structure of CMIP5 monopole mode, which concentrates on interannual scale and increases again on multi-decadal and longer time scales (see Fig. 5.12a). Both EOF-2 and EOF-3 are dipole modes and illustrates strong spectral peaks around the dominant period of the advection (Fig. 12b-c). The out-of-phase correlation ($r = 0.8$) of their PC time series also confirms these two modes are both representing SST anomaly propagation.

Without advection, the EOF patterns become more chaotic in H-NO-WIND. All three leading modes own unsmooth wave-train like structures and their PC time series mostly follows the AR-1 processes (Fig. 5.12d-f). This result proves that ocean horizontal advection creates homogenous-like basin-wide SST patterns and also modulates its spectrum.

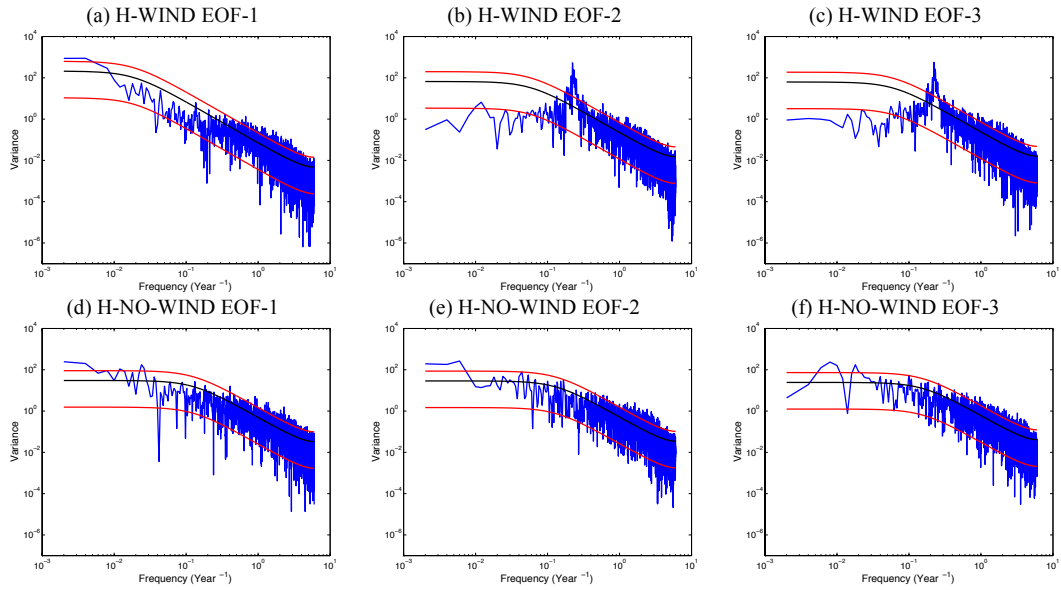


Fig. 5.12 Spectrum of normalized time series of the three leading EOF-modes of the monthly mean SSTA for H-WIND and H-NO-WIND (as in Fig. 5.11 a-f). The black line is a red noise fit to the time series and the red lines mark the 95% confidence interval relative to the red noise.

To conclude, the impact of advection is essential for SST spectral structure in the Southern Ocean. The advection along with strong eastward ACC, not only influences the generation of basin-wide modes, but also redistributes the SST variation on different time scales. In other words, the unique circumpolar current strongly affects specific SST modes of variability in the Southern Ocean both temporally and spatially.

5.3 Simple Band Model Experiment

The HYCOM experiments suggest the ACC caused horizontal advection is the key factor for the specific SST spectral structure. In this section, a simple one-dimensional model is constructed to further prove this conclusion as well as identify the influences of other factors that may affect the SST spectrum.

Following Frankignoul (1985), the SST tendency equation, derived by integrating the heat budget over the mixed layer, can be written as

$$\frac{\partial T_m}{\partial t} = \frac{Q_{net}}{\rho_0 c_p h} + \left(\frac{w+w_e}{h} \right) (T_b - T_m) - \vec{v} \cdot \nabla T_m - \frac{Q_{sw h}}{\rho_0 c_p h} + A \nabla^2 T_m \quad (5.1)$$

where T_m is the mixed layer temperature, which is equivalent to the SST for well-mixed surface layer; t is time; Q_{net} is the net surface heat flux; h is mixed layer depth; ρ_0 and c_p are density and specific heat of the sea water, respectively. Together the first term on right hand side represents the effect of surface heating/cooling. w is mean vertical velocity and w_e is entrainment velocity; T_b is the temperature just beneath the mixed layer. v is the velocity in mixed layer depth, thus third term on right hand side means ocean advection. $Q_{sw h}$ is penetrating shortwave radiation and fourth term represents sunlight exiting the base of mixed layer. Last term on right hand side donates ocean diffusion on account of eddies while A is the eddy diffusion coefficient.

Here we simplify the equation to one dimension zonally. Therefore, the vertical terms (second and fourth terms on right hand side) can be eliminated, as only one vertical well-mixed level exists after simplification.

Besides, the surface flux effect is decomposed to two terms as

$$Q_{net} = Q_{forcing} + Q_{damping} \quad (5.2)$$

where $Q_{forcing}$ is direct heat forcing including surface shortwave and longwave radiation. $Q_{damping}$ is the atmospheric damping term in the combination of surface latent heat flux and sensible heat flux. We neglect latent heat flux here in order to avoid introducing new humidity variables, and making sensible heat flux only to represent the damping effect.

$$Q_{damping} = Q_{sen} = \rho_{air} C_p C_h U (T_a - SST) \quad (5.3)$$

, where ρ_{air} is air density, C_p is the specific heat of surface air at constant pressure (= 1004 J K⁻¹ kg⁻¹); U is the surface wind speed, C_h is the heat bulk transfer coefficient (=0.0012 under constant bulk parameterization). (Park et al., 2005)

Therefore, the new equation could be written as

$$\frac{\partial T_m}{\partial t} = \frac{Q_{forcing}}{\rho_0 c_p h} - \frac{\rho_{air} C_p C_h U (T_m - T_a)}{\rho_0 c_p h} - \vec{v} \cdot \nabla T_m + A \nabla^2 T_m \quad (5.4)$$

, where the SST/mixed layer temperature is only affected by direct flux forcing, atmospheric damping, horizontal advection and diffusive process. Based on equation (5.4), a simple 1-D band model is designed which only has the x-axis along zonal direction at 50°S with a 2.5° resolution (144 grids) and applied to test the role of each term in the new equation. Given that the diffusion in the Southern Ocean are mainly caused by mesoscale eddies, A is set to geostrophic eddy diffusivity (Holloway, 1986; Ledwell et al., 1998). v here is a constant value of 0.2 m s⁻¹ guaranteeing it takes 4 years to finish a circle travelling. See Table 5.1 for model configuration.

Table. 5.1 1-D band model configuration

Variable	Description	Value
$Q_{forcing}$	Direct flux into the ocean (W m ⁻²)	Random
ρ_0	Sea water density (kg m ⁻³)	1000
c_p	Sea water specific heat (J K ⁻¹ kg ⁻¹)	4000
h	Mixed layer depth (m)	200
ρ_{air}	Air density (kg m ⁻³)	1.2
C_p	Specific heat of surface air at constant pressure (J K ⁻¹ kg ⁻¹)	1004
C_h	Heat bulk transfer coefficient	0.0012
U	Wind speed (m s ⁻¹)	5
T_a	Air temperature (K)	273.15
v	Zonal velocity in the ocean (m s ⁻¹)	0.2
A	Horizontal diffusion coefficient (m ² s ⁻¹)	500

The model runs with the daily random $Q_{forcing}$ for each grid box. Similar as the net flux in HYCOM simplified experiments, $Q_{forcing}$ here also fluctuates with a STDV of 16.7 W m^{-2} . The model starts with T_m of 15°C and while T_a is a constant of 15°C . The simple model is integrated for 1000 years and the control run is referred as B-ALL.

In order to identify the influences of specific elements, four sensitivity experiments are conducted with one term missing in the equation. That is, experiment B-NO-DAMP is without atmospheric damping effect, B-NO-AD removes horizontal advection and B-NO-DIFF has no eddy diffusion. We also run each experiment for 1000 years.

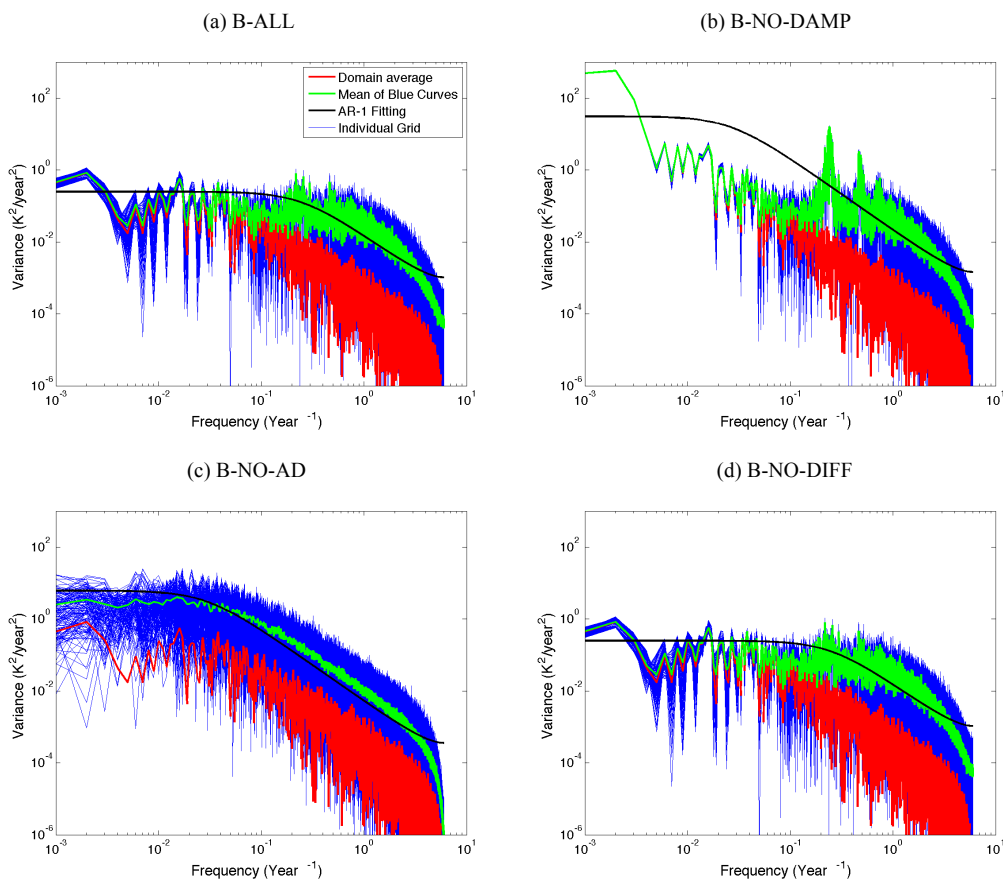


Fig. 5.13 Spectrum of monthly mean SSTA in (a): B-ALL; (b): B-NO-DAMP; (c) B-NO-AD; (d): B-NO-DIFF. Red Curve is the spectrum for domain-averaged SSTA; blue curves are the SSTA spectrum for individual model grids. Green Curve is the average of all blue curves. The black line is a red noise fit to the green curves.

Fig. 5.13 shows SST power spectrums of the four experiments. In B-ALL the averaged spectrum (green curve in Fig. 5.13a) also concentrates within the scale of 4~6 years, same as the advection propagation period, and then it keeps steady on decadal scale. This distribution is similar to H-WIND, providing that the model is capable of capturing most features of SST temporal variability. Individual grids also demonstrate similar variability on longer time scales (blue curves in Fig. 5.13a), implying the consistency of low-frequency fluctuation in the whole domain.

In the experiment without atmospheric damping, significant increase of SST variation is found in B-NO-DAMP both for individual grids and the domain average, especially on longer time scales (Fig. 5.13b). That is, without temperature relaxation, the amplitude of SST fluctuation gets much larger than the control run. For the grid-averaged spectrum (green curve), the peak becomes prominent around period of circumpolar circulation. This feature is similar as H-WIND, as H-WIND does not include damping effect, either. These changes of spectral distribution indicates the importance of atmospheric damping effect, which restores the SST to the balanced status, reduces the overall SST variability and smooths the power spectrum.

Not unexpectedly, without horizontal advection B-NO-AD shows similar spectral structure as H-NO-WIND, which confirms the influence of advection on spectrum redistribution. The spectrums keep growing smoothly without any pause or peaks. The grid-averaged spectrum follows the red noise and the individual points present different variations on all time scales (Fig. 5.13c). Hence, without the strong mixing caused by advection, the homogenous variability disappears on long-term time scales.

It is difficult to present the accurate impact of diffusion in the Southern Ocean for its small temporal and spatial scales (Sallée et al., 2008). In the idealized experiment B-

NO-DIFF, its does not show essential differences to the control run B-ALL for their spectrums are almost identical (Fig. 5.13d and Fig. 5.14). The monthly mean SST STDV is 0.126 for B-ALL, compared to 0.127 in B-NO-DIFF, indicating the existence of diffusion slightly mixes the domain and reduces the fluctuation for individual grids. However, the band model is highly simplified without complex horizontal structure or ocean eddies, and cannot include all diffusive effects in the real Southern Ocean. The role of diffusion might require further discussion.

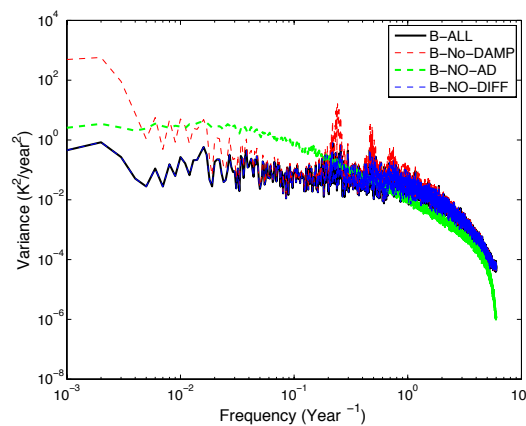


Fig. 5.14 Comparison of the averaged spectrum of all grid points SSTA in B-family experiments.

The comparison of grid-averaged spectrum further presents the differences with and without ocean advection (see Fig. 5.14). Compared to other three experiments, B-NO-AD clearly presents weaker variability on interannual scales but stronger fluctuation on decadal to multi-decadal scales. Hence, in the real world, as the horizontal advection is mostly within interannual cycle, it creates corresponding spectral growth on this frequency band and the variability concentrates around its instinct period. The aggregation of the variation also causes spectrum stops growing on decadal scale. On the even longer scale, the impact of advection gets weaker and the spectrum starts to increase again mostly due to the instability of stochastic forcing (e.g. Alexander and Penland, 1996).

To sum up, without any external forcing pattern, SST spectral structure in the SO can be simulated using 1-D idealized mixed layer model. These band ocean experiments suggest that the ocean advection is the main factor creating the spectral distribution due to its concentrating effect around the circumpolar circulation period.

5.4 Summary and Discussion

In this chapter we qualitatively discussed the causes of power spectral distribution of the SST modes in the Southern Ocean. Based on several simplified numerical experiments, several factors are tested to identify their influences on SST spectral structure. We list the main findings below.

- The deep mixed layer, for its large heat capacity, mediates the air-sea interactions and is responsible for the maintenance of the long-term variability in the Southern Ocean. The mixed layer must be deep enough to keep the proportion of low-frequency anomalies within total variations.
- The ocean dynamics especially the ocean advection, on the other hand, further adjusts the variation distribution among different time scales. Throughout the horizontal transport, the anomalous signals get well distributed and spread. On the same time, the SST variability gets aggregated around the circumpolar circulation period. This variation concentration also raises the increase of the SST spectrum on interannual variability and relative stagnation of the spectrum on longer time scale. Thus, the ocean advection is not only to create homogenous-like modes, but also affects the spectral distribution.
- Atmospheric damping is able to reduce the SST variability caused by stochastic heat flux forcing and smooth the SST spectrum. Similarly, ocean

diffusion mixes the temperature and also weakens the sea temperature fluctuation, though the impact is not apparent in the simplified experiments.

Therefore, most of the long-term variability is reserved within the ocean itself. The specific features of the Southern Ocean, such as deep mixed layer depth, circumpolar current system and strong air-sea interaction, generates the temporal variation of the SST modes together. A homogenous basin-wide monopole pattern could be generated with stochastic atmospheric forcing and ocean advection; as a result it is essentially an ocean-only mode of variability. However, as we discussed in Chapter 3, the atmospheric wave-train forcing leads to the uneven distribution of the variation for the real monopole mode in CMIP5 simulations.

More detailed quantitative study is still desirable for the temporal SST variation. In addition, some missing factors within the simplified models merit attention as well. One notable element is the variability of the MLD. In our experiments, we focus on the thermodynamical property of the mixed layer as MLD is mostly fixed to a constant depth. However, in the real Southern Ocean, MLD demonstrates intense seasonality and even longer scale variation related with SAM and ENSO, which further alters the surface heat balance and affects SST variability (e.g. Dong et al., 2008; Morioka et al., 2013). The dynamical feature of the MLD requires more detailed study. Another factor is the deep ocean circulation. For its long time-scale feature, the overturning circulation has been suggested to modulate the SST on centennial scale and possibly affect the spectrum structure on corresponding frequency band (e.g. Latif et al., 2013).

The instability of the advection is another remarkable feature in the Southern Ocean. The ACC demonstrates large uncertainties and variability on its structure, path and

transport on interannual time scale (Fu and Chelton, 1985; Rintoul and Sokolov, 2001; Zlotnicki et al., 2007; Sallée et al., 2008b), and have presented significant responds to recent climate change as well (e.g. Böning et al., 2008). The varying ACC might cause the redistribution of the SST power spectrum at different time scales. A simple experiment (B-VARYING-U) is done here on the basis of B-ALL but with non-constant ACC zonal velocity. The ACC horizontal speed follows a uniform distribution of $[0.1 \text{ } 0.25] \text{ m s}^{-1}$. Thus the propagation period of ACC ranges from 3 to 8 years. Clearly the new experiment illustrates larger variability within low-frequency band compared to the B-ALL, which is more obvious on interannual and centennial scale (see Fig. 5.15). The instability of the ACC, therefore, may lead to more fluctuation of the SST variation, which requires more detailed discussions.

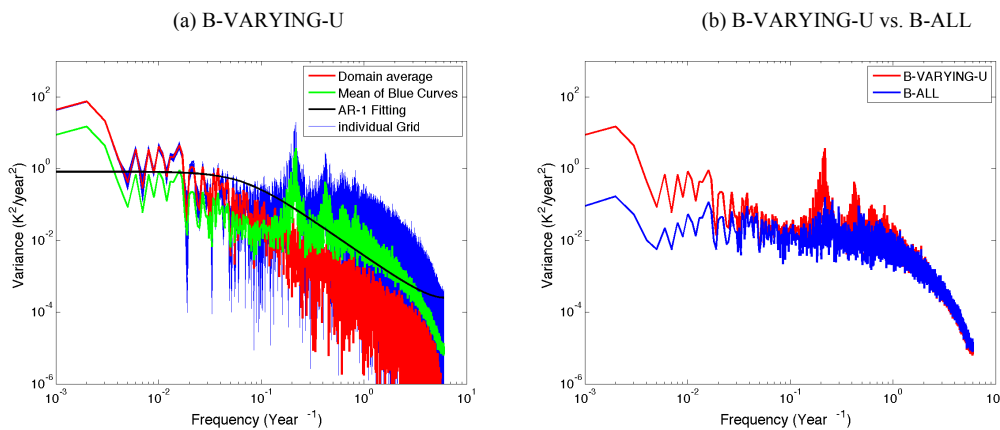


Fig. 5.15 (a). Spectrum of monthly mean SSTA in B-VARYING-U. Red Curve is the spectrum for domain-averaged SSTA; blue curves are the SSTA spectrum for individual model grids. Green Curve is the average of all blue curves. The black line is a red noise fit to the green curves. (b): Comparison of the averaged spectrum of all grid points SSTA between B-VARYING-U and B-ALL.

Besides, eddies and jets along the ACC cannot be neglected. The eddies, originating from the baroclinic instability in the Southern Ocean, play an important role in water mixing and subduction. On the other hand, the ACC consists of multiple jets while the paths and strengths of these jets are mostly affected by topography and eddy-mean flow interaction (e.g. Hughes and Ash, 2001, Williams et al. 2007). Both eddies and

jets can deeply influence the diffusion and advection in the Southern Ocean. Their impacts cannot be totally represented by a simple mean flow plus diffusion parameterization scheme in the simplified experiments, and require a better understanding with more complicated analyses.

Chapter 6

Conclusions

6.1 Summary of Findings

Long-term variability exists in the Southern Ocean and it can be represented as the atmosphere-ocean coupled modes. Given the important role of the Southern Ocean on the global climate system, a detailed understanding of these coupled modes is paramount to our knowledge and better predictions on global climate variability and climate change.

In Chapter 2, we introduced the evaluation of the CMIP models in their skill of simulating the spatial structure of SST variability. We found that some models show good skill in simulating the observed spatial structure of the SST variability in the tropical domains and less so in the extra-tropical domains. However, most models show substantial deviations from the observations and from each other in most domains and particularly in the North Atlantic and Southern Ocean on the longer time scale. The CMIP5 ensemble shows some improvement over the CMIP3 ensemble, mostly in the tropical domains. Further, the spatial structure of the SST modes of the CMIP3 and CMIP5 super ensemble is more realistic than any single model, if the relative explained variances of these modes are scaled by the observed eigenvalues.

In Chapter 3, we analysed the leading SST modes in the Southern Ocean based on CMIP5 super ensemble and observations. Though individual models show large deviation in the spatial structure from each other, the model super ensemble demonstrates similar modes to the limited satellite observations. We found that the annular mode, monopole mode and South Pacific dipole are the principle patterns with statistically significant low-frequency variability in the Southern Ocean. ENSO and SAM dominate the annular mode together, while the impact of ENSO is mostly restricted within the South Pacific. The monopole mode and South Pacific dipole

mode, which both demonstrates strong decadal variability, are firstly inducted by atmospheric wave patterns and further developed via ocean dynamics.

In Chapter 4, we further investigated the factors affecting the spatial features of SST variability with the HYCOM ocean model experiments. The results suggest that the atmospheric forcing is the triggering mechanism of the coupled modes, while the air-sea interaction and amplification have a strong impact on the intensity of the modes. The ocean dynamics, especially the ocean horizontal advection is responsible for the transformation of the modes from atmospheric wave trains to homogeneous-like structures. The sea ice variability, though it can change the strength of SST variation, does not really affect the spatial shapes of the coupled decadal modes in the Southern Ocean.

Chapter 5 discussed the causes of the temporal variability in the Southern Ocean based on simplified numerical experiments. The deep mixed layer depth, due to its large heat capacity, modulates the air-sea interaction and makes the long-term variability predominant in the Southern Ocean. On the other hand, the ocean advection redistributes the spectrum of the SST variability in the Southern Ocean and gathers the variation along the circulation frequency band. Together they maintain the specific power spectral distribution of SST modes.

6.2 Synthesis of Results

Here we simply synthesise the results presented in the preceding chapters as: each mode has its coupling characteristics. The ocean and atmosphere are both necessary and crucial for the mode generation, propagation and development.

The annular mode is the direct result of two coupled modes, namely ENSO and SAM. Thus, as the passive response of other modes, it does not show strong decadal variability. The monopole mode and South Pacific dipole are firstly the duplications of the wave trains in the atmosphere, and then slowly get transformed via ocean dynamics. With the development of the spatial structures, their temporal variability gets further adjustment within the deep mixed layer and by strong zonal advection.

Specifically, the Southern Ocean low-frequency modes could be likened to a classical music concert. The seawater can be compared to the musical instruments, as both of them are the objectives to produce the variability. The atmosphere plays a role as the music scores, which give the direct instructions (e.g. ENSO, SAM and wave trains) to the variation. The deep mixed layer within the Southern Ocean has the similarity as the musicians for their common matureness. The musicians must be well trained while the mixed layer must be deep enough to maintain the long-term variability. Ocean dynamics is similar to the conductor for it connects the entire ocean, modulates the temporal distribution of the variability, and creates the homogeneous-like modes. Last but not least, the sea ice is like the audience. Though it cannot significantly change the spatial structure of the modes, it could affect the variation strength on longer scales. Every element is indispensable and they form the long-term modes together in the Southern Ocean.

6.3 Future Work

In this thesis, we discussed the long-term coupled modes and their mechanisms in the Southern Ocean. In this section, we present some questions encountered but left unsolved or unexplored.

The first one is more complex phenomenon in the Southern Ocean and their influence on the coupled modes. Due to the limitation of the data and approaches, we did not finish the analyses on Southern Ocean topography effect, eddies, jets, deep circulation, water masses evolution, planetary waves propagation and sea ice dynamical interaction, while all of these factors may affect the long-term variability in the Southern Ocean. Further research is needed with more sophisticated experiments.

Another worthwhile application is the mode evolution in the future. Some relevant external modes have been suggested to change their frequency and spatial features under climate change. For example, ENSO events possibly will increase with especially for the central Pacific El Niño (e.g. Yeh et al., 2009, Lee and McPhaden, 2010) and more extreme ENSO events might occur more frequently (Cai et al., 2014; Cai et al., 2015). Quite likely the annular mode in the Southern Ocean will demonstrate similar change with ENSO and SAM. On the other hand, the strengthened westerlies above the Southern Ocean in the future projection may alter local ocean circulation pattern. Though it is still controversial whether the ACC transport will increase in response of the westerlies (e.g. Bi et al., 2002; Fyfe and Saenko, 2006), the increased wind possibly intensifies the eddy and jet field and introduces more mixing within sea surface (e.g. Meredith and Hogg, 2006; Boning et al., 2008). The changes of the ocean dynamics may lead to the modulation of the spectrum and transformation of the spatial modes.

Lastly, it is still unclear how these Southern Ocean modes influence the climate system. The teleconnections from the topics promote the Southern Ocean patterns via atmospheric circulation. But further research is needed to identify how the tropics responses to the Southern Ocean modes and whether the northern hemisphere modes

have corresponding analogues and interactions. As the ACC transportation redistributes the seawater temperature and salinity, regional climate patterns may also change adjacent to the Southern Ocean. The impact of the modes on thermohaline circulation and global hyper modes also requires further study as well.

References

Alexander MA, Penland C (1996) Variability in a mixed layer ocean model driven by stochastic atmospheric forcing. *J Clim* 9: 2424–2442

Bayr T, Dommenges D (2014) Comparing the spatial structure of variability in two datasets against each other on the basis of EOF modes. *Clim Dyn* 42: 1631-1648

Bi D, Budd WF, Hirst AC, Wu X (2002) Response of the Antarctic circumpolar current transport to global warming in a coupled model. *Geophys Res Lett* 29(24): 2173. doi:10.1029/2002GL015919

Bindoff N, Willebrand J, Artale V, Cazenave A, Gregory J, Gulev S, Hanawa K, Le Quéré C, Levitus S, Nojiri Y, Shum C, Talley L, Unnikrishnan A (2007) Observations: oceanic climate change and sea level. *Climate Change 2007: The Physical Science Basis. Contribution of Working Group 1 to the Fourth Assessment Report of the Intergovernmental Panel on Climate Change* [Solomon S, Qin D, Manning M, Chen Z, Marquis M, Averyt KB, Tignor M & H.L. Miller (eds.)]. Cambridge University Press, Cambridge, United Kingdom and New York, NY, USA.

Bleck R (2002). An oceanic general circulation model framed in hybrid isopycnic-Cartesian coordinates. *Ocean Modell* 37: 55–88

Bleck R, Halliwell G (2001) Energy loan sea ice model. HYCOM, unpublished, 2 pp., URL https://hycom.org/attachments/067_ice.pdf

Boer GJ, Fourest S, Yu B (2001) The signature of the annular modes in the moisture budget. *J Clim* 14:3655–3665

Boer GJ, Lambert SJ (2001) Second order space–time climate difference statistics. *Clim Dyn* 17: 213-218

Böning CW, Dispert A, Visbeck M, Rintoul SR, Schwarzkopf FU (2008) The response of the Antarctic Circumpolar Current to recent climate change. *Nature Geosci* 1: 864-869

Bretherton CS, Widmann M, Dymnikov VP, Wallace JM, Bladé I (1999) The effective number of spatial degrees of freedom of a time-varying field. *J Clim* 12: 1990-2009

Bryan FO, Gent PR, Tomas R (2014) Can Southern Ocean eddy effects be parameterized in climate models? *J Clim* 27: 411-425

Cahalan RF, Wharton LE, Wu W-L (1996) Empirical orthogonal functions of monthly precipitation and temperature over the United States and homogeneous stochastic models. *J Geophys Res* 101: 26309-26318

Cai W, Borlace S, Lengaigne M, van Rensch P, Collins M, Vecchi G, Timmermann A, Santoso A, McPhaden MJ, Wu L, England MH, Wang G, Guilyardi E, Jin F-F (2014) Increasing frequency of extreme El Niño events due to greenhouse warming. *Nature Clim Change* 4:111-116

Cai W, Wang G, Santoso A, McPhaden M, Wu L, Jin F-F, Timmermann A, Collins M, Vecchi G, Lengaigne M, England MH, Dommenges D, Takahashi K, Guilyardi E (2015) Increased frequency of extreme La Niña events under greenhouse warming. *Nature Clim Change* 5:132-137

Cai W, Watterson IG (2002) Modes of interannual variability of the southern hemisphere circulation simulated by the CSIRO climate model. *J Clim* 15:1159–1174

Carleton AM (1989) Antarctic sea-ice relationships with indices of the atmospheric circulation of the Southern Hemisphere. *Clim Dyn* 3: 207–220

Cavalieri DJ, Parkinson CL (2008) Antarctic sea ice variability and trends, 1979–2006, *J Geophys Res* 113: C07004, doi: 10.1029/2007JC004564

Chelton DB, deSzoeke RA, Schlax MG, El Naggar K, Siwertz N (1998) Geographical variability of the first-baroclinic Rossby radius of deformation. *J Phys Oceanogr* 28: 433-460

Chen WY (1982) Assessment of Southern Oscillation sea-level pressure indices. *Mon Wea Rev* 110: 800–807

Comiso JC, Nishio F (2008). Trends in the sea ice cover using enhanced and compatible AMSR-E, SSM/I, and SMMR data. *J Geophys Res* 113: C02S07, doi: 10.1029/2007JC004257

Cook ER, Buckley BM, D'Arrigo RD, Peterson MJ (2000) Warm-season temperatures since 1600 BC reconstructed from Tasmanian tree rings and their relationship to large-scale sea surface temperature anomalies. *Clim Dyn* 16 (2–3): 79–91

Cook ER, Palmer JG, D'Arrigo RD (2002) Evidence for a 'Medieval Warm Period' in a 1,100 year tree-ring reconstruction of past austral summer temperatures in New Zealand. *Geophys Res Lett* 29(14): 1667. doi: 10.1029/2001GL014580

Curry JA, Schramm JL, Ebert EE (1995) Sea ice-albedo climate feedback mechanism. *J Clim* 8(2): 240–247

Davies T, Cullen MJP, Malcolm AJ, Mawson MH, Staniforth A, White AA, Wood N (2005) A new dynamical core for the Met Office's global and regional modelling of the atmosphere. *Quart J Roy Meteor Soc* 131: 1759-1782

de Boyer Montégut C, Madec G, Fischer AS, Lazar A, Iudicone D (2004) Mixed layer depth over the global ocean: an examination of profile data and a profile-based climatology, *J Geophys Res* 109: C12003, doi:10.1029/2004JC002378

Deser C, Blackmon ML (1993) Surface climate variations over the North Atlantic Ocean during winter: 1900-89. *J Clim* 6: 1743-1753

Dima M, Lohmann G (2004) Fundamental and derived modes of climate variability. Concept and application to interannual variability. *Tellus A* 56A: 229-249

Dommenget D (2007) Evaluating EOF modes against a stochastic null hypothesis. *Clim Dyn* 28(5): 517-531

Dommenget D (2010) The slab ocean El Niño. *Geophys Res Lett* 37: L20701. doi:10.1029/2010GL044888

Dommenget D (2011) An Objective Analysis of the Observed Spatial Structure of the Tropical Indian Ocean SST Variability. *Clim Dyn* 36: 2129-2145

Dommenget D, Latif M (2002) Analysis of observed and simulated SST spectra in the midlatitudes. *Clim Dyn* 19: 277-288

Dong S, Sprintall J, Gille ST, Talley L (2008) Southern Ocean mixed-layer depth from Argo float profiles. *Geophys Res Lett* 113: C06013. doi:10.1029/2006JC004051

Farneti R, Vallis GK (2011) Mechanisms of interdecadal climate variability and the role of ocean–atmosphere coupling. *Clim Dyn* 36: 289-308

Fletcher JO (1969) Ice extent in the southern oceans and its relation to world climate. *J Glaciol* 15: 417–427

Frankignoul C (1985) Sea surface temperature anomalies, planetary waves, and air-sea feedback in the middle latitudes. *Rev Geophys* 23:357-390

Fu L-L, Chelton DB (1985) Observing large-scale temporal variability of ocean currents by satellite altimetry: With application to the Antarctic Circumpolar Current, *J Geophys Res* 90(C3), 4721–4740, doi:10.1029/JC090iC03p04721.

Fyfe JC (2003) Separating extratropical zonal wind variability and mean change. *J Clim* 16: 863-874

Fyfe JC, Saenko OA (2006) Simulated changes in extratropical Southern Hemisphere winds and currents. *Geophys Res Lett* 33: L06701. doi:10.1029/2005GL025332

Garreaud RD, Battisti DS (1999) Interannual ENSO and interdecadal ENSO-like variability in the Southern Hemisphere tropospheric circulation. *J Clim* 12: 2113-2123.

Gleckler PJ, Taylor KE, Doutriaux C (2008) Performance metrics for climate models. *J Geophys Res* 113: D06104. doi: 10.1029/2007JD008972

Gong DY, Wang SW (1999) Definition of Antarctic Oscillation index. *Geophys Res Lett* 26: 459–462

Gordon AL, Molinelli EJ (1982) Southern Ocean Atlas. Columbia University Press, New York

Gordon AL, Zambianchi E, Orsi A, Visbeck M, Giulivi CF, Whitworth III T, Spezie G (2004) Energetic plumes over the western Ross Sea continental slope. *Geophys Res Lett* 31: L21302. doi:10.1029/2004GL020785

Graham NE (1994) Decadal-scale climate variability in the tropical and North Pacific during the 1970's and 1980's: Observations and model results. *Clim Dyn* 10: 135–162

Guan Y, Zhu J, Huang B, Hu Z-Z, Kinter III JL (2014) South Pacific Ocean Dipole: A predictable mode on multiseasonal time scales. *J Clim* 27: 1648–1658

Guilyardi E (2006) El Niño–mean state–seasonal cycle interactions in a multi-model ensemble. *Clim Dyn* 26: 329–348

Hartmann DL (1994) *Global Physical Climatology*. Academic Press, San Diego, CA.

Hartmann DL, Lo F (1998) Wave-driven flow vacillation in the Southern Hemisphere. *J Atmos Sci* 55: 1303–1315

Hasselmann K (1976) Stochastic climate models Part I. Theory. *Tellus* 28(6): 473–485

Hogg AM, Blundell JR (2006) Interdecadal Variability of the Southern Ocean. *J Phys Oceanogr* 36: 1626–1645

Hogg AM, Meredith MP, Chambers DP, Abrahamsen EP, Hughes CW, Morrison AK (2015) Recent trends in the Southern Ocean eddy field, *J Geophys Res* 120: 257–267

Holloway G (1986) Estimation of oceanic eddy transports from satellite altimetry. *Nature* 323 (6085): 243–244

Hoskins BJ, Karoly DJ (1981) The steady linear response of a spherical atmosphere to thermal and orographic forcing. *J Atmos Sci* 38: 1179–1196

Huang B, Shukla J (2006) Interannual SST variability in the southern subtropical and extra-tropical ocean. Tech Rep 223. Cent for Ocean Land Atmos Stud, Calverton, Md

Huang SP, Pollack HN, Shen PY (2000) Temperature trends over the past five centuries reconstructed from borehole temperatures. *Nature* 403(6771): 756-758

Hughes CW, Ash ER (2001) Eddy forcing of the mean flow in the Southern Ocean. *J Geophys Res* 106(C2): 2713–2722.

Hurrell JW (1995) Decadal trends in the North Atlantic Oscillation and relationships to regional temperature and precipitation. *Science* 269: 676-679

IPCC (2001) *Climate Change 2001: The Scientific Basis. Contribution of Working Group I to the Third Assessment Report of the Intergovernmental Panel on Climate Change* [Houghton JT, Ding Y, Griggs DJ, Noguer M, van der Linden PJ, Dai X, Maskell K, & Johnson CA (eds.)]. Cambridge University Press, Cambridge, United Kingdom and New York, NY, USA

Jacobs SS, Amos AF, Bruchhau PM (1970) Ross Sea oceanography and Antarctic Bottom Water formation. *Deep Sea Res* 17: 935-962

Jamison N, Kravtsov S (2010) Decadal Variations of North Atlantic Sea Surface Temperature in Observations and CMIP3 Simulations. *J Clim* 23: 4619-4636

Jansen E, Overpeck J, Briffa KR, Duplessy JC, Joos F, Masson-Delmotte V, Olago D, Otto-Bliesner B, Peltier WR, Rahmstorf S, Ramesh R, Raynaud D, Rind D, Solomina O, Villalba R, Zhang D (2007) *Palaeoclimate. Climate Change 2007: The Physical Science Basis. Contribution of Working Group I to the Fourth Assessment Report of the Intergovernmental Panel on Climate Change* [Solomon S, Qin D, Manning M, Chen Z, Marquis M, Averyt KB, Tignor M & H.L. Miller (eds.)]. Cambridge University Press, Cambridge, United Kingdom and New York, NY, USA

Johnson GC, Bryden HL (1989) On the size of the Antarctic Circumpolar Current. *Deep Sea Res* 36: 39-53

Jolliffe I (2002) *Principal component analysis. 2nd Edn.* Springer, New York

- Jones JM, Fogt RL, Widmann M, Marshall GJ, Jones PD, Visbeck M (2009) Historical SAM Variability. Part I: Century length seasonal reconstructions. *J Clim* 22: 5319-5345
- Jones PD, Salinger MJ, Mullan AB (1999) Extratropical circulation indices in the Southern Hemisphere based on station data. *Int J Climatol* 19: 1301-1317
- Kanamitsu M, Ebisuzaki W, Woollen J, Yang S-K, Hnilo JJ, Fiorino M, Potter GL (2002) NCEP–DOE AMIP-II Reanalysis (R-2). *Bull Amer Meteor Soc* 83: 1631-1643.
- Kao H, Yu J (2009) Contrasting Eastern-Pacific and Central-Pacific Types of ENSO. *J. Clim* 22(3): 615–632
- Karoly DJ (1989) Southern hemisphere circulation features associated with El Niño–Southern Oscillation events. *J Clim* 2: 1239-1252
- Karoly DJ (1990) The role of transient eddies in low-frequency zonal variations of the Southern Hemisphere circulation. *Tellus* 42A: 41–50
- Kidson JW (1998) Indices of the Southern Hemisphere zonal wind. *J Clim* 1: 183-194
- Kidson JW, Renwick JA (2002) The Southern Hemisphere evolution of ENSO during 1981-1999. *J Clim* 15: 847-863
- Kirtman BP, Bitz C, Bryan F, Collins W, Dennis J, Hearn N, Kinter III JL, Loft R, Rousset C, Siqueira L, Stan C, Tomas R, Vertenstein M (2012) Impact of ocean model resolution on CCSM climate simulations. *Clim Dyn* 39: 1303-1328
- Knutti R, Furrer R, Tebaldi C, Cermak J, Meehl GA (2010) Challenges in combining projections from multiple models. *J Clim* 23: 2739-2758
- Krzanowski WJ (1979) Between-groups comparison of principal components. *J Amer Stat Assoc* 74: 703-707
- Kushnir Y (1994) Interdecadal variations in north Atlantic sea surface temperature and associated atmospheric conditions. *J Clim* 7: 141–157

Kwok R, Comiso JC (2002) Southern Ocean climate and sea ice anomalies associated with the Southern Oscillation. *J Clim* 15: 487-501

Latif M, Barnett TP (1996) Decadal climate variability over the north Pacific and north America: dynamics and predictability. *J Clim* 9: 2407–2423

Latif M, Martin T, Park W (2013) Southern Ocean sector centennial climate variability and recent decadal trends. *J Clim* 26: 7767–7782

Ledley TS, Huang Z (1997) A possible ENSO signal in the Ross Sea. *J Geophys Res* 24: 3253–3256

Ledwell JR, Watson , Law CS (1998) Mixing of a tracer in the pycnocline. *J Geophys Res* 103(C10): 21499–21529

Lee T, McPhaden MJ (2010) Increasing intensity of El Niño in the central-equatorial Pacific. *Geophys Res Lett* 37: L14603. doi:10.1029/ 2010GL044007

Lefebvre W, Goose H, Timmermann R, Fichefet T (2004) Influence of the Southern Annular Mode on the sea ice-ocean system. *J Geophys Res* 109, C09005. doi:10.1029/2004JC002403

Limpasuvan V, Hartmann DL (1999). Eddies and the annular modes of climate variability. *Geophys Res Lett* 26: doi: 10.1029/1999GL010478

Mantua NJ, Hare SR (2002) The Pacific Decadal Oscillation. *J Oceanogr* 58: 35-44

Mantua NJ, Hare SR, Zhang Y, Wallace JM, Francis RC (1997) A Pacific decadal climate oscillation with impacts on salmon. *Bull Amer Meteor Soc* 78: 1069-1079

Marsh R, Nurser AJ, Megann AP, New AL (2000) Water mass transformation in the Southern Ocean of a global isopycnal coordinate GCM. *J Phys Oceanogr* 30: 1013–1045

Martin GM, Bellouin N, Collins WJ, Culverwell ID, Halloran P, Hardiman S, Hinton TJ, Jones CD, McLaren A, O’Connor F, Rodriguez J, Woodward S, et al. (2011) The

HadGEM2 family of Met Office Unified Model climate configurations. *Geosci Model Dev Discuss* 4: 723-757

Martin GM, Milton SF, Senior CA, Brooks ME, Ineson S, Reichler T, Kim J (2010) Analysis and reduction of systematic errors through a seamless approach to modelling weather and climate. *J Clim* 23: 5933-5957

Martin T, Park W, Latif M (2013) Multi- centennial variability controlled by Southern Ocean convection in the Kiel Climate Model, *Clim Dyn*, 40(7): 2005-2022

Maze G, D'Andrea F, Colin de Verdière A (2006) Low-frequency variability in the Southern Ocean region in a simplified coupled model. *J Geophys Res* 111: C05010. doi: 10.1029/2005JC003181

Mazloff M, Heimbach P, Wunsch C (2010) An eddy-permitting Southern Ocean state estimate. *J Phys Oceanogr* 40: 880-899

McClean JL, Bader DC, Bryan FO, Maltrud ME, Dennis JM, Mirin AA, Jones OW, Kim YY, Ivanova DP, Vertenstein M, Boyle JS, Jacob RL, Norton N, Craig A, Worley PH (2011) A prototype two-decade fully-coupled fine-resolution CCSM simulation. *Ocean Model* 39: 10-30

McPhaden MJ, Zebiak SE, Glantz MH (2006) ENSO as an integrating concept in Earth science. *Science* 314: 1740-1745

Meehl GA, Covey C, Delworth T, Latif M, McAvaney B, Mitchell JFB, Stouffer RJ, Taylor KE (2007) The WCRP CMIP3 multi-model dataset: A new era in climate change research. *Bull Amer Meteor Soc* 88: 1383-1394

Mellor GL, Durbin PA (1975) The structure and dynamics of the ocean surface mixed layer. *J Phys Oceanogr* 5: 718–728

Menemenlis D, Campin J, Heimbach P, Hill C, Lee T, Nguyen A, Schodlok M, Zhang H (2008) ECCO2: High resolution global ocean and sea ice data synthesis. *Mercator Ocean Quarterly Newsletter* 31: 13-21

Meredith MP, Hogg AM (2006) Circumpolar response of Southern Ocean eddy activity to a change in the Southern Annular Mode. *Geophys Res Lett* 33: L16608, doi: 10.1029/2006GL026499

Metzger EJ, Smedstad OM, Thoppil PG, Hurlburt HE, Cummings JA, Wallcraft AJ, Zamudio L, Franklin DS, Posey PG, Phelps MW, Hogan PJ, Bub FL, DeHaan CJ (2014) US Navy Operational Global Ocean and Arctic Ice Prediction Systems. *Oceanogr* 27(3): 32–43

Mo KC, Higgins RW (1998) Tropical influences on California precipitation. *J Clim* 11: 412–430

Monselesan DP, O’Kane TJ, Risbey JS, Church J (2015) Internal climate memory in observations and models. *Geophys Res Lett* 42, 1232–1242, doi: 10.1002/2014GL062765.

Monterey GI, Levitus S (1997) Climatological cycle of mixed layer depth in the world ocean. U.S. Gov. Printing Office, NOAA NESDIS, 5pp.

Morioka Y, Ratnam JV, Sasaki W, Masumoto Y (2013) Generation mechanism of the South Pacific Subtropical Dipole. *J Clim* 26: 6033–6045

Murphy JM, Sexton DMH, Barnett DN, Jones GS, Webb MJ, Collins M, Stainforth DA (2004) Quantification of modeling uncertainties in a large ensemble of climate change simulations. *Nature* 430: 768-772

North GR, Bell TL, Cahalan RF, Moeng FJ (1982) Sampling errors in the estimation of empirical orthogonal functions. *Mon Wea Rev* 110: 699-706

O’Kane TJ, Matear RJ, Chamberlain MA, Risbey JS, Sloyan BM, Horenko I (2013) Decadal variability in an OGCM Southern Ocean: Intrinsic modes, forced modes and metastable states. *Ocean Model* 69: 1-21

Orsi AH, Johnson GC, Bullister JL (1999) Circulation, mixing, and production of Antarctic Bottom Water. *Prog Oceanogr* 43: 55-109

Park S, Deser C, Alexander MA (2005) Estimation of the surface heat flux response to sea surface temperature anomalies over the global oceans. *J Clim* 18: 4582-4599

Patra PK, Maksyutov S, Ishizawa M, Nakazawa T, Takahashi, T, Ukita J (2005) Interannual and decadal changes in the sea-air CO₂ flux from atmospheric CO₂ inverse modeling, *Global Biogeochem Cy* 19: GB4013. doi:10.1029/2004gb002257

Philander SGH (1985) El Niño and La Niña. *J Atmos Sci* 42:2652–2662

Pierce DW, Barnett TP, Schneider N, Saravanan R, Dommenges D, Mojiib L (2001) The role of ocean dynamics in producing decadal climate variability in the North Pacific. *Clim Dyn* 18 (1-2): 51-70

Raphael, M.N., 2004: A zonal wave 3 index for the Southern Hemisphere. *Geophys. Res. Lett.*, 31, L23212, doi: 10.1029/2004GL020365

Rayner NA, Parker DE, Horton EB, Folland CK, Alexander LV, Rowell DP, Kent EC, Kaplan A (2003) Global analyses of sea surface temperature, sea ice, and night marine air temperature since the late nineteenth century. *J Geophys Res* 108: D144407, doi:10.1029/2002JD002670

Reifen C, Toumi R (2009) Climate projections: past performance no guarantee of future skill? *Geophys Res Lett* 36: L13704. doi: 10. 1029/ 2009GL038082

Renwick JA (2002) Southern Hemisphere circulation and relations with sea ice and sea surface temperature. *J Clim* 15: 3058-3068

Reynolds RW., Rayner NA, Smith TM, Stokes DC, Wang W (2002) An improved in situ and satellite SST analysis for climate. *J Clim* 15: 1609-1625

Rind D, Healy R, Parkinson C, Martinson DG (1995) The role of sea ice in 2×CO₂ climate model sensitivity. Part I: The total influence of sea ice thickness and extent. *J Clim* 8: 449–463

Rintoul SR, Hughes CW, Olbers D (2001) The Antarctic Circumpolar System. *Ocean Circulation and Climate* [Siedler G, Church J & Gould J(eds.)]. Academic, London

Rintoul SR, Sokolov S (2001) Baroclinic transport variability of the Antarctic Circumpolar Current south of Australia (WOCE repeat section SR3). *J Geophys Res* 106(C2), 2815–2832, doi:10.1029/2000JC900107.

Sabine CL, Feely RA, Gruber N, Key N, Lee K, Bullister JL, Wanninkhof R, Wong CS, Wallace DWR, Tilbrook B, Millero FJ, Peng T-H, Kozyr A, Ono T, Rios, AF (2004) The oceanic sink for anthropogenic CO₂. *Science* 305(5682): 367-371

Sallée JB, Rintoul S (2011) Parameterization of eddy-induced subduction in the Southern Ocean surface-layer. *Ocean Model* 39: 146–153

Sallée JB, Shuckburgh E, Bruneau N, Meijers AJF, Bracegirdle TJ, Wang Z (2013) Assessment of Southern Ocean mixed-layer depths in CMIP5 models: Historical bias and forcing response. *J Geophys Res-OCEANS* 18: 1845–1862

Sallée JB, Speer K, Morrow R, Lumpkin R (2008) An estimate of Lagrangian eddy statistics and diffusion in the mixed layer of the Southern Ocean. *Journ of Marine Res* 66(4): 441-463

Sallée JB, Speer KG, Rintoul SR (2010) Zonally asymmetric response of the Southern Ocean mixed-layer depth to the Southern Annular Mode. *Nature Geosci* 3: 273-279

Santer BD, Taylor KE, Gleckler PJ, Bonfils C, Barnett TP, Pierce DW, Wigley TML, Mears C, Wentz FJ, Brüggemann W, Gillett NP, Klein SA, Solomon S, Stott PA, Wehner MF (2009) Incorporating model quality information in climate change detection and attribution studies. *Proc Natl Acad Sci USA* 106: 14778-14783

Screen JA, Gillett NP, Karpechko AY, Stevens DP (2010) Mixed layer temperature response to the Southern Annular Mode: Mechanisms and model representation. *J. Clim* 23: 664–678

Séférian R, Iudicone D, Bopp L, Roy T, Madec G (2012) Water mass analysis of effect of climate change on air–sea CO₂ fluxes: the Southern Ocean. *J Clim* 25: 3894–3908

Shu Q, Song Z, Qiao F (2015) Assessment of sea ice simulations in the CMIP5 models. (2013) *Cryosphere* 9: 399-409, doi:10.5194/tc-9-399-2015

Simmonds I (2003) Modes of atmospheric variability over the Southern Ocean, *J Geophys Res* 108(C4), 8078, doi:10.1029/2000JC000542

Simmonds I, King JC (2004) Global and hemispheric climate variations affecting the Southern Ocean. *Antarct Sci* 16 (4): 401-413

Simmonds I (2015) Comparing and contrasting the behaviour of Arctic and Antarctic sea ice over the 35-year period 1979–2013. *Ann Glaciol* 56: 18–28

Smith TM, Reynolds RW, Peterson TC, Lawrimor J (2008) Improvements to NOAA's Historical Merged Land-Ocean Surface Temperature Analysis (1880-2006). *J Clim* 21: 2283-2296

Taylor KE (2001) Summarizing multiple aspects of model performance in a single diagram. *J Geophys Res* 106 (D7): 7183-7192. doi: 10.1029/2000JD900719

Taylor KE, Stouffer RJ, Meehl GA (2012) An overview of CMIP5 and the experiment design. *Bull Amer Meteor Soc* 93: 485-498

Tebaldi C, Knutti R (2007) The use of the multi-model ensemble in probabilistic climate projections. *Philos Trans R Soc Lond A* 365: 2053-2075

Thompson DWJ, Wallace JM (1998) The Arctic Oscillation signature in the wintertime geopotential height and temperature fields. *Geophys Res Lett* 25: 1297-1300

Thompson DWJ, Wallace JM (2000) Annular modes in the extratropical circulation. Part I: Month-to-month variability. *J Clim* 13: 1000–1016

Thompson DWJ, Wallace JM (2001) Regional Climate Impacts of the Northern Hemisphere Annular Mode. *Science* 293: 85-89

Trenberth KE, Hurrell JW (1994) Decadal atmosphere-ocean variations in the Pacific. *Clim Dyn* 9: 303-319

Turner J (2004) Review, The El Niño Southern Oscillation and Antarctica. *Int J Climatol* 24: 1-31

Turner J, Hosking JS, Bracegirdle TJ, Marshall GJ, Phillips T (2015) Recent changes in Antarctic Sea Ice. *Phil Trans R Soc A* 373, 20140163, doi:10.1098/rsta.2014.0163

van Loon, H., and R. L. Jenne (1972), The zonal harmonic standing waves in the Southern Hemisphere, *J Geophys Res* 77, 992–1003, doi: 10.1029/JC077i006p00992

Verdy A, Marshall J, Czaja A (2006) Sea surface temperature variability along the path of the Antarctic circumpolar current. *J Phys Oceanogr* 36: 1317-1331

Villalba R, Boninsegna JA, Veblen TT, Schmelter A, Rubulis S (1997) Recent trends in tree ring records from high elevation sites in the Andes of northern Patagonia. *Clim Chang* 36: 425-454

Villalba R, Lara A, Boninsegna JA, Masiokas M, Delgado S, Aravena JC, Roig FA, Schmelter A, Wolodarsky, A, Ripalta A (2003) Large-scale temperature changes across the southern Andes: 20th-century variations in the context of the past 400 years. *Clim Change* 59(1–2): 177-232

Walker GT, Bliss EW (1932). *World weather V*. *Mem Roy Meteor Soc* 4: 53–84

Wallace JM, Gutzler DS (1981) Teleconnections in the Geopotential Height Field during the Northern Hemisphere Winter. *Mon Wea Rev* 109: 784–812

Walsh JE (1983) The role of sea ice in climate variability: Theories and Evidence. *Atmos.-Ocean* 21: 229–242

Wang G, Dommenges D, Frauen C (2015) An evaluation of the CMIP3 and CMIP5 simulations in their skill of simulating the spatial structure of SST variability. *Clim Dyn* 44: 95-114

Wang G, Schimel D (2003) Climate change, climate modes, and climate impacts. *Annu Rev Environ Resour* 28: 1-28

- Washington WM, Meehl GA (1984) Seasonal cycle experiment on the climate sensitivity due to a doubling of CO₂ with an atmospheric general circulation model coupled to a simple mixed-layer ocean model. *J Geophys Res* 89(D6): 9475-9503. doi: 10.1029/JD089iD06p09475
- White WB, Chen SC, Peterson RG (1998) The Antarctic Circumpolar Wave: A beta effect in ocean-atmosphere coupling over the Southern Ocean. *J Phys Oceanogr* 28: 2345–2361
- White WB, Gloersen P, Simmonds I (2004) Tropospheric response in the Antarctic Circumpolar Wave along the sea ice edge around Antarctica. *J Clim* 17: 2765-2779.
- White WB, Simmonds I (2006) Sea surface temperature-induced cyclogenesis in the Antarctic circumpolar wave. *J Geophys Res* 111(C8), C08011 doi: 10.1029/2004JC002395
- White WB, Peterson RG (1996) An Antarctic circumpolar wave in surface pressure, wind, temperature, and sea-ice extent. *Nature* 380: 699-702
- Williams RG, Wilson C, Hughes CW (2007) Ocean and atmosphere storm tracks: The role of eddy vorticity forcing. *J Phys Oceanogr* 37: 2267–2289
- Xavier PK, Duvel J-P, Braconnot P, Doblas-Reyes FJ (2010) An evaluation metric for intraseasonal variability and its application to CMIP3 Twentieth-Century simulations. *J Clim* 23: 3497-3508
- Yeh S-W, Kug J-S, Dewitte B, Kwon M-H, Kirtman BP, Jin F-F (2009) El Niño in a changing climate. *Nature* 461: 511-514
- Yeo SR, Kim KY (2015) Decadal changes in the Southern Hemisphere sea surface temperature in association with El Niño-Southern Oscillation and Southern Annular Mode. *Clim Dyn*. DOI 10.1007/s00382-015-2535-z
- Yuan X, Li C (2008) Climate modes in southern high latitudes and their impacts on Antarctic sea ice. *J Geophys Res-Oceans* 113: C06S91

Yuan X, Martinson DG (2000) Antarctic sea ice extent variability and its global connectivity. *J Clim* 13: 1697-1717

Yuan X, Yonekura E (2011). Decadal variability in the Southern Hemisphere. *J Geophys Res* 116: D19115, doi:10.1029/2006JC004067

Zhou T, Wu B, Wang B (2009) How well do atmospheric general circulation models capture the leading modes of the interannual variability of the Asian–Australian monsoon? *J Clim* 22: 1159-1173

Zlotnicki V, Wahr J, Fukumori I, Song YT (2007) Antarctic circumpolar current transport variability during 2003-05 from GRACE. *J Phys Oceanogr* 37: 230–244.

Zunz V, Goosse H, Massonnet F (2013) How does internal variability influence the ability of CMIP5 models to reproduce the recent trend in Southern Ocean sea ice extent? *Cryosphere* 7: 451–468, doi:10.5194/tc-7-451-2013.

Abbreviations

ACC Antarctic Circumpolar Current

ACW Antarctic Circumpolar Wave

CMIP Coupled Model Intercomparison Project

CMIP3 Coupled Model Intercomparison Project Phase 3

CMIP5 Coupled Model Intercomparison Project Phase 5

DEOFs distinct EOFs

ENSO El Niño-Southern Oscillation

EOF empirical orthogonal function

ERSST NOAA Extended Reconstructed sea surface temperature data set

EV eigenvalue

HadISST Hadley Centre Sea Ice and SST data set

HYCOM HYbrid Coordinate Ocean Model

IPCC Intergovernmental Panel on Climate Change

MLD mixed layer depth

NH Northern Hemisphere

OISST NOAA Optimum Interpolation Sea Surface Temperature

PC principal component

PDO Pacific Decadal Oscillation

PEV projected explained variance

PSA Pattern Pacific South America pattern

PSU Practical Salinity Unit

RMSE normalized root-mean-square error

SAM Southern Annular Mode

SH Southern Hemisphere

SLP sea level pressure

SO Southern Ocean

SOI Southern Oscillation Index

SST sea surface temperature

SSTA sea surface temperature anomaly

STDV standard deviation

TPI Trans-Polar Index